OXIDATIVE DEHYDROGENATION OF N-BUTANE OVER CHROMIUM AND VANADIUM SUPPORTED CATALYSTS WITH CO_2 AS A MILD OXIDANT: SYNTHESIS, CHARACTERIZATION AND KINETIC STUDIES

BY

BABAJIDE PATRICK AJAYI

A Thesis Presented to the

DEANSHIP OF GRADUATE STUDIES

KING FAHD UNIVERSITY OF PETROLEUM & MINERALS

DHAHRAN, SAUDI ARABIA

In Partial Fulfillment of the
Requirements for the Degree of

MASTER OF SCIENCE

In

CHEMICAL ENGINEERING

MAY, 2013

KING FAHD UNIVERSITY OF PETROLEUM & MINERALS

DHAHRAN- 31261, SAUDI ARABIA

DEANSHIP OF GRADUATE STUDIES

This thesis, written by **Babajide Ajayi** under the direction his thesis advisor and approved by his thesis committee, has been presented and accepted by the Dean of Graduate Studies, in partial fulfillment of the requirements for the degree of **MASTER OF SCIENCE IN CHEMICAL ENGINEERING.**

Dr. Basim Abussaud
(Chairman)

Dr. Usamah Al-Mbaiyedh
Department Chairman

Dr. Sulaiman Al-Khattaf
(Co-chairman)

Dr. Salam A. Zummo
Dean of Graduate Studies

Dr. M. Mozarhar Hossain
(Member)

28/5/13
Date

Dr. Nabil Al-Yassir
(Member)

Dr. Abdullah Al-Shammari
(Member)

Dedicated to my loving wife Folashade Anne Ajayi

ACKNOWLEDGMENTS

My first days in Saudi Arabia were filled with ambivalent feelings. On one hand, I was happy about the opportunity of earning a second degree in a competitive and internationally acclaimed institution known to advance the frontiers of research and knowledge. One the other hand, I was unsure whether people here will accept me owing to my diverse background. But the kind of love, concern, professionalism, and meritocracy I experienced here put my fears to bed the instance I enrolled for the program.

I am especially thankful to God for the gift of life, for His guidance, protection and care throughout my sojourn in Saudi Arabia. My sincere gratitude goes to my thesis advisor in the person of Dr Basim Abussaud for his kindness and support throughout my stay here. The door of your office was always open for scientific discussions as well as informal chitchat. Your relaxed character and pragmatic way of working always took away any worries that I had concerning my project. To my indefatigable Director at Center of Research Excellence in Petroleum Refining and Petrochemicals who also doubled as my co-advisor, Professor Sulaiman Saleh Al-Khattaf: I am so lucky to have passed through you in training because your constructive criticism and chastisements will come handy in my future career and for this reason I say a big thank you!

I can never forget in a hurry the contributions of Dr Balasamy Radindran Jermy. His work rate, professionalism, honesty, dedication and humility will resonate in my mind for years to come, and I sincerely hope a little of his positive traits rubs off on my

personality. My appreciation goes to my thesis committee members: Dr Abdullah Al-Shammari, Dr Nabil Al-Yassir, Dr Mohammed Mozahar Hossian. I am most especially indebted to Dr Mohammed Mozahar Hossain for helpful discussions during the kinetic modeling phase of this research work. I would also like to thank late Mr Alam Khurshid and Mr Mariano Gica who both helped out with some experimental works.

I am grateful for the support from Ministry of Higher Education, Saudi Arabia for the establishment of the Center of Research Excellence in Petroleum Refining and Petrochemicals at King Fahd University of Petroleum and Minerals and the Department of Chemical Engineering both at King Fahd University of Petroleum & Minerals. I would also acknowledge Japan Cooperation Center, Petroleum (JCCP) which gave the opportunity for collaborative research. I have received a world class exposure to the field of catalysis research thanks to the following JCCP consultants: Dr Katsuomi Takehira, Dr Hideshi Hatori, Dr Sachio Asaoka. JCCP's technology transfer program with Saudi Arabia has been very fruitful to say the least, especially in the area of graduate education.

In conclusion, I am thankful to my wife, my parents and my sisters especially Josephine for their patience, prayers and support and to the Nigerian community here in KFUPM for making my stay a pleasant one. I will like to also extend my profound gratitude to many others too numerous to mention, who have in many ways contributed to this milestone achievement.

TABLE OF CONTENTS

LIST OF TABLES

LIST OF FIGURES

LIST OF ABBREVIATIONS

BET ……Bernet Emette Teller

BJH……. …… Barret Joyner Halenda

BTX ……Benzene Toluene Xylene

CP…… Cracked Products

EB ……. ……Ethyl Benzene

EDX……..…….. Energy Dispersive X-ray

FB ……Fixed Bed

FID……. …Flame Ionization Detector

FTIR……. ….Fourier Transform Infra Red

GC……. Gas Chromatography

GHSV…….. Gas Hourly Space Velocity

HMS…….…… Hexagonal Mesoporous Silica

HPIL……. Hewlett-Packard Interface Loop

HTC…… High Temperature Ceramics

ID ……..……. Internal Diameter

JCPDS ……..Joint Committee on Powder Diffraction Standards

LAB…….. Linear Alkyl Benzene

LSQCURVEFIT…….. Least Square Curve Fit

MB…….…….. Membrane

MATLAB…… Matrix Laboratory

NDIR……..……Non-Dispersive Infra Red

ODE……Ordinary Differential Equation

ODH…… Oxidative Dehydrogenation

Q-MASS……..Quadrupole Mass Analyser

SEM…….….. Scanning Electron Microscopy

SS…….…… Sum of Square Errors

TCD…….. Thermal Conductivity Detector

Torr. ……..…. Torricelli

TPD…….. Temperature Programmable Desorption

TPO ……Temperature Programmable Oxidation

TPR……. Temperature Programmable Reduction

VITA ……. Verweilzeitgekoppette Integration fur TOC Analysen

WHSV …… Weight Hourly Space Velocity

XRD…… X-Ray Diffraction

ABSTRACT

Full Name : [Babajide Patrick Ajayi]

Thesis Title : [Oxidation Dehydrogenation of n-Butane over Chromium and Vanadium Supported Catalysts with CO2 as Mild Oxidant: Synthesis, Characterization and Kinetics]

Major Field : [Chemical Engineering]

Date of Degree : [May 2013]

The study investigates the simple dehydrogenation of *n*-butane over mono (Cr or V) and bimetal (Cr-V) loaded MCM-41 catalysts. Wet impregnation technique was used, where the metal content maintained around 4wt.%. The unique properties of bimetal supported catalysts were evaluated by means of XRD, N_2 adsorption, pyridine FT-IR, Raman spectroscopy, SEM-EDX, temperature programmed analysis (H_2-TPR, NH_3-TPD, CO_2-TPD). The catalytic evaluation shows that Cr content of 1.2wt% and V content of 2.8wt% over MCM-41 designated as 1.2Cr2.8V/M-41 exhibited the highest butane conversion of 20.1% and butenes selectivity of 88.5% at 600 °C. In the presence of CO_2, the stability of 1.2Cr2.8V/M-41catalyst was quite improved. The improved performance of bimetal catalysts can be correlated to synergetic effect of uniformly dispersed Cr-V-O mixed oxides over MCM-41, high reducibility and surface acidity. Oxidative dehydrogenation of *n*-butane was tested using CO_2 as a mild oxidant over bimetallic Cr-V supported catalysts (MCM-41, ZSM-5, MCM-22 and mesoZSM-5). The metal content of Cr and V was maintained around 1.2wt.% and 2.8wt.% for the catalytic test in packed bed reactor at different temperatures (525-600°C) for 180 min. 1.2Cr2.8V/MCM-41 and 1.2Cr2.8V/ZSM-5 exhibited maximum conversion of 14 % and 13.1%, respectively at 10 min and 600 °C. Significantly, high butenes selectivity was observed over MCM-41 (86.27%) than ZSM-5 support (58.1%). The mesoporousity in ZSM-5 had a negative impact on conversion level (7.1%) but improved the butenes selectivity slightly. 1.2Cr2.8V/M-22 showed the highest cracking ability leading to overall reduced butenes selectivity (57.9%). The study shows that over all catalysts, *n*-butane conversion is independent of CO_2 conversion. 1.2Cr2.8V/M-22 showed highest CO_2 conversion in the range 2.35-2.2% between 525-550^{o}C. The kinetics of *n*-butane dehydrogenation over 1.2Cr2.8V/M-41 catalyst was studied. The models were developed based on the catalyst tests carried out in a fixed bed reactor at reaction temperature varied from 525-575°C. Based on the experimental observations, power law type models were formulated and parameters were estimated by fitting the experimental data implemented in MATLAB.

جامعة الملك فهد للبترول و المعادن

قسم الهندسة الكيميائية

نزع الهيدروجين التأكسدي للبيوتان على العوامل الحفازة المدعمة بالكروم و الفناديوم في وجود ثاني أوكسيد الكربون كمؤكسد معتدل: التحضير, الوصف و الحركية

الملخص

هذا البحث يختص بدراسة عماية نزع الهيدروجين من البيوتان على العامل الحفاز MCM-41 محمل بأحادي (Cr أو V) أو ثنائي المعدن (Cr-V). تم إستخدام طريقة التلقيح الرطب حيث تم الحفاظ على كمية المعدن ليكون حوالي 4% بالوزن. الخواص الفريدة للعامل الحفاز المدعم بثنائي المعدن تم تقييمها بإستخدام XRD ,تقنية إمتزاز النيتروجين, Raman , pyridine FTIR الطيفي, SEM-EDX و تجارب الحرارة المبرمجة (H_2-TPR, NH_3-TPD, CO_2-TPD). تقييم العامل الحفاز وضح أن Cr بنسبة 1.2% و V بنسبة 2.8% على MCM-41 المعرف ب (1.2Cr2.8V/M-41) أظهر أعلى نسبة تحويل للبيوتان بنسبة 20.1% و إنتاجية بيوتين بنسبة 88.5% عند درجة حرارة 600 درجة مئوية. في وجود ثاني أوكسيد الكربون تحسنت الإستقرارية ل 1.2Cr2.8V/M-41. و يمكن إرجاع هذا الأداء العالي للحفاز ثنائي المعدن إلى الأثر التعاضدي للتوزيع المتجانس لخليط أوكسيدات Cr-V-O على MCM-41, الإختزالية العالية و حامضية السطح. تم إختبار نزع الهيدروجين التأكسدي للبيوتان بإستخدام ثاني أوكسيد الكربون كمؤكسد معتدل للحفاز المدعم بثنائي المعدن (Cr, V) (MCM-41,ZSM-5, MCM-22, mesoZSM-5). المحتوى المعدني من Cr و V تم تم الحفاظ عليه عند 1.2% و 2.8% على التوالي لعملية إختبار العامل الحفاز في المفاعل عند درجات حرارة مختلفة بين 525 و 600 درجة مئوية لمدة 180 دقيقة. 1.2Cr2.8V/M-41 و 1.2Cr2.8V/ZSM-5 أظهرا اعلى نسبة تحويل بقيمة 14% و 13.1% على التوالي عند 10 دقائق و 600 درجة مئوية. بشكل واضح تم ملاحظة إنتاجية عالية للبيوتين على MCM-41 بنسبة 86.27% بالمقارنة مع 58.1% ل ZSM-5. المسامية الدقيقة ل ZSM-5 كان لها تأثير سلبي على درجة التحويل بقيمة 7.1% و لكنها حسنت بدرجة قليلة الإنتقائية للبيوتين. أظهر 1.2Cr2.8V/M-41 أعلى قدرة على التكسير مؤديا لتقليل عام في إنتقائية البيوتين (57.9%). أظهرت هذه الدراسة أنه على جميع العوامل الحفاز المستخدمة أن نسبة التحويل للبيوتان لا تعتمد على درجة تحويل ثاني أوكسيد الكربون. أظهر 1.2Cr2.8V/M-41 أعلى نسبة تحويل لثاني أوكسيد الكربون في المدى 2.35% إلى 2.2% بين 525 و 550 درجة مئوية. تم دراسة حركية عملية نزع الهيدروجين من البيوتان على العامل الحفاز 1.2Cr2.8V/M-41. تم تطوير منظومة معادلات بناء على تجارب تقييم العامل الحفاز التي أجريت في المفاعل عند درجات حرارة بين 525 و 575 درجة مئوية. بناء على نتائج التجارب, تم تكوين معادلات من نوع المعادلات الأسية و تم حساب قيم الثوابت في هذه المعادلات بمقارنة النتائج المعملية مع المعادلات الأسية المقترحة بإستخدام برنامج MATLAB.

CHAPTER 1

INTRODUCTION

1.1 Background

The petrochemical industry in Saudi Arabia has a small domestic market with a large raw materials resource base, resulting in an export oriented industrial structure. To realize better economic benefits, conversion of lower hydrocarbons such as C_1 to C_4 alkanes to higher value products is being investigated. The plan is to spend efforts in this direction, investigating new processes with higher efficiencies and better economic returns than current commercial processes.

The abundance and lower cost of light alkanes have generated extraordinary interest in oxidative catalytic conversion of alkanes to olefins, oxygenates or nitriles in the petroleum and petrochemical industries due to both the potential economic and environmental advantages [1]. The direct conversion of light alkanes to commodity chemical intermediates has the potential to radically transform the chemical industry. The effectiveness of the catalyst, i.e. the activity for alkane conversion and the selectivity to desired products, will ultimately determine the economic attractiveness of an alkane-based chemical process. The successful commercial technologies will be those that link catalyst performance characteristics with innovative process designs [2].

The importance of catalytic dehydrogenation of paraffin hydrocarbons to olefins has been growing steadily in recent years. Light olefins, such as butenes, are important raw materials for the synthesis of polymers, gasoline additives and various other petrochemical products. The current world capacity for 1-butene is about 1.3 million metric tpy, and the demand is expected to increase 5 – 6%/yr through 2015. Similarly, global consumption of butadiene is expected to increase from 10 million tons in 2006 to 13 million tons by 2015.The cracking processes especially fluid catalytic cracking and steam cracker produce high-purity mono-olefins, such as 1-butene or butadiene. Despite such processes, currently more research is focused on developing alternatives such as oxidative dehydrogenation (ODH) for two reasons: (1) undesired reactions take place at high temperature leading to coking and catalyst deactivation, making frequent regeneration of the catalyst unavoidable, (2) it consumes a large amount of heat and requires high reaction temperatures. Oxidative dehydrogenation (ODH) of n-butane is an alternative to classical dehydrogenation, steam cracking and fluid catalytic cracking processes.

1.2 Industrial Technologies

Commercially, dehydrogenation units use Pt/Al_2O_3 or $Pt/Sn/Al_2O_3$ or Cr/Al_2O_3 catalysts, respectively, refer to Table 1.1 [3]. The support alumina has high thermal stability, mechanical strength, and catalyst regeneration capabilities. However, alumina tends to have acidic sites that accelerate undesired side reactions such as skeletal isomerization and cracking that enhance coke formation. The catalyst is cycled through

dehydrogenation, coke burn-off and reduction cycles within approximately 20 minutes. This environment is extremely challenging for any catalyst and significant catalyst degradation is seen in the plant process within 2-3 years.

In addition to the above Pt and Cr based catalysts, zeolite based catalysts (modified and impregnated ZSM-5, ZSM-11, MCM-41, SBA-15, etc), gallium oxides, and catalytic membrane reactors have been investigated [4,5]. However, in parallel to the catalyst effects, there are various process parameters that have direct impact on catalyst performance that needs to be addressed. These parameters include reaction conditions, feed and product purity requirements. Alternatively, ODH of butane by an oxidant is free from thermodynamics constraints and can be operated at moderate temperatures in an exothermic reaction [6, 7]

.

Table 1.1: Industrial Butane Dehydrogenation Processes

Process name	Catofin	Oleflex	STAR	FBD	Linde/BASF
Licensor	Lummus	UOP	Uhde	Snamprogetti	BASF
Catalyst	CrO_x/Al_2O_3	$Pt/Sn/Al_2O_3$	Pt/Sn/Zn/Ca/Al	CrO_x/Al_2O_3	Pt-Sn/Zr
	Adiabatic	Adiabatic			Isothermal
Reactor	FB	MB	Adiabatic/Oxy	Continuous	FB
Temp/° C	590-650	550-620	550-590	550-600	500-600
Conversion/%	48-65	25	40	40	45-50
Selectivity/%	82-87	89-91	89	89	90

1.3 Motivation

Research and development of new catalysts, reactor designs, and process routes has been continuously pursued to achieve process improvement. There are very many collaborations going on between catalyst research and process development, and such collaboration have enabled the development of a new energy saving catalytic process, to reduce the cost of raw materials and to enhance production capability. BASF and DOW processes composed of multi-tubular fixed bed reactor, whereas Lummus and Badger processes composed of radial flow type reactor recently used due to its adiabatic character applicable for large scale production. In view of this, a plausible catalytic process of n-butane dehydrogenation to improve butene and butadiene production is being developed. This process is going to utilize CO_2, a well known greenhouse gas. The development of this process depends primarily on the fundamental studies of catalyst preparations as well as the catalytic reactions involved in the process. For the dehydrogenation at low temperatures, a highly dispersed Cr and V catalyst with zeolite carriers is a promising candidate due to its high activity. We aim to optimize the catalysts by modifying the preparative conditions and metal compositions. The catalytic process will make use of a fixed bed micro-reactor made from quartz material. The reaction will be studied under several conditions for catalyst testing and kinetic modeling. Finally, by optimizing the reaction conditions, a highly efficient process can be established in the dehydrogenation of n-butane to butene and /or butadiene, as well as enable an energy saving and environmental benign chemical process.

This project tests the effectiveness of using carbon dioxide as a mild oxidant. The motivation for the choice of carbon dioxide is predicated on the following reasoning:

- It is inexpensive.
- It is a renewable feedstock.
- Offers new routes to chemical intermediates and products.
- Carbon dioxide removes the hydrogen adsorbed on the surface of the catalysts through the reverse water gas shift reaction.
- Stability of catalysts improves in carbon dioxide atmosphere because solid coke deposited on the surface of the catalyst is removed through reaction with carbon dioxide to form gas phase carbon mono-oxide.

1.4 Objectives

The main objectives are three folds:

- To develop highly efficient bimetallic catalysts for catalytic dehydrogenation of n-butane
- To test the influence of zeolites supports
- Kinetic studies of the reactions using the most efficient catalyst.

The detailed objectives are highlighted in the sub-header below

1.4.1 Synthesis and characterization of chromium and vanadium based catalysts supported on MCM-41.

- Preparation of mono and bimetallic chromium and vanadium based MCM-41 supported catalysts.
- Determination of the physico-chemical properties of the catalysts through some characterization techniques.

- Catalyst testing to determine the optimum catalyst in nitrogen atmosphere.

1.4.2 Oxidative dehydrogenation of n-butane over chromium and vanadium catalyst supported on four selected zeolites using CO_2 as a soft oxidant.

- Impregnation of optimum Cr-V on four selected zeolite support of micro and mesoporousity.
- Determination of the physico-chemical properties of the catalysts through some characterization techniques.
- Catalyst testing in CO_2 atmosphere to determine the best catalyst as per n-butane and CO_2 reactivity and catalyst stability.

1.4.3 Kinetic modeling of optimum Cr-V catalyst loaded on MCM-41 carrier in a fixed bed reactor.

An important aspect of process development is the availability of design parameters such as activation energy of reaction, rate constants, etc. This involves the following;

- To predict the rate mechanistic steps by incorporating Cr-V bimetallic system using the power law model.
- To estimate the kinetic parameters underlying the rate equation.
- Fitting experimental data into proposed models to check the suitability of the models.

1.5 Scope & Outline of Work

Chapter two presents a comprehensive literature survey on catalytic n-butane dehydrogenation. Challenges facing the industrial catalysts, and what has been done to ameliorate these problems were discussed.

Chapter three deals with the experimental section of this research work. The description of the equipment used for the experimental set-up as well as the procedure adopted to accomplish various tasks vis-à-vis catalyst synthesis, characterization and evaluation.

Chapter four focuses on the results of the experimental work. All characterization results of the prepared catalysts are discussed in details here. Discussion of the effects of reaction conditions such as temperature effects, effect of time on stream, effect of oxidants, contact time, etc, are all explained in details. Also, kinetic modeling results are presented starting first with model development to the estimation of kinetic parameters using a non-linear regression analysis.

Chapter five includes the summary of research work and the conclusions drawn from it. Also, recommendations for future work were discussed here.

CHAPTER 2

LITERATURE REVIEW

2.1 Background

The principal catalytic systems that have a dehydrogenation activity reported in scientific and patent literature are:

- Group VIII metals (mainly platinum with tin) supported on alumina and with promoters [3].
- Chromium oxides on alumina or zirconium, with promoters.
- Vanadium oxides supported on zeolites and silica.
- Iron oxides supported, with promoters.
- Gallium, as a supported oxide or included in zeolitic structures.
- Copper, for the dehydrogenation of alcohols to aldehydes.

Including the most recent literature, the situation for dehydrogenation catalysts and their applications is outlined in **Table 2.1**. Commercial application has restricted potential catalysts to those indicated below:

Table 2.1 Performance of dehydrogenation catalysts

Active component of Catalysts	Dehydrogenation of Light Paraffin	Dehydrogenation of Paraffin C_{10}-C_{14}	Dehydrogenation of Ethyl Benzene to Styrene
Pt/sn	Excellent	Excellent	Poor
Cr oxides	Excellent	Moderate	Good
V oxides	Excellent	Moderate	Good
Fe oxides	Absent/poor	Not available	Excellent
Ga systems	Excellent	Not available	Excellent

Source: www.trecanni.it

- For the dehydrogenation of ethyl benzene to styrene, oxides of Fe as the only choice.
- For long chain paraffins for LAB, Pt/Sn promoted on Al_2O_3.
- For light paraffins and olefins, Pt/Sn promoted on Al_2O_3 and Cr_2O_3 on Al_2O_3.

The two large families of catalysts for the dehydrogenation of paraffins (based on Pt and Cr) were developed at the same time. The two families do not differ substantially in terms of activity and selectivity, but rather in the quality of some by-products and in the treatment needed to complete the regeneration after the combustion of the coke. In addition, the phenomena that lead to the irreversible deactivation (sintering, volatilization of the active components and transformations of the morphology or the state of the support) are typically connected to the chemical types that characterize the various catalysts.

2.2 Kinetics and Thermodynamics of Dehydrogenation Reactions

Dehydrogenation removes a molecule of hydrogen from paraffin forming an olefinic double bond that will be the preferred point of attack for successive reactions. Notwithstanding its apparent simplicity, the dehydrogenation of paraffin is one of the most complex chemical processes to realize industrially, since the thermodynamic equilibrium limits the conversion possible per pass and the reaction is highly endothermic, that is to say, a large amount of heat must be supplied to the reactant system. In F**ig. 2.1**, the conversion equilibrium is shown versus the temperature, for paraffins with 2 to 15 atoms of carbon. It is clear that, in order to make the industrial

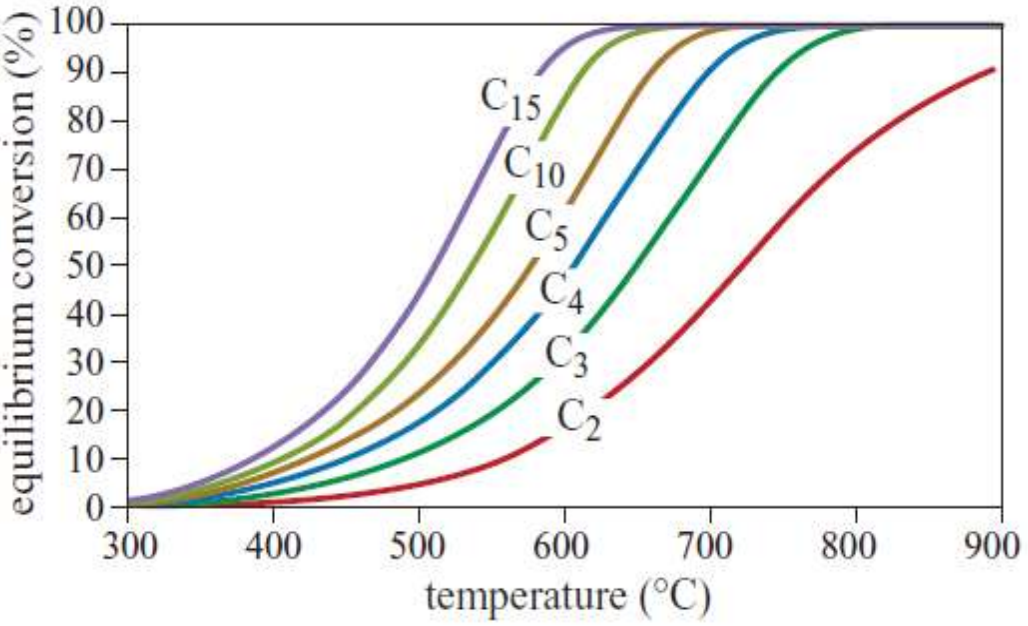

Fig. 2.1. Equilibrium conversion in the dehydrogenation of some paraffins at atmospheric pressure. *Source: www.trecanni.it*

process more economic, it is advisable to increase the conversion per pass as much as possible, so that the cost of recycling the unconverted reagent and that of separating the reagent and the product is reduced. As shown in Fig.2.1, it is evident that temperatures between 500 and above 700°C are needed to reach a conversion rate of 50%. However, high temperatures also enhance an undesired parallel process, i.e., thermal cracking reactions that reduce the selectivity to the desired product and make purification operations downstream the reaction zone necessary. Oxidative dehydrogenation has been widely studied, as one route to circumvent the thermodynamic limitations. This involves supplying oxygen to the reagent mixture so that it combines with the hydrogen produced by dehydrogenation and forms water. The removal of the hydrogen allows the dehydrogenation reaction to proceed with a higher conversion than would be suggested by the equilibrium. However, the practical application of this approach ran into the problem of making the oxygen react only with the hydrogen, without causing direct combustion of the hydrocarbons and a resulting loss of selectivity. An additional advantage of this approach results from the exothermic nature of the reaction producing water, which contributes heat for the dehydrogenation reaction, reducing the need for an external source. In non-oxidative dehydrogenation, in order to reach high reaction rates and minimize the effect of its complex secondary reactions, a suitable heterogeneous catalyst is needed. The energy required to remove two atoms of hydrogen from the alkane molecule is almost independent of the molecular weight of the paraffin and in the range of 113-134 KJ/mol. The highly endothermic nature of the main reaction (and of the greater part of the secondary reactions) leads to a strong temperature decrease, if the reaction is carried out in an adiabatic manner. For example, in the case of the

dehydrogenation of propane with a 25% conversion, there is an adiabatic temperature decrease of 200°C. Since no catalyst is able to operate in such a wide temperature range, it is clear that a single adiabatic reactor cannot be used, and a heat source must also be supplied in the course of the reaction.

2.3 Chromium and Vanadium Catalysts

Over the years, a significant progress has been made in the development of catalysts for ODH of *n*-butane (C_4H_{10}) and isobutane (*i*-C_4H_{10}) to C_4H_8 and *i*-C_4H_8. Among the oxide catalysts, vanadium and chromium oxide supported catalysts have been most promising for ODH due to their high catalytic activity. The mononuclear Cr^{3+} species dispersed on the surface of silica support are reported to be responsible for dehydrogenation of light alkanes. These species predominate at low Cr loadings, while at higher loadings less active crystalline Cr_2O_3 tends to dominate [8]. Hakuli et al. [9] reported that silica- and alumina-supported chromium oxides were effective for the production of lower alkenes such as propylene and isobutene. Botavina et al. [10] stated that for ODH of propane and isobutane, the highest activity, selectivity and stability were achieved over 5.0 wt% CrOx/silica catalysts prepared by wet impregnation method. Volpe et al. [11] investigated *n*-butane dehydrogenation using VO*x* supported on USY, NaY, γ-Al_2O_3 and α-Al_2O_3. The high catalytic activity of VO*x*/USY and butene selectivity was related to the VO*x* monolayer and mild acidity. Recently, chromium oxide catalysts supported on high surface area, pore expanded MCM-41 silica was investigated for ethane dehydrogenation. The studies showed that the ethane conversion strongly depend on the chromia loading and the catalyst preparation method [12]. Similarly, VO_X species supported on hexagonal

mesoporous silica (HMS) were found to be active in ODH of n-butane, where the isolated monomeric VO_X species were determined to play most active catalytic role [13]. The comparative study on V-containing different mesoporous siliceous materials such HMS, SBA-16, SBA-15 and MCM-48 in ODH of propane and n-butane highlights the importance of population of tetrahedrally coordinated VOx complexes and isolated monomeric VOx complexes [14].

2.4 Carbon Dioxide Assisted Dehydrogenation

The dehydrogenation of propane using CO_2 as a mild oxidant has been recently explored as an alternative to the equilibrium controlled dehydrogenation. Oxygen assisted dehydrogenation is less attractive because the abstracted hydrogen is oxidized, releasing heat in an exothermic reaction. Due to the exothermic property of these reactions, it is expedient to remove heat [15] and avoid the over-oxidation of n-butane to CO_2 in order to reach high selectivity to butene. Nakagawa et al. [16] have shown that CO_2 improves the stability of Ga_2O_3 loaded catalyst by the removal of the coke deposited on its surface according to the Boudouard reaction:

$$C_{(s)} + CO_{2(g)} \rightleftharpoons 2CO_{(g)} \qquad (2.1)$$

Also, CO_2 removes the H_2 adsorbed on the surface of the catalyst through the reverse water gas shift reaction (RWGSR):

$$CO_2 + H_2 \rightleftharpoons CO + H_2O \qquad (2.2)$$

RWGSR is very important because it removes one of the products (H_2) and shifts the equilibrium to the products, thereby improving the conversion. Wang et al. [17]

reported, for *i*-C_4H_{10} dehydrogenation with Cr/MCM41 catalyst, a selectivity of 90.4% at an *i*-C_4H_{10} conversion of 18.3%. Shimada et al. [18] discussed that iron loaded on activated carbon produced an *i*-C_4H_{10} conversion of 48% with 80% *i*-C_4H_8 selectivity at 600 °C in the ODH of *i*-C_4H_{10} by CO_2.

The literature shows that ODH in n-butane are little and are primarily based on monometallic system. It is well established that the incorporation of two different metals might create new redox and acidic properties [19]. Yuan et al. [20] reported on the synthesis of metallosilicate MCM-41 with hierarchical structure containing Cr and V species. The synthesis and catalytic application of single or two transition metals systems have been already reported [21, 22, 23 and 24]. MCM-41 mesoporous molecular sieve is extensively used as support or catalysts as documented in recent review papers [25, 26].

Therefore, in the present study, we extend the investigation using Cr and V based bimetallic impregnated MCM-41 in dehydrogenation of n-butane at different reaction conditions via temperature, time on stream, contact time, feed and catalyst type.

The literature reports show that dehydrogenation reaction has been exhaustively carried out in the presence of conventional oxygen as oxidant. Like pointed out previously, such oxygen assisted dehydrogenation is less attractive due to its exothermicity, necessitating the removal of heat in order to avoid the deep oxidation to CO_2. The heat removal step is necessary in order to achieve high selectivity to butenes. In the current trend, emissions of greenhouse gas such as carbon dioxide have become major problem in global climate changes. Recently, there are several attempts is being made either to capture CO_2 [27] or

utilize it as co-feed gas in dehydrogenation of ethylbenzene and light alkanes [28]. Unlike oxygen, CO_2 exists as gaseous state during whole reaction steps and possesses high heat capacity. Moreover, reaction coupling, namely processes combining dehydrogenation with reverse water-gas shift reaction, is an attractive approach to improve the equilibrium conversion in the dehydrogenation reactions [29]. However, the best known commercial $CrOx/Al_2O_3$ catalyst was found to be inhibited by CO_2, while over $CrOx/SiO_2$ and CrOx/ZSM-5, the presence of CO_2 showed a promoting effect [30]. Until now, ODH of *n*-butane in CO_2 atmosphere over bimetal (Cr-V) containing mesoporous material (MCM-41, mesoZSM-5) and microporous zeolites (MCM-22, ZSM-5) has not been explored. In the present study, we have investigated the influence of time on stream and different temperatures over the four catalysts. The conversion of *n*-butane and CO_2, molar selectivity of dehydrogenation products, distribution of butene isomers, apparent activation energy, olefin to paraffin ratio, ratio of conversion to coke weight percent were all investigated.

CHAPTER 3

EXPERIMENTAL

3.1 Experimental Set-up

3.1.1 Set-up for Catalyst Evaluation

3.1.1.1 BELCAT microreactor

The catalytic runs were carried out in a fully integrated, fixed bed continuous flow reactor system (BELCAT). The system consists of one tubular quartz reactor attached with stainless steel one-zone furnace assembly through reactor furnace wall thermo well. The catalysts sample (0.15g) was packed in the reactor and activated with flowing N_2 at 823 K for 2 h. After which the flow rate of reactants were maintained at 4.0 ml/min; n-butane, 96 ml/min;N_2, (non-oxidative reaction) and 56ml/min N_2, 40ml/min CO_2, (oxidative reaction) respectively. The gas product samples were analyzed by online gas chromatograph (Agilent, 7890N) equipped with J&W Scientfic HP-5 capillary column (length: 30 m, ID: 0.32 mm, and film thickness 0.25 μm) and FID detector. The gas products, including H_2, CO and CO_2, were analyzed with a TCD and a GS-GASPRO capillary column. The products were identified by comparison with authentic samples. See Fig 3.1 for the schematics and appendix for the complete specifications.

3.1.1.2 Gas chromatograph (GC)

The quantitative analysis of the reactor products were carried out online using Agilent GC (Agilent Chromatograph Model 7890N) equipped with one Flame Ionization Detector (FID) and two Thermal Conductivity Detectors (TCD), equipped with GS-GASPRO capillary column (Polyethylene glycol, length:60m, internal diameter:0.32mm, film thickness: 0.50µm). Helium is used as the carrier gas, while air and hydrogen gases are used for the FID. Furthermore, liquid nitrogen is used to facilitate the initial cryogenic operation of the GC temperature program. The liquid nitrogen cools the GC oven to -30°C. The flow of liquid nitrogen is administered by a solenoid valve actuated from the GC's internal oven temperature controller. The integrator allows strip chart recording as well as integration of the GC detector signal. The integrator is connected to the GC via a HPIL instrument network cabling system.

3.1.1.3 Coke Analyzer

A carbon analyzer multi EA 2000 was used. This multi EA 2000 equipped with CS module is specially developed system which permits simultaneous or separate determination of the total carbon and total sulphur in the samples of solids, pastes and liquids by means of high temperature oxidation in a current of xygen supplied directly to the unit. It is based on a special high temperature ceramics (HTC) technology which renders a catalyst superfluous. By combining the finely tuned non-dispersive infra red gas analysis (NDIR) detection which is selective to CO_2/SO_2 with the patented Verweilzeitgekoppelte Integration fur TOC-Analysen (VITA) procedure, which takes into account the dwelling time, the analysis possible is very precise. The aliquot of the

sample is accurately weighed into the combustion boat and delivered complete into the hot zone of the furnace. There, pyrolysis and oxidation of the sample occurs at a high temperature in the stream of oxygen. The gas produced in the pyrolysis is drawn through a glass tube filled with a specialist dessicant. This dessication tube also serves as a particle filter so that no water or dust can get into the detection system of the device. NDIR detector is used to determine the CO_2 content in the carrier gas. Gases whose molecules are composed of different types of atoms possess specific adsorption bands in the infra red wavelength range. The concentration of CO_2 is signaled several times per second. An integral over time is created from the series of signals. The integration is proportional to the concentration of the carbon in the sample analyzed. The calibrations allows for any changes to flow arising over time because of such factors such as ageing process, dirt getting into flow regulators, or the dessicants going lumpy, will not automatically necessitate re-calibration, which is a positive factor reducing the frequency of the dessicant replacement. A small amount of the spent catalyst(0.09 – 0.1g) is used for the analysis.

3.1.2 Set-up for catalyst characterization

BELCAT Catalyst analyzer can evaluate catalysis by using the following methods; Temperature Programmed Desorption spectrum measurement (TPD), Temperature Programmed Reaction spectrum measurement (TPReaction), Temperature Programmed Reduction spectrum measurement (TPReduction), Temperature Programmed Oxidation spectrum measurement (TPO), metal dispersion measurement, pulse injection

measurement, and single-point BET method to measure the specific area of sample. You can program BELCAT to automatically do pretreatment of sample, measurement, and calculation.

3.1.2.1 Temperature Programmed Desorption (TPD)

Temperature-Programmed Desorption (TPD) is one of the most widely used and flexible techniques for characterizing the acid sites on oxide surfaces. Determining the quantity and strength of the acid sites on alumina, amorphous silica-alumina, and zeolites is crucial to understanding and predicting the performance of a catalyst.

This method can also be said to be useful for measuring the status of physical adsorption and chemisorptions. It is obtained by measuring desorption or decomposition of adsorbed molecules from the surface while continually supplying heat [31]. By this method, one can determine the number of desorption peaks (type of adsorption sites) from the spectrum of desorbed molecules, desorbed temperature (activation energy of desorption), and volume of desorption (number of adsorption active sites)

There are three types of molecular probes commonly used for characterizing acid sites using TPD

- Ammonia
- Non-reactive vapors
- Reactive vapors

For our experiment, ammonia was adopted as the molecular probes. TPD of ammonia is a widely used method for characterization of site densities in solid acids due to the simplicity of the technique. Ammonia often overestimates the quantity of acid sites. Its small molecular size allows ammonia to penetrate into all pores of the solid where larger molecules commonly found in cracking and hydrocracking reactions only have access to large micropores and mesopores.

Also, ammonia is a very basic molecule which is capable of titrating weak acid sites which may not contribute to the activity of catalysts. The strongly polar adsorbed ammonia is also capable of adsorbing additional ammonia from the gas phase.

3.1.2.2 Temperature Programmable Reduction (TPR)

TPR is the method to measure the characteristics of reduction, and reactivity of adsorbed molecules. They can be determined by measuring the consumption volume of reactive gas.

In order to do TPR measurement, we use the same instrument that was used for TPD measurement without many changes. In TPR, molecules are generally adsorbed by pulse injection method, volumetric method under the vacuum, or flow method. TPR measures the reduction under the H_2 flow during a temperature increase; there are various categories depending on the gas you use and purposes. The measurement varies depending on the condition (ambient pressure, etc), but basically, it is done by the heating under the carrier gas flow. Desorbed gas can be detected by Thermal Conductivity Detector [TCD] or mass analyzer [Q-mass].

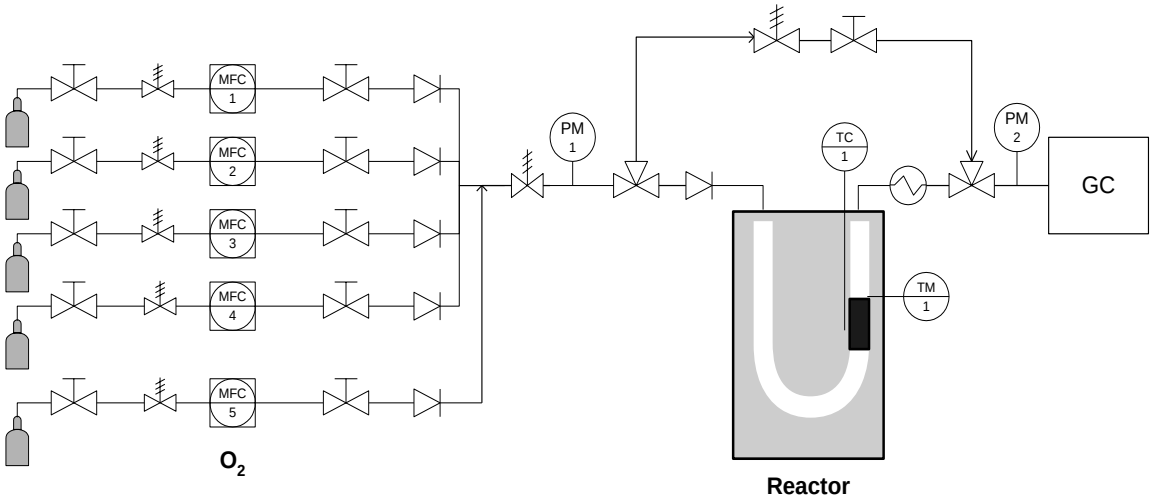

Figure 3.1 Schematic diagram of the BELCAT microreactor experimental set-up

3.1.2.3 Raman Spectroscopy

It is a spectroscopic technique used to observe vibrational, rotational, and other low-frequency modes in a system[32] It relies on inelastic scattering, or Raman scattering, of monochromatic light, usually from a laser in the visible, near infrared, or near ultraviolet range. The laser light interacts with molecular vibrations, phonons or other excitations in the system, resulting in the energy of the laser photons being shifted up or down. The shift in energy gives information about the vibrational modes in the system. Infrared spectroscopy yields similar, but complementary, information.

Typically, a sample is illuminated with a laser beam. Light from the illuminated spot is collected with a lens and sent through a monochromator. Wavelengths close to the laser line due to elastic Rayleigh scattering are filtered out while the rest of the collected light is dispersed onto a detector.

3.1.2.4 SEM/EDX

A SEM is essentially a high magnification microscope, which uses a focused scanned electron beam to produce images of the sample, both top-down and, with the necessary sample preparation, cross-sections. The primary electron beam interacts with the sample in a number of key ways:-

- Primary electrons generate low energy secondary electrons, which tend to emphasize the topographic nature of the specimen.
- Primary electrons can be backscattered which produces images with a high degree of atomic number (Z) contrast.

- Ionized atoms can relax by electron shell-to-shell transitions, which lead to either X-ray emission or Auger electron ejection. The X-rays emitted are characteristic of the elements in the top few μm of the sample and are measured by the EDX detector.

3.2 Experimental Procedure

3.2.1 Materials

The ZSM-5 was procured from Catal International, while the MCM-22 zeolite was obtained from Industrial Chemicals, USA. The Meso-ZSM-5 zeolite having a Si/Al of 30 was obtained from the J. Heyrovsky´ Institute of Physical Chemistry, Czech Republic. It was synthesized using carbon black (CBP 2000, Cabot Corporation) as a secondary template with an average particle diameter of 12 nm [33]. The H-form of catalysts were turned into Na form by repeated ion-exchange with $NaNO_3$ at 60 ^oC for 3 h, filtered, dried and calcined at 550 ^oC for 4 h.

3.2.2 Catalyst Preparation

3.2.2.1 Synthesis of Si-MCM-41 by direct hydrothermal method

MCM-41 was synthesized as follows: 10.6 g of sodium meta silicate (Aldrich) and appropriate amount of chromium nitrate was dissolved in 50 g of water and then thoroughly stirred until a clear solution was obtained. 4.45 g of cetyltrimethylammonium bromide (Aldrich) was dissolved in 30 g of distilled H_2O. The resultant mixture was stirred for 2h, and then the pH of the resulting gel was adjusted to 10.5 with 4N sulfuric

acid followed by stirring for 3 h. The resulting homogenous solution was transferred into an autoclave and heated to 140 ^{o}C in static conditions for 12 h. The solid product was filtered, washed thoroughly using distilled water, dried at 80 oC overnight, then calcined at 550 °C for 6 h to remove the surfactant.

3.2.2.2 Synthesis of Cr-MCM-41(CrM-41) by direct hydrothermal method

10.6 g of sodium meta silicate (Aldrich) and appropriate amount of chromium nitrate was dissolved in 50 g of water and then thoroughly stirred until a clear solution was obtained. 4.45 g of cetyltrimethylammonium bromide (Aldrich) was dissolved in 30 g of distilled H_2O. The resultant mixture was stirred for 2h, and then the pH of the resulting gel was adjusted to 10.5 with 4N sulfuric acid followed by stirring for 3 h. The resulting homogenous solution was transferred into an autoclave and heated to 413K in static conditions for 12 h. The solid product was filtered, washed thoroughly using distilled water, dried at 80 ^{o}C overnight, then calcined at 550 °C for 6 h to remove the surfactant.

3.2.2.3 Synthesis of Cr-V/support (Si-MCM-41 (M-41), Na-MCM-22(M-22), Na-ZSM-5 (Z-5) and mesoporous Na-ZSM-5 (mesoZ-5)) by wet impregnation method:

Cr-V bimetals was impregnated onto support by wet impregnation method. For 1.2wt.% Cr and 2.8wt.% V impregnation over MCM-41(1.2Cr2.8V/M-41), 0.092g of chromium nitrate and 0.064g of ammonium metavanadate was dissolved in 30mL deionized water and then added to 1 g of support. The resulting mixture was stirred, dried overnight at 80 ^{o}C and then calcined at 550 ^{o}C for 4 h (3^{o}C/min).

3.2.3 Catalyst characterization

3.2.3.1 BET surface area and pore size distribution

The textural properties of the synthesized samples were characterized by nitrogen adsorption measurements at 77K using Quantochrome Autosorb1-c adsorption analyzer. Samples were outgassed at 220°C under vacuum (10^{-5} Torr.) for 3h before nitrogen physisorption. The BET specific surface areas were determined from the adsorption data in the relative pressure (P/P_0) range from 0.06-0.2, assuming a value of 0.164nm^2 for the cross section of the nitrogen molecule. The pore size distribution was calculated from the adsorption branch using the Barrett-Joyner-Halenda (BJH) method.

3.2.3.2 Atomic adsorption

The chemical compositions of the synthesized catalysts were determined by the atomic adsorption spectroscopy Perkin-Elmer equipment of model AAnalyst 100 using a mixed gas of acetylene-N_2O-air.

3.2.3.3 X-ray diffraction

The Powder X-ray diffraction (XRD) was recorded on Rigaku Miniflex II system using nickel filtered CuKα radiation λ = 1.5406 Å at 40 kV and 30 mA. The diffraction patterns were identified through comparison with those included in the Joint Committee of Powder Diffraction Standards (JCPDS) literatures and database.

3.2.3.4 Pyridine Fourier Transform Infra Red Spectroscopy

The acidity of the zeolites was measured using a Nicolet 6700 FT-IR spectrophotometer (Thermo Scientific) equipped with a high temperature vacuum chamber using pyridine as a probe. The sample (50 mg) was pressed and placed in a sample holder for pretreatment at 400 °C under vacuum for 1 h. The sample was then cooled and the spectrum was recorded. After pyridine adsorption, the sample was heated at 150 °C, 250 °C and 400 °C under vacuum (10^{-5} mbar) for 30 min. The removed material was then cooled to room temperature and then the spectrum was recorded again. The acidity was calculated using the extinction coefficient (0.75) of the bands of pyridine adsorbed Brönsted and Lewis acid sites.

3.2.3.5 Raman Spectroscopy

Raman spectroscopy of catalysts was recorded at ambient conditions on a Bruker Senterra in a frequency range of 65 – 4000 cm^{-1} with a resolution of 9 – 13 cm^{-1}. A laser wavelength of 532 cm^{-1} with 10 mW power was used for zeolite supported catalysts.

3.2.3.6 SEM-EDX

The morphological characterization and elemental composition of the catalyst was carried by SEM on a JEOL JSM 5600LV instrument coupled with an EDX analyser.

3.2.3.7 Temperature Programmable Analysis (TPx)

TPR and TPD (temperature-programmed reduction and ammonia or CO_2 desorption) experiments were performed in BEL-CAT-A-200, chemisorption apparatus that consists

of a gas mixing unit allowing both continuous and pulsed reactant dosing, U-tube quartz microreactor with a thermocouple placed inside the sample, and a thermal conductivity detector (TCD). The linearity of the TCD response was proven by the injection of gas pulses of various known compositions, and the quantitative hydrogen consumption was calibrated in every measurement by a series of calibration gas pulses. TPR analysis was performed using Ar/H_2 gas mixture (95/5 vol%). The total flow rate of the feed was 50 ml/min. Before the experiment, the sample (50mg) was preheated in He at 300 ^oC for 3 hr, and then cooled to room temperature. The sample was heated at 10 $^oC\ min^{-1}$ to the final temperature of 700 ^oC. The H_2 consumption was measured by a thermal conductivity detector and CuO was used as a reference for the calibration of H_2 consumption. Temperature programmed ammonia (NH_3-TPD) was carried out on the same instrument. The sample (50mg) was pretreated in a flow of He (50 mL/min) at 500 ^oC for 1 h. Then the sample was exposed to He/NH_3 mixture (95/5 vol%) or He/CO_2 (95/5 vol%) at room temperature for 30 min. The gas phase was removed by He purging for 1 h followed by which TPD was performed in He flow (50 mL/min) at a heating rate of 10 ^oC/min, and the desorbed NH_3 or CO_2 was monitored by a TCD detector.

3.3 Catalyst Evaluation

n-Butane dehydrogenation was carried out over synthesized Cr and/or V catalysts wet impregnated on the following zeolites supports: MCM-41, MCM-22, ZSM-5, meso-ZSM-5 in order to test their catalytic activity. These catalysts were evaluated for their reactivity at reactions temperature 525, 550, 575 and 600 °C. From reaction temperatures 525-600 C, the activity of the first 30 min were tested while at 550C reaction

temperature, the catalyst was tested for 3h in order to establish their stability at steady state.

3.3.1 Testing Procedure

The catalytic runs were carried out in a fully integrated, fixed bed continuous flow reactor system (BELCAT). The system consists of one tubular quartz reactor attached with stainless steel one-zone furnace assembly through reactor furnace wall thermo well. The catalysts sample (0.15g) was packed in the reactor and activated with flowing N_2 at 823 K for 2 h. In the case of the oxidative dehydrogenation reactions, the flow rate of reactant (*n*-butane and CO_2) and the diluents N_2 was maintained at 4.0 ml/min, 40 ml/min and 56 ml/min, respectively while for the simple dehydrogenation reactions (non-oxidative) the flow rate of reactant (*n*-butane) and the diluents N_2 was maintained at 4.0 ml/min, 96 ml/min. The gas product samples were analyzed by online gas chromatograph (Agilent, 7890N) equipped with J&W Scientfic HP-5 capillary column (length: 30 m, ID: 0.32 mm, and film thickness 0.25 μm) and FID detector. The gas products, including H_2, CO and CO_2, were analyzed with a TCD and a GS-GASPRO capillary column. The products were identified by comparison with authentic samples.

The term gas hourly space velocity (GHSV) is the inverse of contact time (τ) and is defined as the mass flow rate of *n*-butane in g/min over the weight of the catalyst. The contact times were varied by changing the partial pressure of *n*-butane in the mixed gas containing n-butane and nitrogen while keeping the catalyst weight fixed.

$$\tau = \frac{1}{GHSV}\left(\frac{g_{cat}min}{g_{butane}}\right)$$

GC analyzed data were further processed to evaluate conversion and selectivity using the following equations:

$$\textit{Conversion of n-butane} = \frac{moles\ of\ n{-}butane\ converted}{moles\ of\ butane\ fed} \times 100\% \quad (3.1)$$

$$\textit{Selectivity of product } i = \frac{moles\ of\ product\ i}{butane\ conversion} \times 100\% \quad (3.2)$$

The yield to product i is expressed as follows:

$$Yield\ to\ product\ i = \frac{selectivity\ of\ product\ i}{butane\ conversion} \quad (3.3)$$

To ascertain the reaction stoichiometry, the molar selectivities were estimated with the equation:

$$S_i^{molar} = \frac{weight\ fraction\ of\ product\ i}{molecular\ weight\ of\ product\ i} \times molecular\ weight\ of\ butane \quad (3.4)$$

3.4 Reactor product analysis

3.4.1 GC Calibration

The calibration of the gas chromatograph used in determining the product stream composition of n-butane dehydrogenation reaction was done as explained in the sub-header below.

3.4.1.1 Determination of Retention Time

The retention times of all compounds of interest in this study were determined by analyzing pure samples of each of the compounds in GC in turns. The retention times were used to identify each component of the reaction products.

3.4.1.2 Correlating GC Response and Actual Weight% of Each Compound

In calibrating the GC, standard samples of different compositions containing n-butane, main reaction products (1-butene, cis-2-butene, trans-2-butene, 1,3 butadiene) and cracked products (methane, ethane, ethene, propane, propene) were prepared. The composition of the prepared samples were carefully chosen to reflect all possible product compositions (obtained from preliminary experimental runs) under different reaction conditions to be investigated. 0.2µL of the first sample was then injected into the GC and the GC response (area %) for each of the components in the sample were obtained. This procedure was repeated for all other samples.

3.5 Coke Analysis

The amount of coke deposited on the spent catalysts was determined by the combustion principle of the carbon analyzer multi EA 2000. A small amount of the spent catalyst (100mg) was weighed into a combustion boat and fed completely into a hot zone of the furnace, oxygen is fed directly into the unit and the coke deposited on the spent catalyst is completely burnt, converting the carbonaceous deposit into carbon dioxide. The amount of coke formed is determined by measuring the number of moles of CO_2 released. This technique however cannot be used to determine the nature of coke formed.

CHAPTER 4

RESULTS & DISCUSSIONS

4.1 *n*-Butane dehydrogenation over mono and bimetallic MCM-41 catalysts under nitrogen atmosphere.

4.1.1 Characterization

4.1.1.1 X-ray Diffraction

The X-ray diffraction patterns for impregnated samples (3.5Cr/M-41, 3.8V/M-41, 1.2Cr2.8V/M-41, 2Cr2V/M-41, 2.7Cr1.2V/M-41) and hydrothermally synthesized Cr-M-41 (Si/Cr = 50) are shown in Figure 4.1(a-f). CrM-41 showed characteristics XRD diffraction patterns indexed to hexagonal symmetry [34] (Figure 1(a)). But apart from intense (100) peak, a significant reduction in the higher order peaks occurs indicating a decreased structural ordering of mesostructure. The d-spacing of CrM-41 decreased to 3.29 nm compared to 3.67 nm of SiMCM-41. In general, the incorporation of Cr^{3+} (0.76 A°) into the silicate framework is expected to increase lattice parameter. However, in the case of Cr substituted MCM-41 sample, the d-spacing was found to be less similar to the observation of Kevan et al. [35].

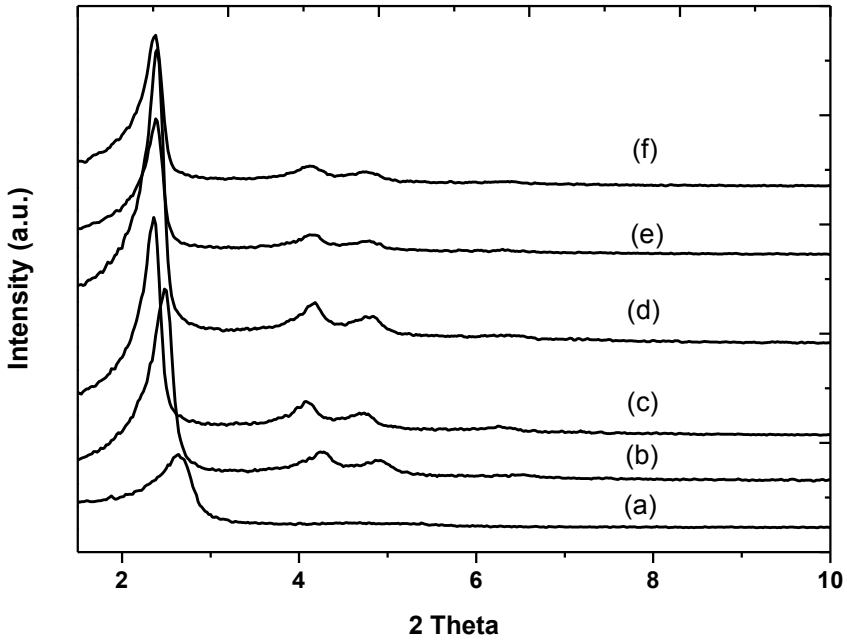

Figure 4.1. X-ray diffraction analysis of CrM-41, Cr or V and Cr-V impregnated MCM-41: (a) CrM-41 (Si/Cr = 50), (b) 3.5Cr/M-41 (c) 3.8V/M-41, (d) 1.2Cr2.8V/M-41, (e)2.0Cr2.0V/M-41, and (f) 2.7Cr1.2V/M-41.

indicating less incorporation of chromium into MCM-41 framework. Overall, the impregnated samples showed high orderedness irrespective of such high metal loadings. The samples showed well resolved three diffraction lines at 2θ range of 2.4, 4.2, 4.8 indexed to (100), (110) and (111) peaks corresponding to hexagonal symmetry (Figure 1(b-f)). Comparatively, 3.8V/M-41 showed the highest d-spacing at 3.74 nm, while 3.5Cr/M-41 showed lowest d-spacing at 3.53 nm. Such increase after vanadium impregnation is usually attributed to incorporation of vanadium to certain degree in the lattice position due to its longer V-O bond length (~1.58 Å) compared with Si-O bond length (~1.50 Å) [36]. In the case of bimetal impregnated samples such as 1.2Cr2.8VM-41 and 2Cr2V/M-41 (Figure 4.1(d and e)), the d-spacing remained at 3.67 nm similar to that of SiMCM-41, which then decreased to 3.61 with Cr content of 2.7wt.% and vanadium content of 1.2 wt.% (2.7Cr1.2V/M-41). Klinowski et al. [37] observed that such a decrease occurs due to difference in the condensation of silicate polyanions and metallosilicate polyanions. The absence of crystalline α-Cr_2O_3 and V_2O_5 between 2θ range 10-50^o shows the highly disbursed metal oxide phase over the support.

Table 4.1 Physico-chemical properties of Cr or V and Cr-V supported MCM-41 catalysts

Catalyst	Metal content (wt.%)		$d_{spacing}$ (A^o)	Surface area (m^2/g)	Pore volume (cc/g)	Pore diameter (nm)
	Cr	V				
SiMCM-41	-	-	36.78	1229	0.81	2.6
Cr-M-41(Si/Cr = 50)	1.5	-	32.93	577	0.39	2.7
3.5Cr/M-41	3.5	-	35.31	946	0.57	2.4
3.8V/M-41	3.8	-	37.40	939	0.61	2.6
1.2Cr2.8V/M-41	1.2	2.8	36.78	1079	0.66	2.5
2Cr2V//M-41	2.0	2.0	36.78	959	0.59	2.5
2.7Cr1.2V//M-41	2.7	1.2	36.17	866	0.63	2.9

4.1.1.2 Nitrogen adsorption isotherms

The textural characteristics of CrM-41, mono and bimetal impregnated MCM-41 samples are presented in Table 1. All samples showed characteristic type IV isotherms typical to that of siliceous MCM-41(Figure 4.2(a-f)). Hydrothermally synthesized Cr-M-41 showed a less sharp inflection at P/P_0 range between 0.2-0.3 indicating a slight decrease in textural characteristic after chromium incorporation (Figure 4.2(a)). The surface area reduced considerably at 577 m^2/g compared with Si-MCM-41 (1229 m^2/g), while pore volume decreased from 0.81 cc/g to 0.39 cc/g. Jha et al. [38] attributed such a trend to the presence of large amount of chromium species outside the framework of MCM-41. In the case of impregnated samples, a sharp inflection can be observed reflecting uniform mesopore size distribution (Figure 4.2(b-f). When compared with SiMCM-41, only a slight decrease in the surface area and pore volume is observed (Table 4.1). 1.2Cr2.8V/M-41 showed the highest surface area of 1079 m^2/g and pore volume of 0.66 cc/g. The pore size distribution curves of all samples as calculated by BJH method are centered in the range 2.4-2.9 nm.

4.1.1.3 Temperature Programmed Reduction

In ODH of alkanes over transition metal oxides supported catalysts, the reaction proceeds via redox mechanism, in which the reducibility is a key factor for the catalyst activity [39]. XRD is a relatively known to be an insensitive method for the detection of crystallites [40]. Therefore, the materials were characterized by H_2-TPR. Figure 4.3(a-f)

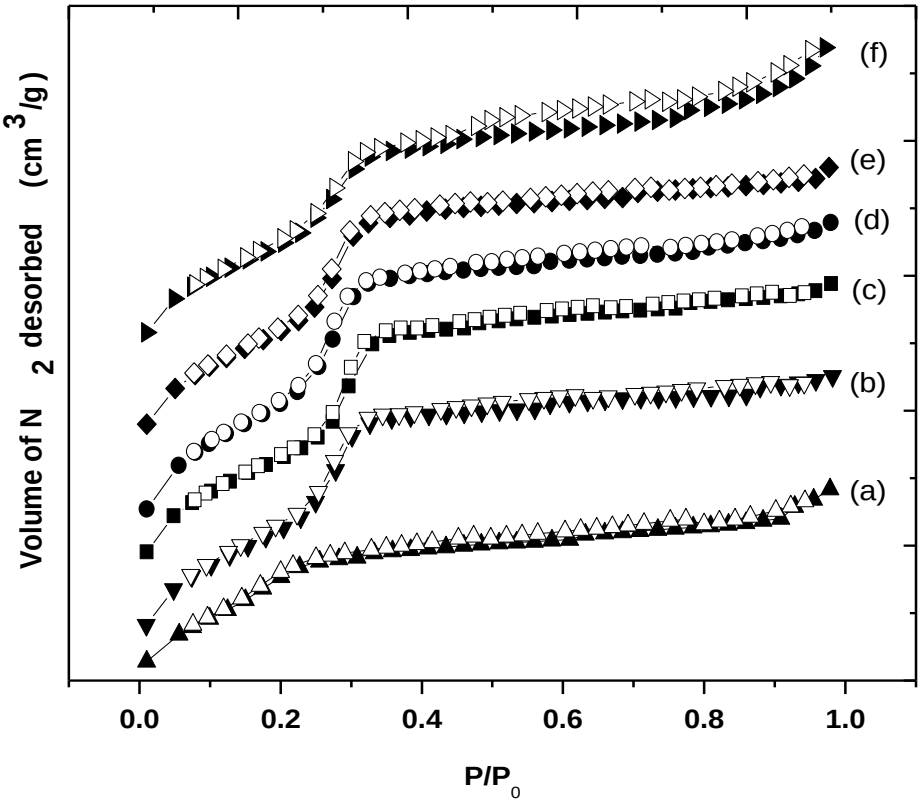

Figure 4.2 N_2 adsorption isotherm of CrM-41, Cr or V and Cr-V impregnated MCM-41: (a) CrMCM-41 (Si/Cr = 50), (b) 3.5Cr/M-41 (c) 3.8V/M-41, (d) 1.2Cr2.8V/M-41, (e)2.0Cr2.0V/M-41, and (f) 2.7Cr1.2V/M-41.

shows the reducibility of Cr, V or Cr-V impregnated MCM-41 support. The TPR results are presented in Table 4.2. A significant difference in the reducibility is observed between the mono or bimetallic supported system. CrM-41 showed a sharp reduction peak at the temperature around 444 ^{o}C. This peak can be attributed to the reduction of Cr^{6+} species [41]. In the case of 3.5Cr/M-41, two reduction peaks are observed at 354 and 435 ^{o}C, respectively. Ellison et al. [42] attributed such peaks to CrO_3 clusters with smaller interaction over the silica support. However, the H_2 consumption was found to be smaller than for other samples. In the case of 3.8V/M-41, two reduction peaks are observed around 535 and 617 ^{o}C, respectively. The reduction peak maxima between 500-550 ^{o}C is attributed to the reduction of surface V^{5+} species to surface V^{3+} species [43, 44, 45 and 46]]. The presence of a less intense peak between 580 and 630 ^{o}C for 3.8V/M-41 is attributed to the reduction of polymeric and bulk vanadia species [47]. In the case of bimetal loading, for 1.2Cr2.8V/M-41 sample, a shift in the onset of reduction peak towards lower temperature between 335 and 520 ^{o}C compared to 3.8V/M-41 indicating more reducible species due to the Cr-V oxide interaction leading to mixed oxide phase over the support. A small reduction peaks at 431 ^{o}C and a distinct reduction band at 457 ^{o}C were observed. Gasper et al. [48] ascribed such reduction to Cr^{6+} species that is interacted at different locations over the silica support. The presence of high temperature peak at 497 ^{o}C, which extends up to 540 ^{o}C can be due to monomeric or low oligomeric surface dispersed tetrahedral species [49, 50].

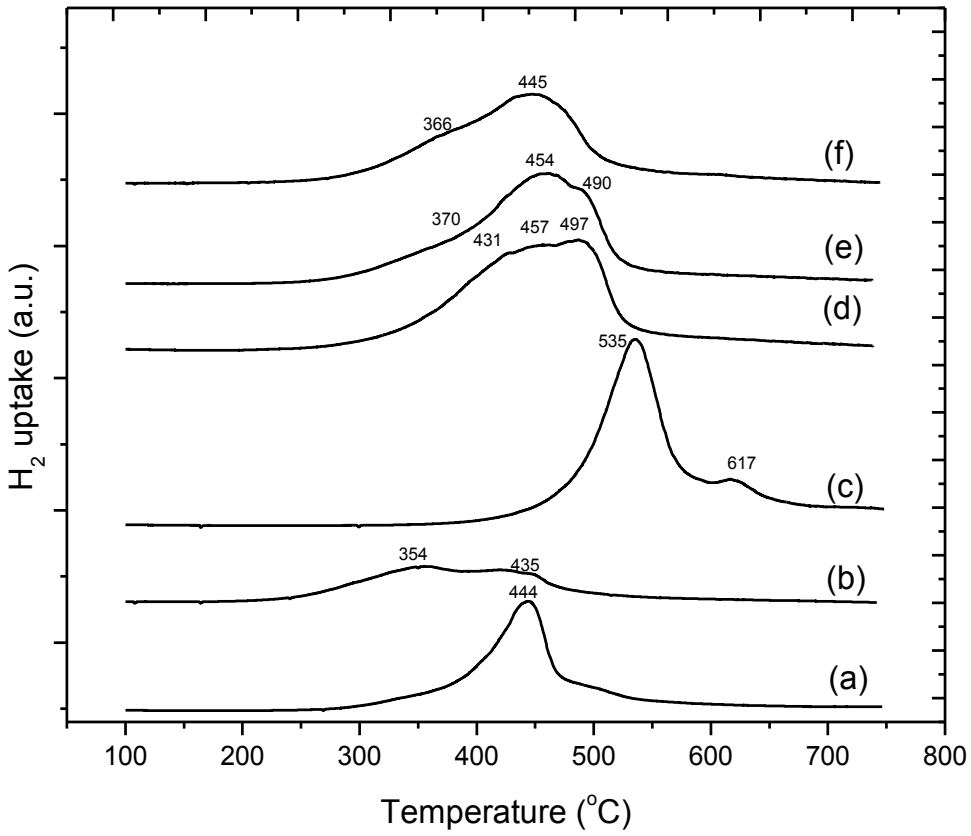

Figure 4.3 H_2-TPR profile of CrM-41, Cr or V and Cr-V impregnated MCM-41: (a) CrMCM-41 (Si/Cr = 50), (b) 3.5Cr/M-41 (c) 3.8V/M-41, (d) 1.2Cr2.8V/M-41, (e)2.0Cr2.0V/M-41, and (f) 2.7Cr1.2V/M-41.

Table 4.2. Temperature programmed analysis (H_2-TPR and NH_3-TPD) of Cr or V and Cr-V supported MCM-41 catalysts.

Catalyst	TPR	TPD	
	T_M (^oC)	H_2uptake (mmol/g)	Total acidity (mmol NH_3/g)
SiMCM-41	-	-	0.071
Cr-M-41(Si/Cr = 50)	444	0.385	0.087
3.5Cr/M-41	354, 435	0.285	0.323
3.8V/M-41	535, 617	0.655	0.319
1.2Cr2.8V/M-41	431, 457,497	0.790	0.533
2.0Cr2.0V//M-41	370,454, 490	0.605	0.410
2.7Cr1.2V//M-41	366, 445	0.495	0.539

Thus it can be pointed out that the VOx species in the presence of CrOx species tends to inhibit the agglomerization of vanadia species and hence the formation of bulk-like vanadia species becomes less prominent. The peaks at 366 and 445 ^{o}C became dominant for the samples 2Cr2V/M-41 and 2.7Cr1.2V/M-41 with increasing chromium content indicating the formation of polychromates. Airaksinen et al. [51] observed that such polychromates species on the chromia/alumina sample are more reducible than monochromates species. The H_2 consumptions (mmol/g) were in the following order: 1.2Cr2.8V/M-41 > 3.8V/M-41 (0.655) > 2.0Cr2.0V/M-41 (0.605) > 2.7Cr1.2V/M-41 (0.495) > CrM-41 (0.385) > 3.5Cr/M-41 (0.285), respectively. The depreciation of H_2 consumption with high Cr loading indicates increasing Cr–V oxide interactions, which may lead to the formation of mixed oxide phases and, therefore, may inhibit the thermal decomposition of chromium species in oxidation states VI and/or V during calcination [52, 53].

4.1.1.4 Temperature Programmed Desorption

Particular, in the case of monometallic Cr or V impregnation, a major desorption peak appear between 100-220 ^{o}C indicating an increased acid amount of weak acidity. This is reflected in the overall concentration of acid sites of bimetallic Cr-V impregnated MCM-41 (Table 4.2). Santamaria-Gonzalez et al. [55] attributed such a rise due to the enhancement of acid strength of silanol groups caused by the strong interaction with metal oxides. The amount of ammonia consumed in the samples is as follows: 1.2Cr2.8V/M-41 ~ 2.7Cr1.2V/M-41 > 2Cr2V/M-41 > 3.5Cr/M-41 ~ 3.8V/M-41 > CrM-41 > SiMCM-41. The increased surface acidity shows the stronger interaction of mixed oxides over support than that of the mono metal oxide supported catalysts. Raju et al.

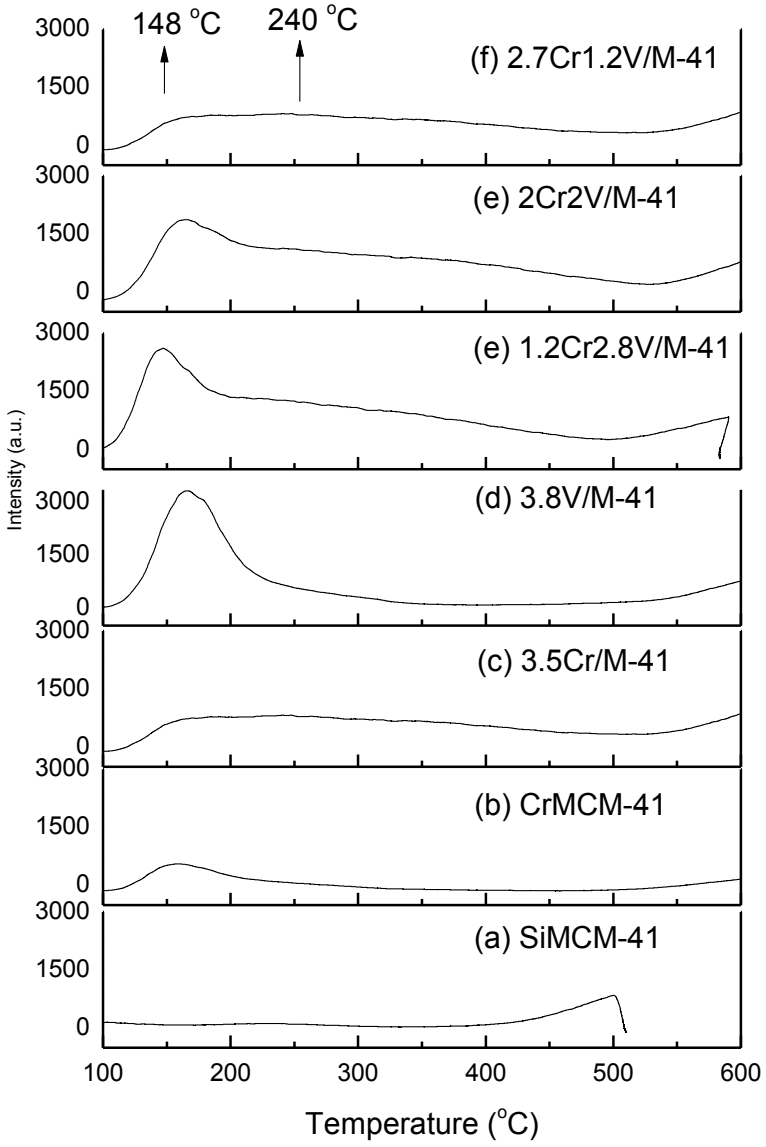

Figure 4.4 NH_3-TPD of SiMCM-41, CrM-41 and different weight percentage Cr or V and Cr-V impregnatedMCM-41.

[56] indicated that such type of increased acidity to the existence of synergistic effect between the metal oxides.

4.1.2 Dehydrogenation of n-butane

The catalyst performances are as shown in Figure 4.5. The dehydrogenation of n-butane was carried out in the presence of nitrogen at 550°C over V/M-41, Cr/M-41 and Cr-V/M-41 catalysts with different metal loadings. The flow rate of n-butane was 4ml/min while nitrogen flow rate was 96ml/min, and the catalyst loading was 0.15g. The major reaction products observed were methane, ethane, ethylene, propane, propene, isobutene, t-2-butene, 1-butene, isobutylene, cis-2-butene, and 1,3-butadiene. CrO_x and VO_x based mesoporous catalysts have been proposed to be catalytically active in the dehydrogenation of light alkanes [8, 57]. The main factors affecting the selectivity are reported to be the metal content, nature of the support (structure, acidity) and the reactions temperature [58]. In agreement with this report, hydrothermally synthesized CrM-41 (Si/Cr molar ratio 50) exhibited a low dehydrogenation activity as well as a low selectivity. The dehydrogenation selectivity was 81%, for the n-butane conversion of 3.74 % at 10 min. It indicates that in butane dehydrogenation, in addition to dispersion, a high metal loading higher than 1.5wt.% and large surface area is significant for high dehydrogenation activity. 3.8V/M-41 shows a better stability than 3.5Cr/M-41 even though the first 10min initial activity of 3.5Cr/M-41 was better (9.2% conversion, compared with 6.0% conversion for 3.8V/M-41). The selectivity to butenes of 3.8V/M-41 was slightly better. However, it is interesting to observe that the catalysts modified with bimetals over MCM-41 shows an enhanced dehydrogenation activity. The impregnation

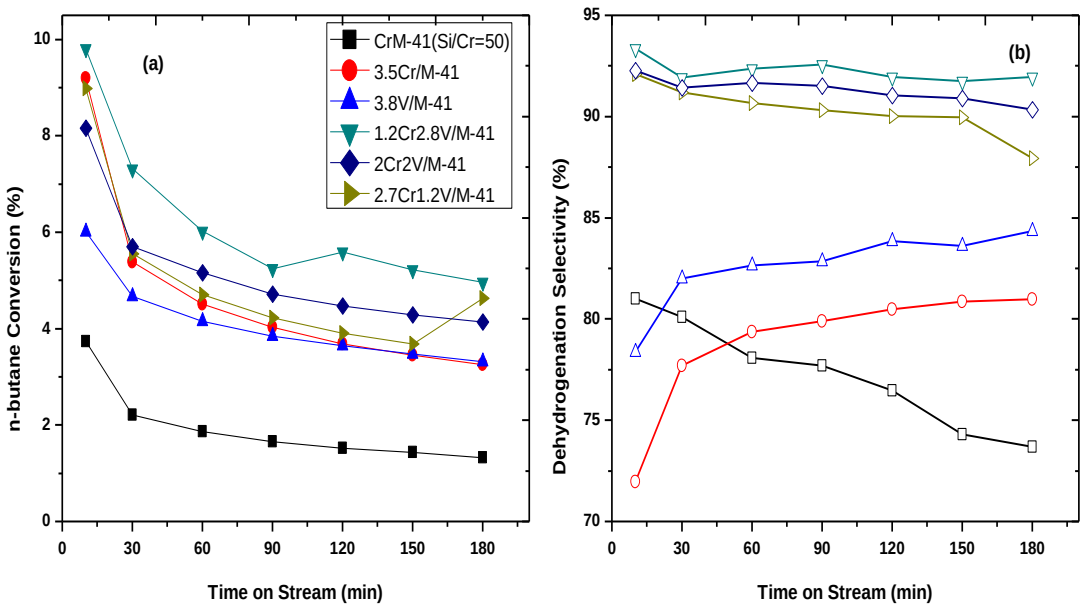

Figure 4.5. Simple dehydrogenation activity of Cr or V and Cr-V supported MCM41 against the time on stream in N_2 atmosphere at 550°C.

of 1.2wt.% Cr and 2.8 wt.% V over MCM-41 (1.2Cr2.8V/M-41) significantly affects the conversion of butane and butenes selectivity. The maximum conversion was 9.8% at 10 min of reaction time, whereas the selectivity to butenes improved sharply and remains above 90% through the course of entire reaction time. The oxidative dehydrogenation reaction is postulated to occur through a redox cycle, where the catalysts lattice oxygen takes part in the oxidation reaction, and then the reduced catalyst is re-oxidized following a Mars-van Krevelen mechanism [59]. Ruettinger et al. [60] shows that an isolated V=O groups are active sites in the ODH reaction. The VOx species with higher degree of polymerization participate in undesired consecutive reactions with ODH products [13]. The improved results of bimetal impregnated MCM-41 samples can be explained to the synergetic effect of active metals (VOx and/or CrOx species), which according to the results of XRD and TPR, are well dispersed on the surface of mesoporous support. An intermediate reduction temperature between 300 and 520 ^{o}C of the Cr-V/M-41 catalyst determined by TPR than that of Cr and V based MCM-41 catalyst supports the correlation between the higher activity and easier reducibility of the Cr-V/M-41 catalyst. Karamullaoglu and Dogu [59] correlated the activity of Cr-O and Cr-V-O in oxidative dehydrogenation of ethane with the reduction temperature as determined from the TPR data. The Cr-O catalyst showed activity at temperatures over 225 °C, whereas the Cr-V mixed oxide catalyst showed activities at much higher temperatures over 400 °C. In the present study, TPR result of mixed oxides showed an intermediate reduction at about 366 and 490 °C, respectively (Figure 4.3(d-f). The absence of the high temperature reduction peak shows a well dispersed monomeric VO_X species. The observed activity and the TPR result indicate the strong correlation between facile reducibility and the activation

temperature of the catalyst. Thus the bimetallic supported catalysts were found to be most reactive due to its higher reducibility, thus providing additional sites for oxygen activation.

Figure 4.6 shows the influence of total acidity on the yield of butenes over CrM-41, Cr or V and Cr-V impregnated MCM-41 for the reaction time of 10 min at 550°C. The total number of acid sites of Cr-V impregnated MCM-41 samples increases linearly with increased vanadium addition and it has a direct effect on the increase the yield of butenes (Figure 4.6). The order of the amount of ammonia consumed in the samples is as follows: 1.2Cr2.8V/M-41 ~ 2.7Cr1.2V/M-41 > 2Cr2V/M-41 > 3.5Cr/M-41 ~ 3.8V/M-41 > CrM-41 > SiMCM-41. This increase in weak acid sites with increasing vanadium content could probably be due to the increased concentration of surface-isolated tetrahedral vanadium species [61, 62, and 63]. In particular, 1.2Cr2.8V/M-41 showed a high total acidity indicating the presence of large fraction of exposed active V sites. The yield of butenes versus total acidity over CrM-41, Cr or V and Cr-V impregnated MCM-41 measured at the reaction time of 10 min at 550°C are in the following order: 1.2Cr2.8V/M-41 > 2.7Cr1.2V/M-41 > 2.0Cr2.0V/M-41 > 3.5Cr/M-41 > 3.8V/M-41 > CrM-41 > SiMCM-41, respectively. The selectivity to dehydrogenation products over Cr-V-O based MCM-41 can be related to the acid-base character of the catalysts. It has been reported that presence of VOx species favor dehydrogenation, while vanadia over layer or V_2O_5 crystallites play detrimental role by favoring coke formations [11]. The observed high conversion of 1.2Cr2.8V/M-41 followed by 2.7Cr1.2V/M-41 and 2.0Cr2.0V/M-41

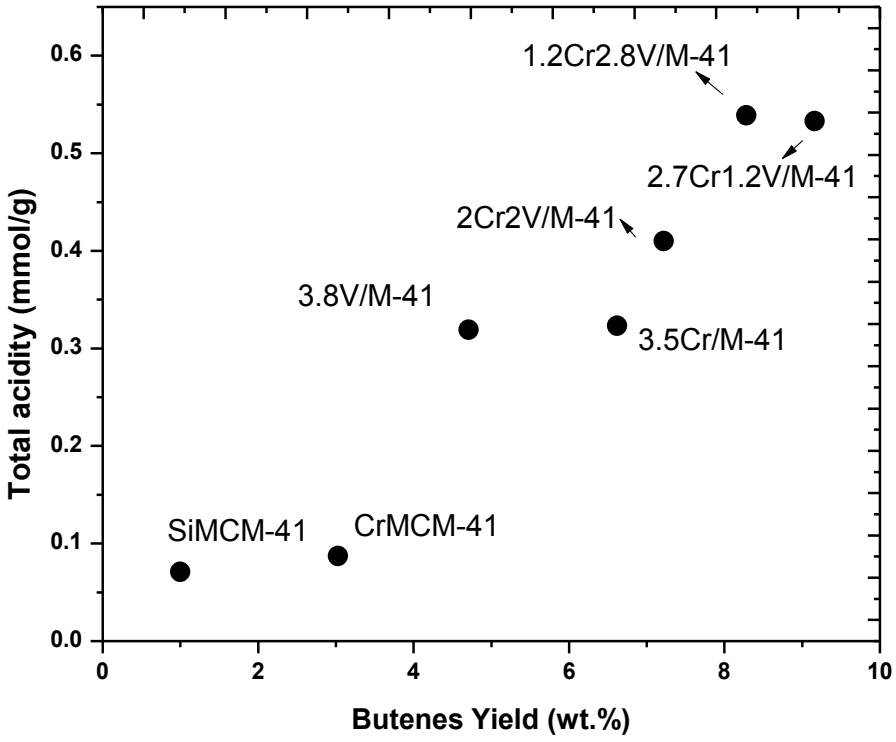

Figure 4.6. The influence of acid sites on the yield of butenes over CrM-41, Cr or V and Cr-V impregnated MCM-41 at the reaction time of 10 min at 550°C.

shows the presence of dispersed CrO_x and VOx species that play an important role for the formation of key intermediate species. The obtained results coincide with the report of Le Bars et al., [64], where they showed a linear relation between conversion rate of ethane and acid surface character of V/SiO_2 catalyst in the ODH of ethane.

Figure 4.7 presents the dependence of conversion and selectivity to butylenes on the reaction temperature over 1.2Cr2.8V/M-41catalyst in the nitrogen atmosphere. It can be observed that an increase of the reaction temperature from 525-600°C resulted in a significant increase in n-butane conversion, but at the expense of butenes selectivity. The conversion improved from 6.12% to 20.12%, while the dehydrogenation selectivity (trans 2-butene, 1-butene, cis 2-butene, isobutylene, 1,3-butadiene) decreased from 94.7% to 88.5% within the temperature range of 525-600°C. The cracked products include light hydrocarbons like methane, ethane, ethene, propane and propene that occur at high temperatures. The absence of aromatic and heavier products suggests that cracking occurs through monomolecular mechanism [65]. The initial step of cracking on zeolite has been considered to be a protonation followed by cracking in three paths: (1) to hydrogen and butene; (2) to methane and propylene; (3) to ethane and ethylene [66]. Narbeshuber [67] attributed the formation of ethene occurs due to secondary cracking of butene isomers via primary carbenium ion formation. The present results with 1.2Cr2.8V/M-41 catalyst are quite similar to dehydrogenation over ZSM-5 based catalyst [68]. The cracking pathways: methane and propene,

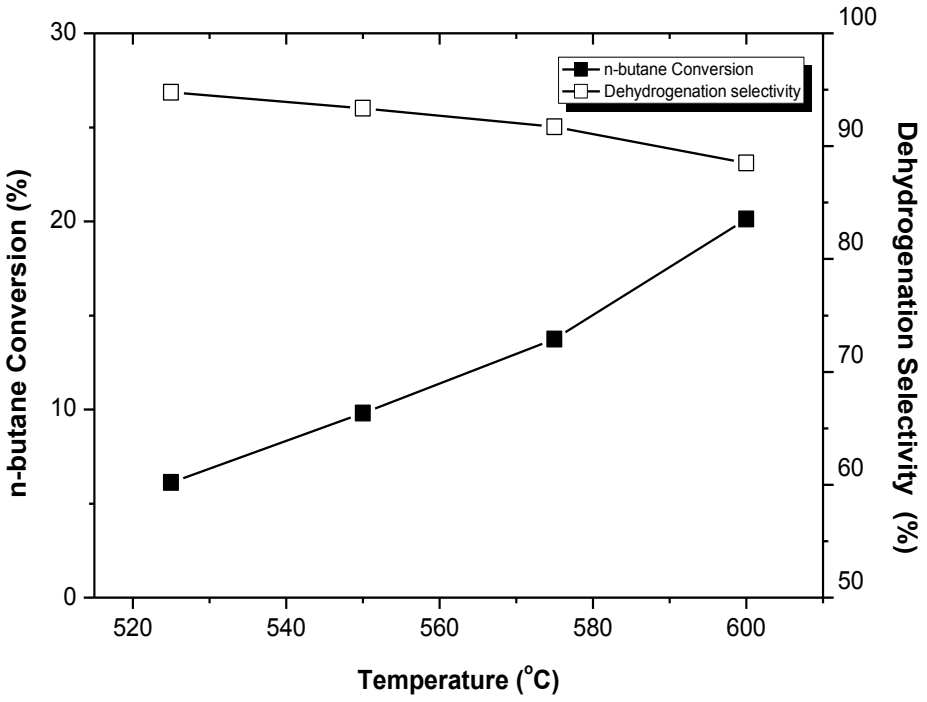

Figure 4.7. Dehydrogenation activity of 1.2Cr2.8V/M-41 with respect to n-butane conversion (■) and butenes selectivity (□) at 525-600°C.

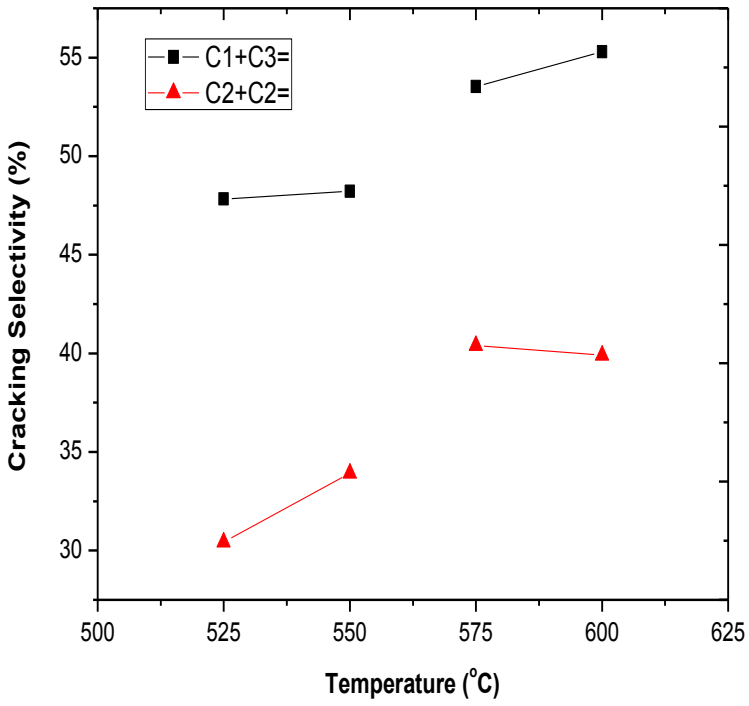

Figure 4.8. Cracking selectivity of 1.2Cr2.8V/M-41 catalysts in n-butane dehydrogenation at 525-600°C.

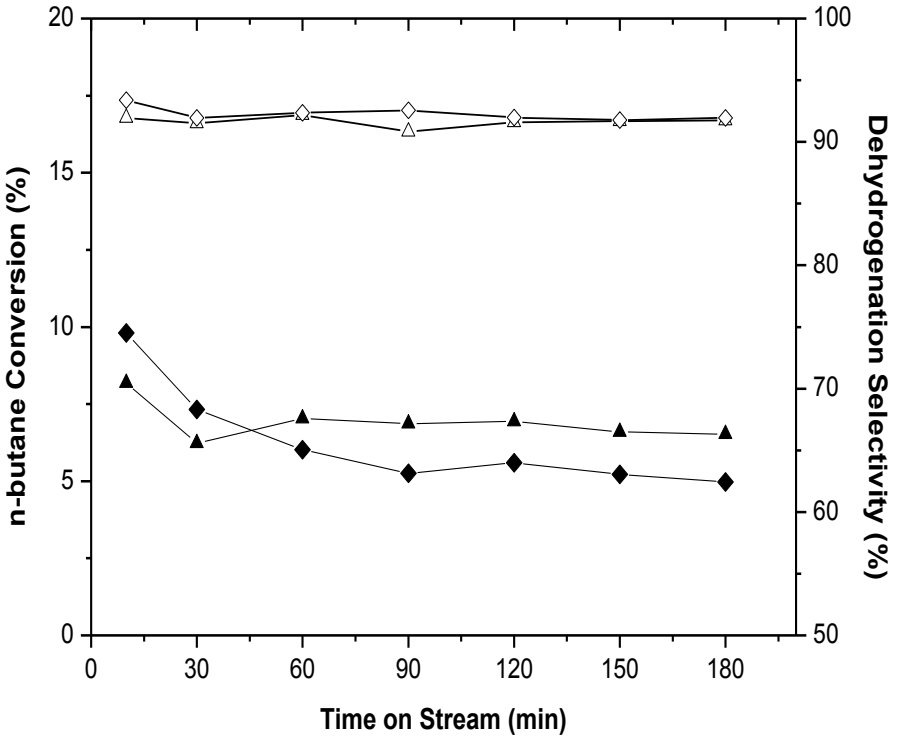

Figure 4.9. Dehydrogenation activity of 1.2Cr2.8V/M-41 with respect to n-butane conversion in N_2 (♦) and CO_2 (▲) and butenes selectivity in N_2 (◊) and CO_2 (Δ) at 550°C for 180 min.

ethane and ethene increases with reaction temperature indicating lower energy activation for dehydrogenation than cracking (Figure 4.8).

Figure 4.9 shows the activity of 1.2Cr2.8V/M-41 in ODH of n-butane in CO_2 or nitrogen atmosphere at an operating temperature of 550°C. The flow rate of the reactant mixture (n-butane/nitrogen/CO_2 was 4:56:40) was 100 ml/min, respectively, while the catalyst loading was 0.15g. In the presence of CO_2, the catalyst showed 6% n-butane conversion with dehydrogenation selectivity above 90% for the duration of 180 min. However, in the case of N_2, though the initial conversion was high at 10%, during the course of reaction time, the conversion fell below 5% indicating rapid deactivation. This result shows that CO_2 can be regarded as a good promoter in butane dehydrogenation. Michorczyk et al., [50] reported similar positive effect in propane dehydrogenation, where the selectivity to propylene was maintained above 80%.

4.2 Oxidative dehydrogenation of *n*-butane over 1.2Cr2.8V/MCM-41, 1.2Cr2.8V/MCM-22, 1.2Cr2.8V/ZSM-5 and 1.2Cr2.8V/mesoZSM-5 with CO_2 as mild oxidant

4.2.1 Characterization

4.2.1.1 X-ray diffraction and nitrogen physisorption analysis:

The X-ray diffraction patterns for impregnated samples are shown in Figure 4.10(a-d). 1.2Cr2.8V/M-41 sample showed a well resolved four diffraction lines at 2θ range of 2.3, 4.2, 4.8 and 6.3 indexed to (100), (110), (200) and (210) peaks corresponding to hexagonal symmetry indicating well ordered mesoporous support (Figure 4.10(a). The XRD pattern for 1.2Cr2.8V/M-22 exhibited sharp crystalline peaks typical to that of the parent MCM-22 with MWW structure (Figure (4.10b)). The XRD patterns of conventional and mesoZ-5-supported chromium and vanadium oxide catalysts evidently exhibited the characteristic reflections of the MFI topology (Figure 4.10 (c and d)). The intensity of the diffraction peaks of mesoZ-5 catalyst is lower than that of Z-5, showing that the former has a slightly lower crystallinity. The absence of crystalline α-Cr_2O_3 and V_2O_5 between 2θ range 10-50^o for all the samples show considerable dispersity of metal

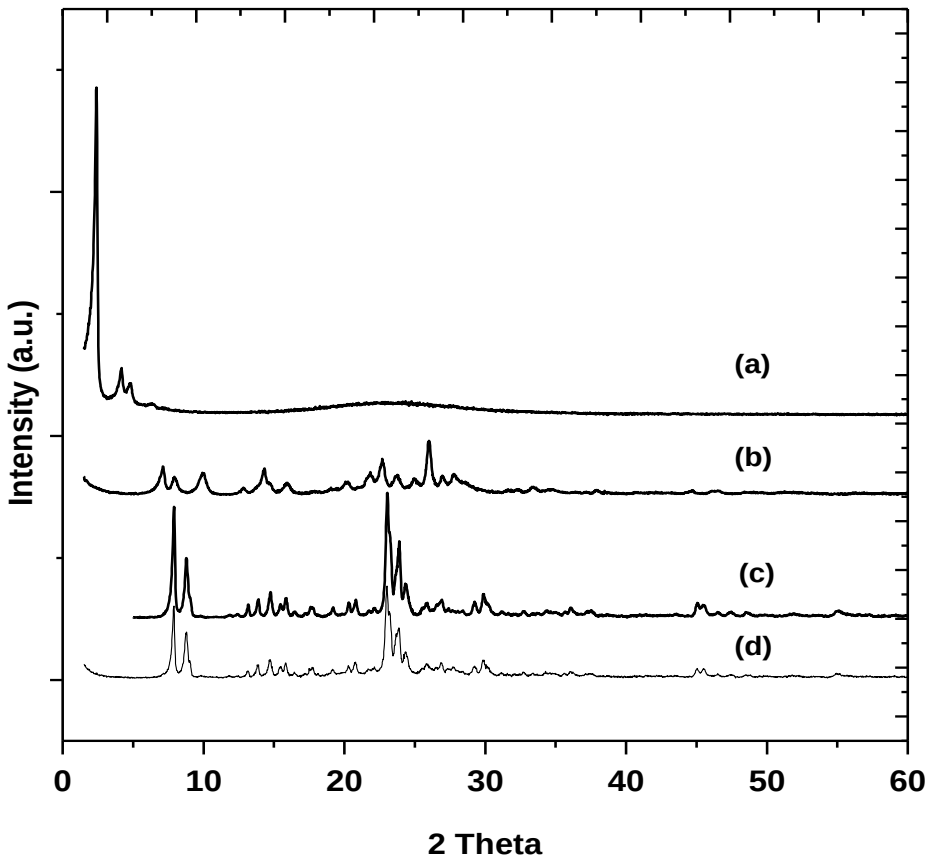

Fig.4.10. XRD profile for (a) 1.2Cr2.8V/M-41 (b) 1.2Cr2.8V/M-22 (c) 1.2Cr2.8V/Z-5 and (d) 1.2Cr2.8V /mesoZ-5.

Table 4.3. Physico-chemical properties of Cr-V supported catalysts.

Catalyst	Si/Al ratio	Surface area (m^2/g)	Pore volume (cc/g)
1.2Cr2.8V/M-41	-	1079	0.66
1.2Cr2.8V/M-22	15	291	0.34
1.2Cr2.8V/Z-5	75	271	0.29
1.2Cr2.8V/mesoZ-5	15	344	0.41

oxide phase over the support. The textural properties of bimetal impregnated samples are presented in Table 4.3. The surface area (1079 m^2/g), and pore volume (0.66 cc/g) calculated from nitrogen adsorption isotherm was highest for 1.2Cr2.8V/M-41 sample (Table 1). On the other hand, MCM-22 exhibited low surface area (291m^2/g) and pore volume (0.34 cc/g) which was slightly higher than commercial ZSM-5 catalysts. As expected, surface area of mesoZ-5 (344 m^2/g) was larger than Z-5 (284 m^2/g) with significantly higher mesopore volume of 0.41 cc/g compared with Z-5 (0.23 cc/g), which includes inter-crystal void volume. The high pore volume of mesoZ-5 catalyst is due to actual mesopores and does not represent intra-crystalline void volume [69].

4.2.1.2 Temperature programmed reduction

In order to analyze the reduction properties of the catalysts, TPR was carried out for 1.2Cr2.8V/M-41, 1.2Cr2.8V/M-22, 1.2Cr2.8V/Z-5, and 1.2Cr2.8V/mesoZ-5 at 100-700 ^oC (Fig. 4.11). The TPR results are presented in Table 4.4. In the case of 1.2Cr2.8V/M-41 sample, two reduction peaks are observed at 457 and 481^oC, respectively. The peak at 457 ^oC can be attributed to the reduction of Cr^{6+} species [30]. A shift in the onset of reduction peak towards lower temperature at 400 ^oC indicates more reducible species due to the Cr-V oxide interaction leading to mixed oxide phase over the support. Gasper et al. [48] ascribed such reduction to Cr^{6+} species that is interacted at different locations over the silica support. The observed onset reduction temperature is less for 1.2Cr2.8V/M-41, followed by 1.2Cr2.8V/Z-5, 1.2Cr2.8V/M-22 and 1.2Cr2.8V/mesoZ-5, respectively. The presence of high temperature peak at 481 ^oC, which extends up to 510 ^oC may be due to monomeric or low oligomeric surface dispersed tetrahedral species.

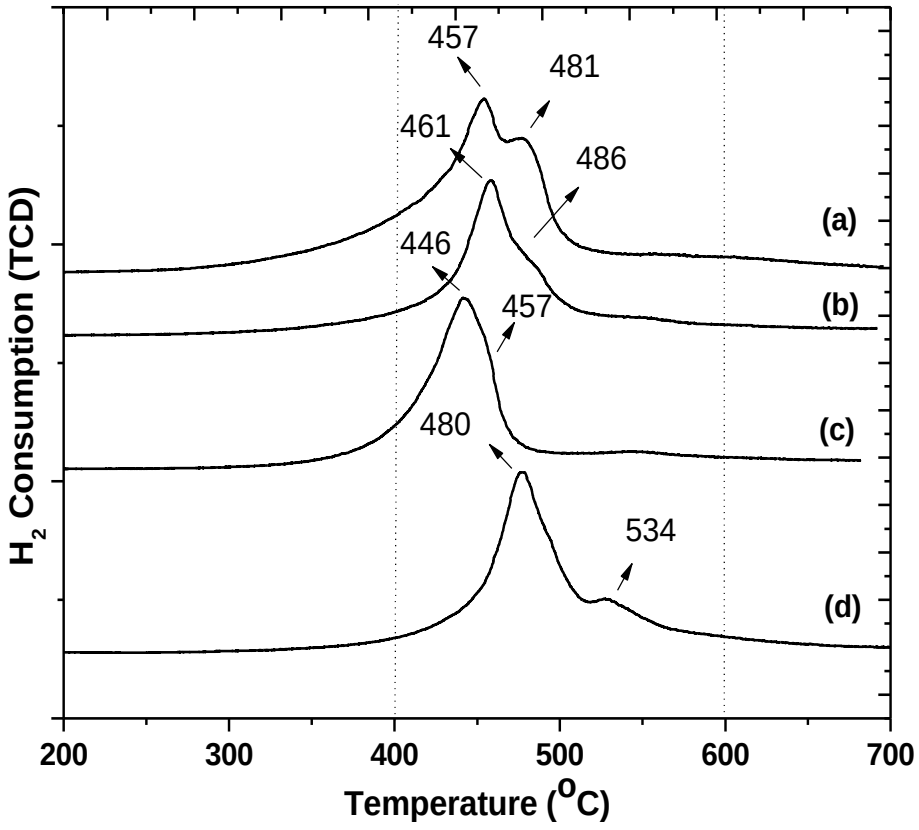

Fig.4.11. TPR profile for (a) 1.2Cr2.8V/M-41 (b) 1.2Cr2.8V/M-22 (c) 1.2Cr2.8V/Z-5 and (d) 1.2Cr2.8V /mesoZ-5.

Table 4.4. Temperature programmed analysis (H_2-TPR and TPD) and Pyridine-FTIR of Cr-V supported catalysts.

Catalyst	TPR		TPD			Pyridine-FTIR at 150 ^oC (mmol/g)	
	T_M (^oC)	H_2 consumption (mmol/g)	acidity (mmol NH_3/g)	basicity (mmol CO_2/g)	acidity/ basicity ratio (mmol/g)	Brønsted	Lewis
1.2Cr2.8V/M-41	457, 481	0.790	0.53	0.053	10.06	0.031	0.097
1.2Cr2.8V/M-22	461, 486	0.291	0.58	0.183	3.17	0.272	0.283
1.2Cr2.8V/Z-5	446, 457	0.372	0.28	0.090	3.08	0.030	0.070
1.2Cr2.8V/mesoZ-5	480, 534	0.370	0.283	0.142	2.00	0.033	0.410

In agreement with earlier reports on the reducibility of vanadium supported silica [49, 50], the peak at 481 ^{o}C is attributable to the reduction of dispersed tetrahedral vanadium species. The H_2 consumption was found to be higher than other samples. Thus the VOx species in the presence of CrOx species tends to inhibit the agglomerization of vanadia species and hence the formation of bulk-like vanadia species becomes less prominent. Similarly, a sharp reduction peak was observed at 461 ^{o}C in the case of 1.2Cr2.8V/M-22, accompanied by a shoulder peak at 486 ^{o}C. However, the presence of a less intense peak between 540 and 580 ^{o}C was attributed to the reduction of polymeric and bulk vanadia species [47]. The onset of reduction temperature of Cr-V supported Z-5 catalyst appears at 370 ^{o}C, while a peak reduction maximum occurs at 445 ^{o}C. In addition, a very less intense peak also appears at 540 ^{o}C. The reduction peak maxima between 500-550 ^{o}C was attributed to the reduction of surface V^{5+} species to surface V^{3+} species [43]. In the case of 1.2Cr2.8V/mesoZ-5, a shift in the onset of reduction peak towards higher temperature occurs compared to other bimetallic supported systems. The onset temperature begins at 380 ^{o}C and maximum reduction temperature peak appeared at 481 ^{o}C with a less intense peak at 496 ^{o}C. In addition, sample showed a distinct peak that extended up to 565 ^{o}C, indicating the formation of less reducible bulk-like vanadia species. The H_2 consumptions (mmol/g) were in the following order: 1.2Cr2.8V/M-41 > 1.2Cr2.8V/Z-5 > 1.2Cr2.8V/MesoZ-5 > 1.2Cr2.8V/M-22. The amount of transition metal reduced for the four catalysts were estimated. In the case of 1.2Cr2.8V/M-41, almost all the metal content in is observed to be reduced, whereas in 1.2Cr2.8V/M-22, 1.2Cr2.8V/Z-5 and 1.2Cr2.8V/mesoZ-5, a reduction of 37.3%, 47.7% and 47.4% of

metals are observed indicating reduction of V^{5+} to V^{3+} and Cr^{6+} to Cr^{3+} species, respectively. The depreciation of H_2 consumption with 1.2Cr2.8V/M-22 indicates increasing Cr–V oxide interactions, which may lead to the formation of mixed oxide phases and, therefore, may inhibit the thermal decomposition of chromium species in oxidation states VI and/or V during calcination [52].

4.2.1.3 Temperature programmed desorption

The acid-base functionality of catalyst plays an important role in the selectivity of dehydrogenation products [61, 70]. A recent report by Reddy et al. [56] also stressed the importance of finding the catalysts with an optimum amount of acid-base catalyst for high C_4 olefins selectivity. In the present study, the acidity and basicity of different supports were compared using TPD of ammonia and carbon dioxide, respectively (Fig. 4.12(a and b)). The total acidity and basicity from corresponding maximum desorption peak are presented in Table 4.4. The total acidity determines the acidity of support and the acidity due to impregnation with bimetals. In case of parent MCM-41, only a small broad peak was observed with very weak acid sites of about 0.071mmol/g mainly due to perturbed silanol groups. However, after impregnation of Cr-V, 1.2Cr2.8V/M-41 showed a broad desorption peak at temperature range of 100-330 ^oC with peak maxima at 136 ^oC indicating a wide distribution of weak acidity (0.533mmol/g). The increased surface acidity indicates the existence of synergistic effect between the metal oxides and shows the stronger interaction of mixed oxides over support [56, 55]. Though TPD analysis cannot provide direct information about interaction energies of ammonia molecule with surface of catalyst, increasing amount of desorbed ammonia, observed for bimetallic

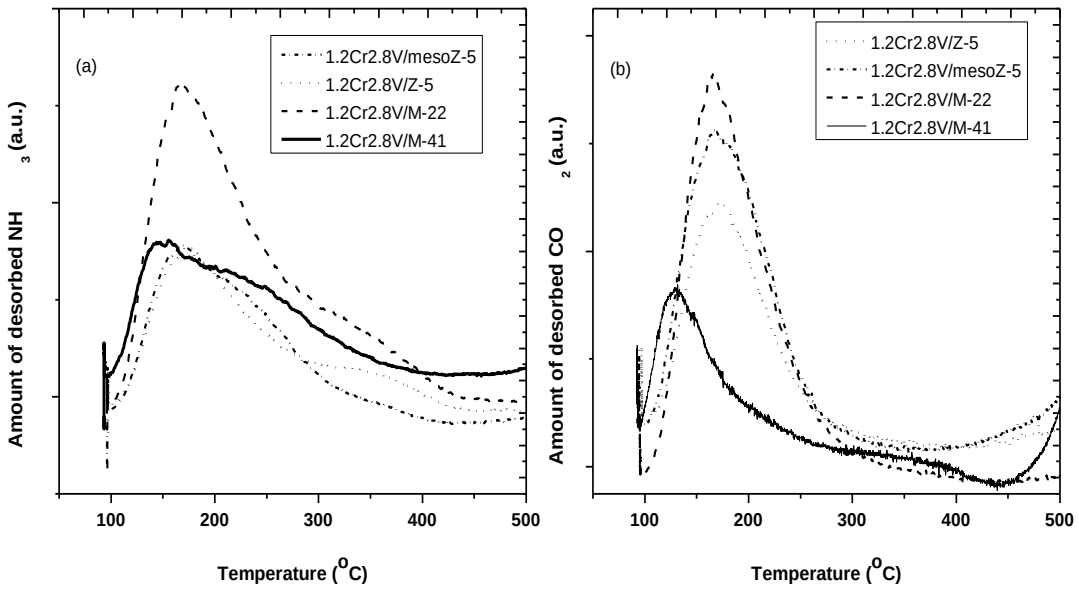

Fig.4.12. NH_3-TPD (a) and CO_2-TPD (b) profile for bimetallic impregnated samples

catalyst, can be caused by increase in number of adsorption site (e.g. better dispersion of oxide species) or by change in nature of oxide species and stoichiometry of adsorption adducts. 1.2Cr2.8V/M-22 showed relatively high number of acid sites with two maximum desorption peaks at 162 and 350 ^{o}C that extend up to 420 ^{o}C suggesting the presence of acidity in moderate range. In the case of 1.2Cr2.8V/Z-5, in addition to the desorption peak at 168 ^{o}C, two additional desorption peak maxima with varying intensity appeared at 344 and 478 ^{o}C indicating the presence of higher acid strength. Over 1.2Cr2.8V/mesoZ-5 sample, a similar broad NH_3 desorption peaks to that of 1.2Cr2.8V/M-41 occurs in the temperature range 100–380 ^{o}C accompanied by a significantly higher amount of weak acid sites.

In case of CO_2-TPD, weak, medium, and strong basic sites are estimated from the curves for the temperature range of 100–250, 250–400, and 400–650 ◦C, respectively. The variation in acidity shows that sodium ion exchanges neutralize part of acidity to generate the observed basicity. The loading of bimetals over Si-MCM-41 has shown to introduce weak basic sites (0.053mmol/g) at 160 ^{o}C on the siliceous surface of the catalyst. In case of 1.2Cr2.8V/M-22, the acid characters of the catalyst are observed to be affected significantly. A single broad desorption peak from 100-300 ^{o}C corresponding to the basic sites is seen that is apparently larger than all the samples (0.188mmol/g). 1.2Cr2.8V/Z-5 exhibited similar desorption peak indicating that the nature of the basic sites only changed less considerably compared to MCM-41. 1.2Cr2.8V/meso-Z-5 shows a similar desorption peak in that range, but with a lower amount of weak basic sites than 1.2Cr2.8V/M-22, and a significantly higher amount than 1.2Cr2.8V/Z-5 and

1.2Cr2.8V/M-41 (Table 2). The total acidity to basicity ratios of the four samples were observed as follows: 1.2Cr2.8V/M-41 > 1.2Cr2.8V/M-22 > 1.2Cr2.8V/Z-5 > 1.2Cr2.8V/mesoZ-5, respectively.

The nature of acid sites in Cr-V impregnated samples was determined using pyridine FTIR spectroscopy technique. The spectra of the samples recorded after desorption at different temperatures (150 ^{o}C, 250 ^{o}C and 400 ^{o}C) are shown in Fig. 4.13 The amount of both Brønsted and Lewis acid sites of zeolite samples are given in Table 4.4. In the case of siliceous MCM-41, only a weak Lewis band appears at 1445 cm^{-1} due to distorted silica sites (Fig. 4.13a). However, after Cr-V impregnation, the number of total acid sites including both Brønsted and Lewis acid sites increased (Fig. 4.13b). Such increase in the acidity over V-SBA-15 samples due to vanadium oxide impregnation is discussed in detail by Liu et al. [71]. The distinct band at 1545 cm^{-1} is associated with the coordination of pyridine over acidic V-OH groups [72], while the additional peak at 1490 cm^{-1} can be attributed to the interaction of both types of acid sites with pyridine. Comparatively, the pyridine spectrum of 1.2Cr2.8V/M-41 showed that the intensity of both acid sites decreases with increasing desorption temperatures (Fig. 4.13(c and d)). The pyridine adsorbed on Brønsted acid site is found to disappear after evacuation at 250 ^{o}C. In contrast, 1.2Cr2.8V/M-22 showed the presence of strong acidity with distinct peaks even after evacuation at 400 ^{o}C. Thus pyridine desorption shows a relatively mild acid strength over MCM-41, while presence of strong acid sites over 1.2Cr2.8V/M-22 (Fig. 4.13(e)). 1.2Cr2.8V/Z-5 and 1.2Cr2.8V/mesoZ-5 showed the presence of acidity with intermediate acid strength (Fig. 4.13(f and g).

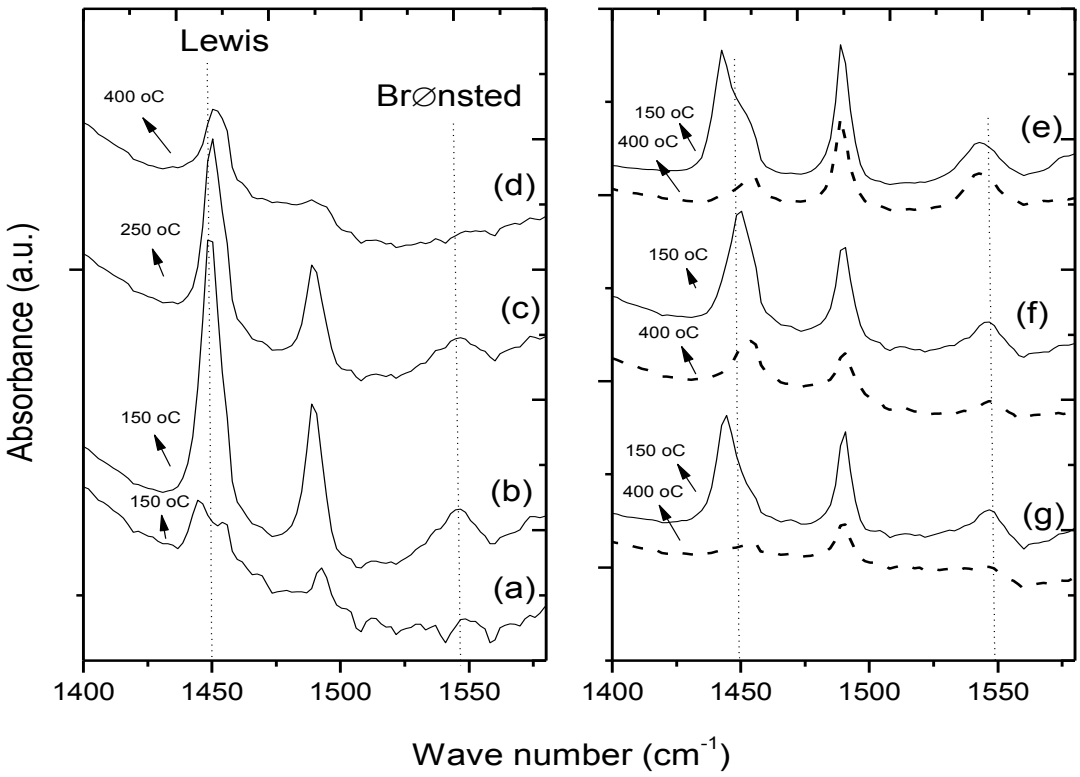

Fig.4.13 FTIR-pyridine profile for impregnated samples evacuated at different temperatures:
(a) SiMCM-41, (b-d) 1.2Cr2.8V/M-41, (e) 1.2Cr2.8V/M-22, (f) 1.2Cr2.8V/Z-5 and (g)1.2Cr2.8V/mesoZ-5.

4.2.1.4 Raman spectra

The Raman spectra of Cr-V catalysts are shown in Fig. 4.14. In general, the presence of typical strong bands at 287, 304, 402, 475, 526, 695, and 996 cm^{-1} were ascribed to crystalline V_2O_5, whereas the bands between 550-560 cm^{-1} are related to the crystalline α-Cr_2O_3 [73]. The absence of such peaks in the samples shows that chromium and vanadium are well dispersed over the support. Over 1.2Cr2.8V/M-41, a well distinguishable peak at 875 cm^{-1} appear due to monochromate Cr^{6+} species. The bands at 900-1000 cm^{-1} are usually assigned to hydrated polymeric vanadium oxide species with different degree of oligomerization [74]. Comparatively, a less intense band at 915 cm^{-1} assigned to V=O symmetric stretching mode of octahedrally coordinated vanadium oxide species is observed. A small band at 1042 cm^{-1} is usually attributable to isolated terminal V=O stretching vibration of monomeric vanadyl species was also observed. In case of Z-5 support, impregnation of bimetals resulted in an equally intense two band formations due to polymeric vanadia band at 915 cm^{-1} and polychromate species at 962 cm^{-1}. This indicates less dispersity of bimetals over Z-5 support. A band at 487 cm^{-1} assigned to the symmetrical Si–O–Si stretching mode of siloxane rings was also observed [75]. For 1.2Cr2.8V/M-22 and 1.2Cr2.8V/mesoZ-5, an intense band of polymeric vanadia was observed. Overall, the result reflects the existence of high bimetal dispersion over 1.2Cr2.8V/M-41.

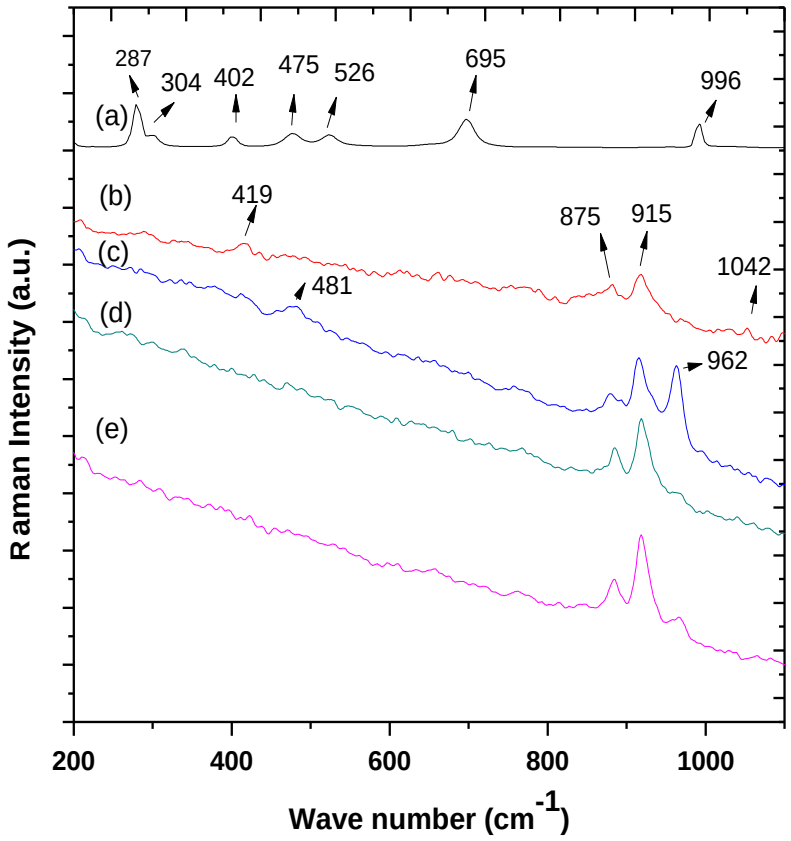

Fig.4.14. FT-Raman spectra for bimetallic impregnated samples (a) V_2O_5 (b) 1.2Cr2.8V/M-41 (c) 1.2Cr2.8V/Z-5 (d) 1.2Cr2.8V/M-22 and (e) 1.2Cr2.8V/mesoZ-5.

4.2.2 Dehydrogenation of n-butane and CO_2 activation

4.2.2.1 Effects of time on stream

The dehydrogenation for *n*-butane was carried out over mesoporous silica (M-41) and zeolite supports (M-22, Z-5 and mesoZ-5) with CO_2 as oxidant at 550°C for 3 h time on stream (Fig. 4.15a). In a typical reaction, the space velocity (WHSV) of *n*-butane was maintained at 4 h^{-1}. In our previous report, we showed dehydrogenation activity of 1.2Cr2.8V/M-41 catalyst in N_2 atmosphere [76]. In the present study, the catalytic activity of four different catalysts is tested in CO_2 atmosphere. The catalytic activity of all the samples showed a decreasing trend with increasing time-on-stream. Interestingly, a significant difference in selectivity to butenes was observed depending on the metal oxide supported system. The high activity is again reciprocated over mesoporous MCM-41 based catalyst 1.2Cr2.8V/M-41 followed by 1.2Cr2.8V/Z-5. At the initial reaction time of 10 min, *n*- butane conversion over 1.2Cr2.8V/M-41 and 1.2Cr2.8V/Z-5 were 8.18% and 6.79%, respectively. Importantly, butenes selectivity over 1.2Cr2.8V/M-41 was about 90% for the studied reaction time, while 1.2Cr2.8V/Z-5 shows lowest selectivity around 70%. It was observed that 1.2Cr2.8V/mesoZ-5 catalyst shows the lowest activity followed by 1.2Cr2.8V/M-22 with intermediate selectivity to butenes of about 77%. Fig.4.15b shows the CO_2 conversion over 1.2Cr2.8V impregnated catalysts (M-41, Z-5, M-22, mesoZ-5) catalysts against the time on stream at 550°C. Sun et al. [77] reported that in ethylbenzene dehydrogenation using Fe/Al_2O3 and V/Al_2O_3

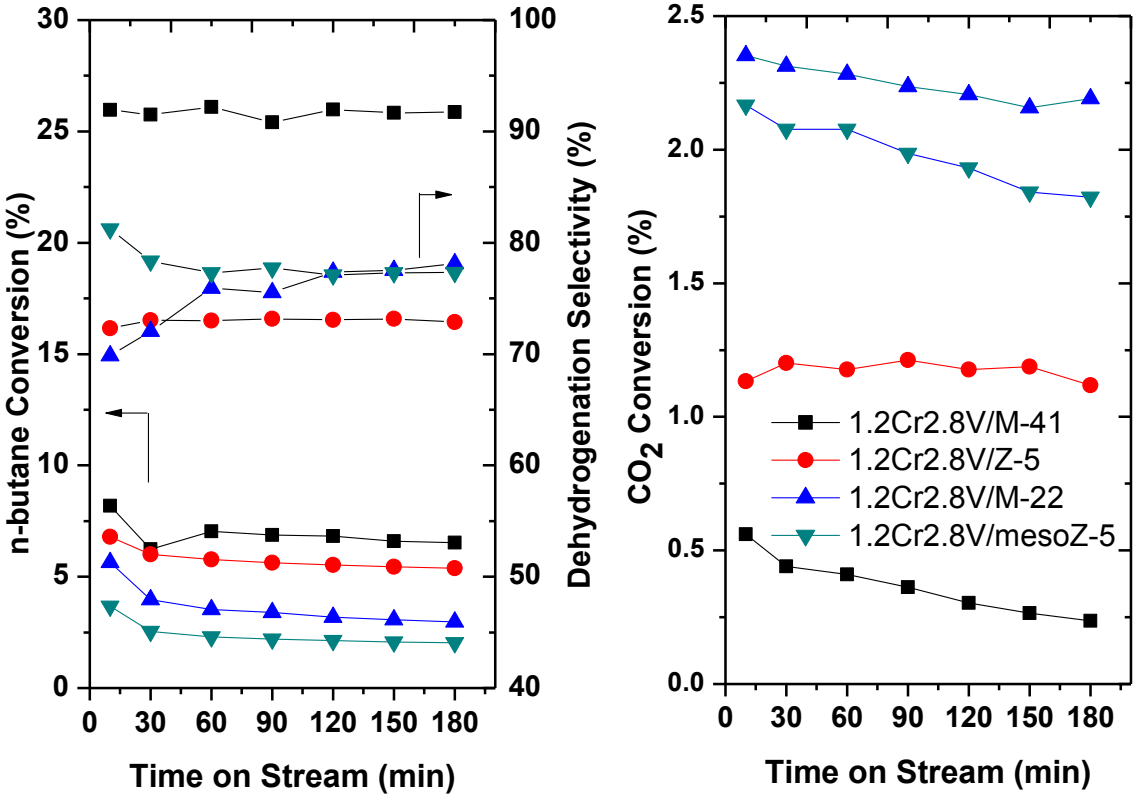

Fig.4.15. *n*-Butane conversion over 1.2Cr2.8V impregnated catalysts (M-41, Z-5, M-22, mesoZ-5) against the time on stream in CO_2 atmosphere at 550 °C. Catalyst weight, 0.15g, n-butane flow rate, 4 ml min^{-1}, CO_2 flow rate 40 ml min^{-1} and N_2 flow rate 56 ml min^{-1}. WHSV value, 4.0 h^{-1}(with respect to butane).

modified catalysts, conversion of CO_2 increased with conversion of EB showing synergetic effect in coupling reaction. In addition, many recent literatures have shown the reverse water gas shift effect in ethane and propane dehydrogenation over MCM-41 [78]. However, in butane dehydrogenation at 550 ^oC, CO_2 activation is observed among the catalysts in the following order: 1.2Cr2.8V/M-22 > 1.2Cr2.8V/meso-Z-5 > 1.2Cr2.8V/Z-5 > 1.2Cr2.8V/M-41**.** With 1.2Cr2.8V/M-22, the highest conversion level of CO_2 was observed, which decreases with time on stream (2.35-2.2%) at 550 ^oC. In case of 1.2Cr2.8V/M-41, the total conversion values were about 4.2 times lower than 1.2Cr2.8V/M-22 despite its high dehydrogenation activity.

4.2.2.2 Effects of temperature

The effects of reaction temperatures (525, 550, 575 and 600 ^oC) on the conversions of *n*-butane and CO_2 were studied (Fig. 4.16 a and b). Ogonowski and Skrzynska [79] showed that the isobutane conversion and the activation of carbon dioxide depend on the reaction temperature. Similarly, a marked difference was observed between the activities of different catalysts. The conversion of *n*-butane tends to increase with increasing reaction temperature. Overall, 1.2Cr2.8V/M-41 maintained high catalytic activity, where conversion of *n*-butane increased from 4.7% at 525 ^oC to the maximum of 14% at 600 ^oC. It has been reported in the literatures that Cr(VI) species are more active than Cr(III) polychromate in alumina based catalysts for dehydrogenation with CO_2 as the oxidant [51]. In the case of vanadium supported catalysts, VOx species with higher degree of polymerization participate in undesired consecutive reactions with ODH products [13]. The high activity of Cr-V supported MCM-41 with overall temperature range is consistent with TPR results indicating the formation of synergy between active metals

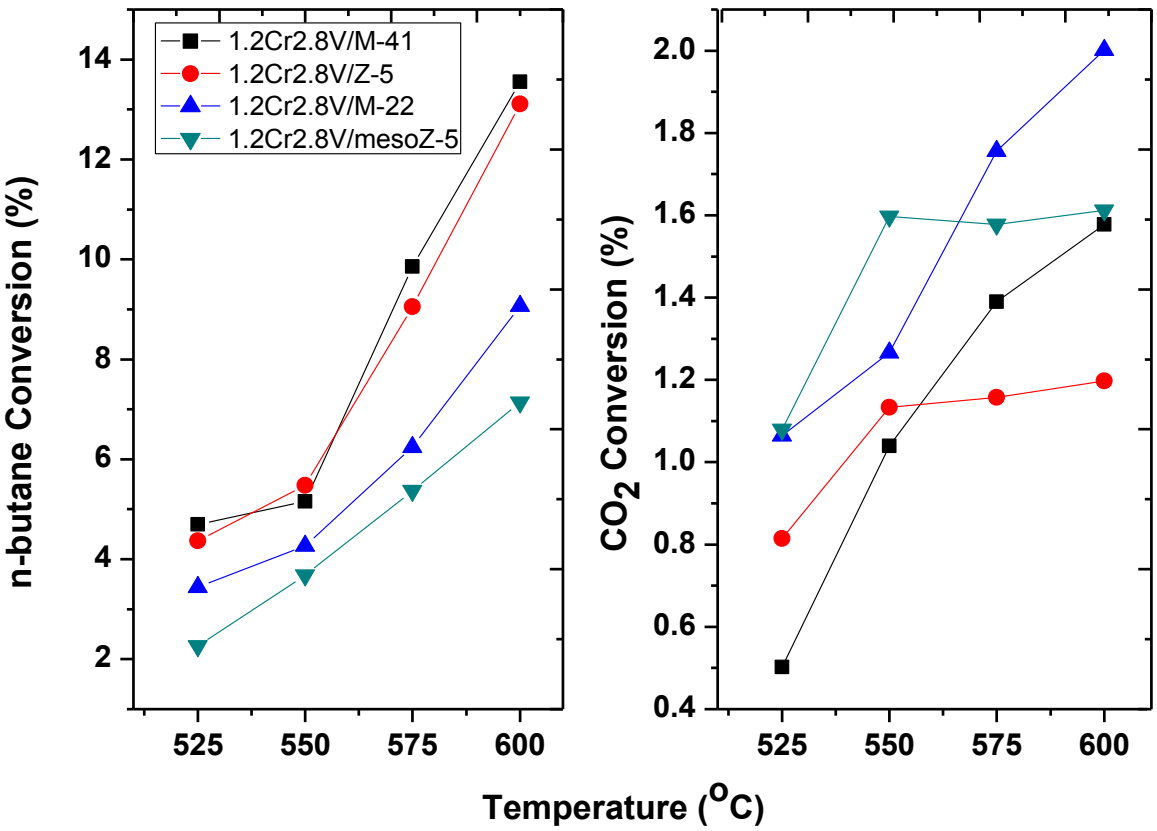

Fig.4.16. Effect of reaction temperature and CO_2 conversion on the oxidative dehydrogenation of *n*-butane over 1.2Cr2.8V impregnated catalysts (M-41, Z-5, M-22, mesoZ-5). Reaction temperature, 525-600 °C; catalyst weight, 0.15g, *n*-butane flow rate, 4 ml min^{-1}, CO_2 flow rate 40 ml min^{-1} and N_2 flow rate 56 ml min^{-1}. All data were collected within the first 10 min.

(VOx and/or CrOx species), leading to the easy reducibility (about 300 ^{o}C) on the high surface area of mesoporous support. Sun et al. [80] showed that in the case of ethylbenzene dehydrogenation coupled reaction in the presence of CO_2, the catalyst which produced a good styrene yield also showed a high CO_2 conversion. However, in the present results with *n*-butane as reactant, quite different results were obtained as shown in Fig. 4.15b. 1.2Cr2.8V/M-41 exhibited high dehydrogenation capacity but on the other hand it showed substantially lower capability to absorb carbon dioxide than 1.2Cr2.8V/Z-5, 1.2Cr2.8V/mesoZ-5 and 1.2Cr2.8V/M-22, respectively. However, CO_2 conversion was observed reasonably well at higher temperature of 600 ^{o}C, where maximum conversion of CO_2 (1.58%) occurred. Such trend in MCM-41 indicates simple dehydrogenation takes place at temperature lower than 550 ^{o}C, where CO_2 behaves as an inert gas. But at higher temperature, carbon dioxide is consumed and shifts the dehydrogenation equilibrium to butenes. 1.2Cr2.8V/Z-5 with reduction temperature of 440 ^{o}C showed competitive catalytic ability with steady increase of conversion from 4.37% to the maximum of 13.1% from 525-600 ^{o}C. Conversely, 1.2Cr2.8V/M-22 catalyst with reduction temperature of 461 ^{o}C containing stronger surface basic sites showed intermediate activity with 3.44 to 9.07% of *n*-butane conversion. The presence of more strong basic sites in 1.2Cr2.8V/M-22 sample than the other samples favours more efficient dissociative adsorption of CO_2 with maximum conversion of 2% at 600 ^{o}C. The activity of 1.2Cr2.8V/mesoZSM-5 catalyst was lowest with a conversion value ranging from 2.26% to 7.14%, indicating that Cr-V was not active on this support. The lower activity can be correlated to the higher reduction temperature (480 ^{o}C) due to the formation of crystalline and high amount of polymerized Cr and V species that are not

active for dehydrogenation. This result indicates the strong relation between reducibility, and catalytic activity for the oxidative dehydrogenation of butane.

4.2.2.3 SEM and EDX

The particle morphology and elemental composition of parent (Fig 4.17a and b) and active catalysts 1.2Cr2.8V/M-41 (Fig 4.17c and d) were investigated using SEM equipped with EDX detector**.** The SEM micrographs for parent and impregnated MCM-41 showed similar particle morphology in the range 5µm. The EDX elemental mapping analysis indicated absence of V_2O_5 and Cr_2O_3 clusters. In addition to the presence of polymeric species, a homogeneous distribution of Cr and V species are observed on the surface of MCM-41. No large clusters of metal species were observed on the surface.

4.2.2.4 Products distribution

The molar selectivity of the dehydrogenation products observed at 600 ^{o}C indicates that along with dehydrogenation, cracking is also increased which is expected at such high reaction temperature (Fig. 4.18). However, it is clearly observed that formation of butenes with respect to 1.2Cr2.8V/M-41 is still the highest with the selectivity of 89%. [51]. It is already been stated that dehydrogenation takes places either by coupling with reverse water-gas shift reaction (Eq. 4.1 and 4. 2) or through redox mechanism (Eq. 4.3 and 4.4) [50]. The high hydrogen consumption of 1.2Cr2.8V/M-41 coupled with high butenes formation shows that reaction mostly favoured through redox cycle mechanism.

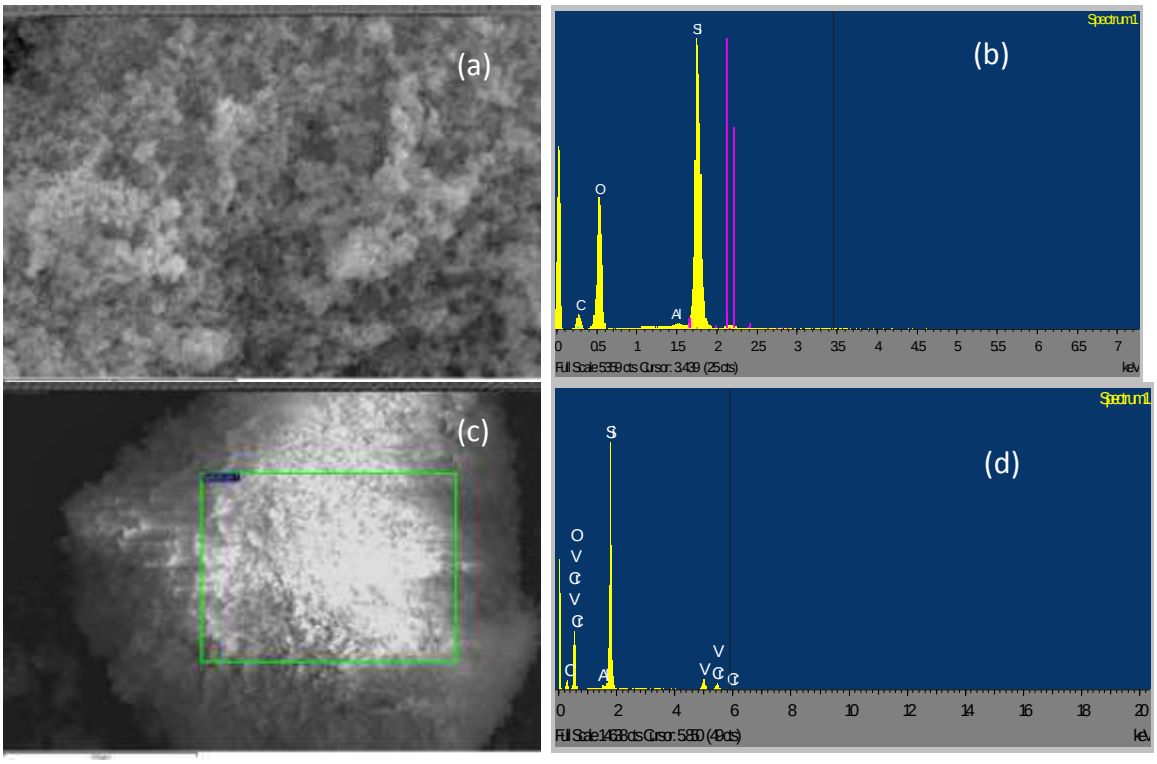

Fig.4.17. SEM-EDX images of parent Si-MCM-41 (a and b) and 1.2Cr2.8V/M-41 (c and d) at 5µm.

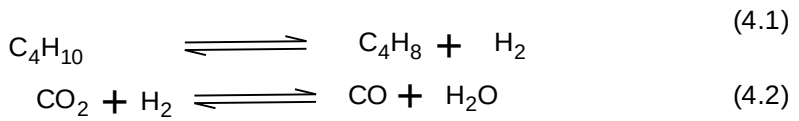

(4.1)

(4.2)

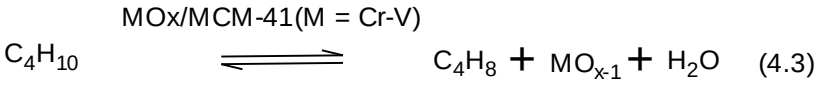

(4.3)

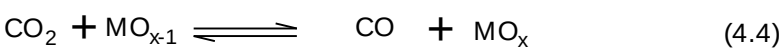

(4.4)

The loading of rare earths on HZSM-5 also had been found to increase the hydrophilicity of the catalyst that suppress bimolecular reactions which form BTX and stimulate monomolecular cracking reactions which form olefins [81]. In this work, absence of aromatic and heavier products suggests that cracking occurs through monomolecular mechanism [65]. In the case of zeolites, the initial step of cracking on zeolite has been considered to be a protonation followed by cracking in three paths [66]. The primary C-C bond cracking leads to the formation of methane and propylene (Eq. 4.5). Narbeshuber [67] attributed the formation of ethene occurs due to secondary cracking of butene isomers via primary carbenium ion formation (Eq. 4.6), whereas monomolecular primary C-C cracking of butane leads to formation of ethane and ethylene (Eq. 4.7). The cracking pathways: methane and propene, ethane and ethene increases with reaction temperature indicating lower energy activation for dehydrogenation than cracking. The monomolecular cracking of primary C-C bond and secondary C-C bond cleavage occurs through acidic proton of zeolites. The formation of high ethene to ethane molar ratio may be attributed to the excess ethene produced from the secondary cracking of butene molecule through the formation of primary carbenium ions.

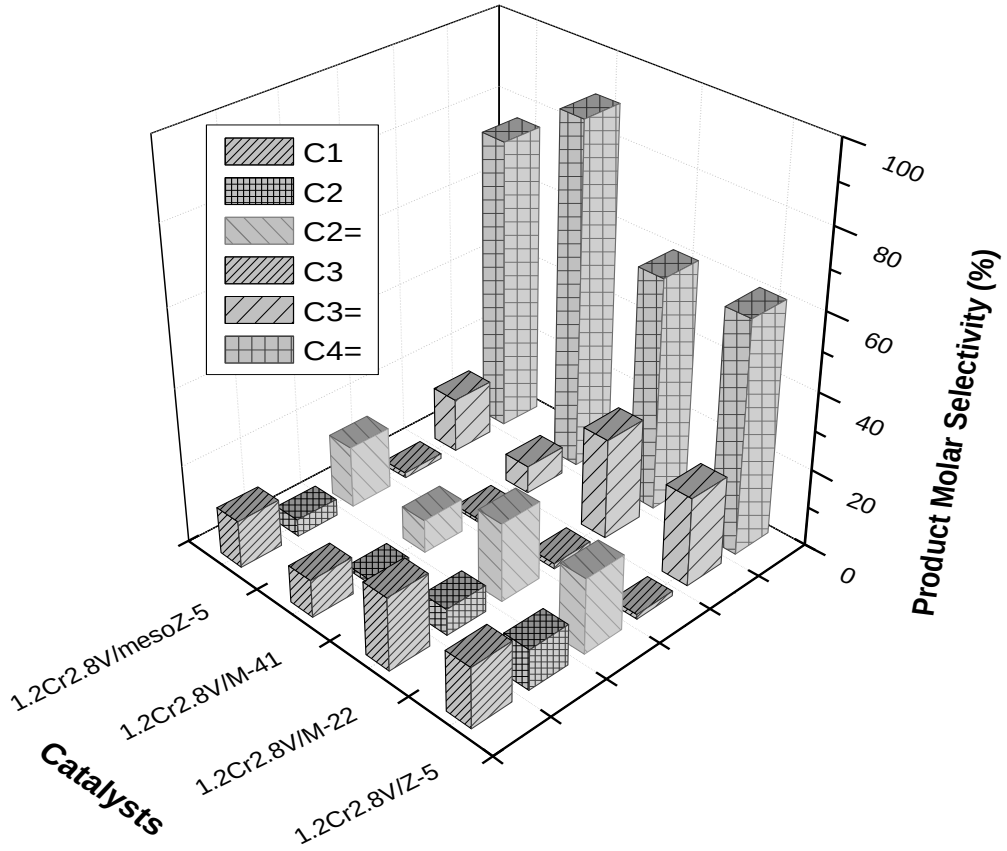

Fig.4.18. Product molar selectivity over 1.2Cr2.8V impregnated catalysts (M-41, Z-5, M-22, mesoZ-5) catalysts. With reaction time of 10minutes, *n*-butane:CO_2:N_2=1:10:14, WHSV=4.0h^{-1}(with respect to butane), reaction temperature of 600 °C and catalyst weight of 0.15g.

$$C_4H_{10} \xrightarrow{H^+} CH_4 + C_3H_6 \quad (4.5)$$

$$C_4H_8 \xrightarrow{H^+} C_4H_9^+ \longrightarrow C_2H_4 + C_2H_5^+ \xrightarrow{-H^+} 2\,C_2H_4 \quad (4.6)$$

monomolecular cracking of secondary C-C bond

$$C_4H_{10} \xrightarrow{H^+} C_2H_6 + C_2H_4 \quad (4.7)$$

monomolecular cracking of primary C-C bond

As expected, the methane/propene molar ratio was fairly equal for 1.2Cr2.8V/M-41 and 1.2Cr2.8V/mesoZ-5 catalysts. However, the methane/propene imbalance in the other two catalysts (1.2Cr2.8V/Z-5 and 1.2Cr2.8V/M-22) may be explained by a similar observation in the work of Wang et al. [82]. The *n*-butane feedstock may have been functionalized by the acidic sites of 1.2Cr2.8V/Z-5 and 1.2Cr2.8V/M-22 catalysts, forming butyl carbenium ions (Eq. 4.8), which is capable of abstracting hydride ions from propane impurity (0.4% of feedstock) to yield butane and adsorbed propyl ions which ultimately transforms into propene (Eq. 4.9). Evidently, this explains the observed low butene yield for 1.2Cr2.8V/Z-5 and 1.2Cr2.8V/M-22 catalysts.

$$C_4H_8 \xrightarrow{H^+} C_4H_9^+ \quad (4.8)$$

$$C_4H_9^+ + C_3H_8 \longrightarrow C_3H_7^+ + C_4H_{10} \quad (4.9)$$

The variation in yield of butene isomers for 1.2Cr2.8V/M-41, 1.2Cr2.8V/Z-5, 1.2Cr2.8V/M-22 and 1.2Cr2.8V/mesoZ-5 are shown in Fig. 4.19. In general, 1-butene and 2-butenes are considered as primary products, while butadiene is a secondary product formed from butenes. Butadiene is reported to oligomerize easily with other olefins over acid based catalysts [83]. In the present study, for 1.2Cr2.8V/M-41 catalyst, the major product was found to be 1, 3-butadiene (6.6 wt %). The formation of some trans 2-butene, 1-butene, cis 2-butene (< 2wt.%) with very less amount of isobutene (0.21wt.%) was observed. It was reported that cerium containing MCM-41

catalyst showed high selectivity (78%) for butadiene at moderate conversion of about 4% [84]. The formation of competitive deep oxidation products is closely related to the interaction of olefin or allylic intermediates with surface medium acid sites during the ODH of propane [85]. The observed selectivity of 1,3- butadiene over 1.2Cr2.8V/M-41 indicates that a very less combustion of olefins occurs due to mild adsorption on the catalyst surface.

With 1.2Cr2.8V/Z-5, a high yield of isobutene (2.5 wt %) was obtained. The dehydroisomerization of *n*-butane to isobutene over Pt–ZSM-5 catalysts with a high Si/Al ratio was studied [86], and the highest yield of isobutene achieved at 560°C and with a feed of 10% *n*-butane and 20% hydrogen was about 12.5%. At the same condition, almost similar formation of primary products cis-2-butene (0.78wt.%), 1-butene (0.9wt.%) and 2-butenes (1.02wt.%) was observed over 1.2Cr2.8V/M-22 and 1.2Cr2.8V/mesoZ-5, respectively. With respect to 1,3-butadiene formation, the selectivity over 1.2Cr2.8V/M-22 was slightly less (1.18wt.%) compared to 1.2Cr2.8V/mesoZ-5 (1.46wt.%). Overall, the formation of primary products and high conversion of CO_2 is observed. This behavior could be related to the presence of Lewis acid sites that is reported to play an important role in the selective oxidative dehydrogenation of ethane

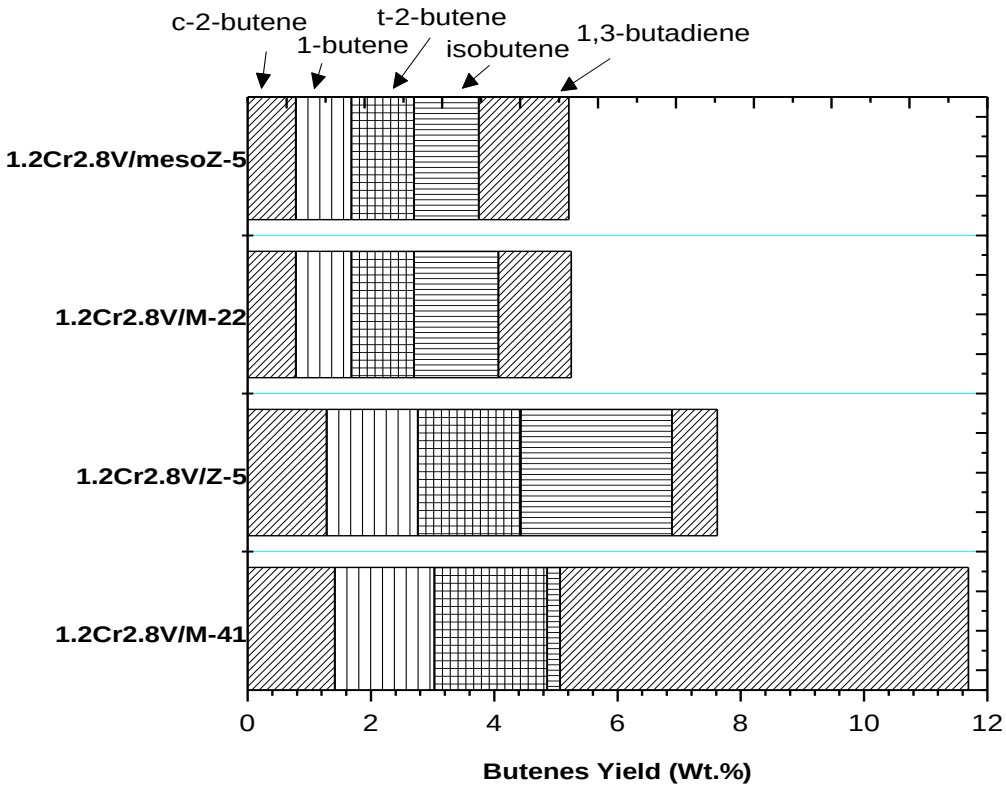

Fig. 4.19. Butenes yields over 1.2Cr2.8V impregnated catalysts (M-41, Z-5, M-22, mesoZ-5) catalysts. With reaction time of 10minutes, n-butane:CO_2:N_2=1:10:14, WHSV=4.0h^{-1}(with respect to butane), reaction temperature of 600 °C and catalyst weight of 0.15g.

[87]. If the strength of Lewis acid sites is higher than a required value, adsorption of the olefin is reported to be too strong and over-oxidation toward combustion products is favored. In the case of 1.2Cr2.8V/M-22, and 1.2Cr2.8V/mesoZ-5, the observed activity could be related to the combustion of olefins strongly adsorbed on the catalysts surface.

4.2.2.5 Apparent activation energy

In order to evaluate the apparent activation energy, we varied the temperature from 525 to 600 °C with a step change of 25 °C each (Table 4.5) (Figure 4.20a and b). The apparent activation energies of dehydrogenation reaction over the four catalysts are quite similar at 72, 71, 69 and 67kJ/mol for 1.2Cr2.8V/M-41, 1.2Cr2.8V/Z-5, 1.2Cr2.8V/M-22 and 1.2Cr2.8V/mesoZ-5 respectively. However, apparent activation energies of cracking shows higher values with a range of about one order of magnitude, with values from 80kJ/mol to 157kJ/mol. These values reflect the relative difficulty of cracking reaction of *n*-butane. The reactant over 1.2Cr2.8V/M-41 catalyst evidently shows the most difficulty to cracking while with 1.2Cr2.8V/M-22 catalyst, cracking was dominant. This is further illustrated by the ratio of the apparent activation energy of cracking to the apparent activation energy of dehydrogenation, in the following order: 1.2Cr2.8V/M-41> 1.2Cr2.8V/mesoZ-5> 1.2Cr2.8V/Z-5> 1.2Cr2.8V/M-22. The different values of the apparent activation energy for cracking confirm that the reaction mechanism changes. Narbeshuber et al [68] reported that the apparent activation energies of simple dehydrogenation and cracking over H-ZSM-5 are 115kJ/mol and 135kJ/mol respectively.

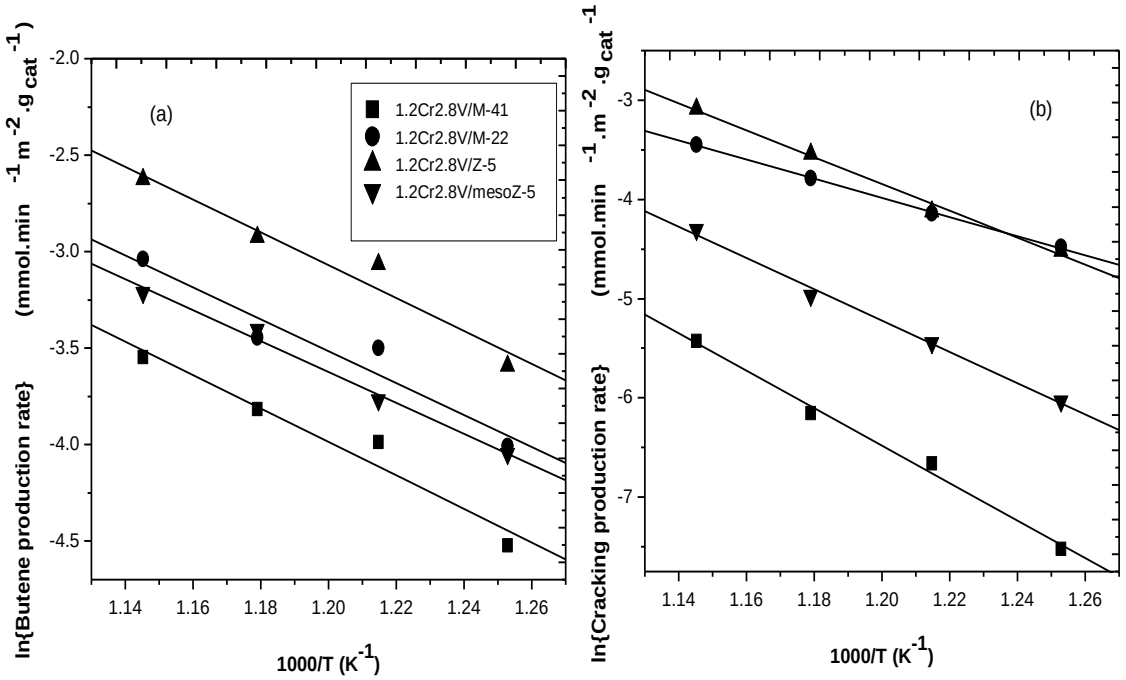

Fig.4.20 Arrhenius plots of n-butane dehydrogenation (a) and cracking (b) over 1.2Cr2.8V/S (S=M-41, Z-5, M-22, mesoZ-5) catalysts. Reaction temperature, 525-600°C; catalyst weight, 0.15g, n-butane flow rate, 4 ml min^{-1}, CO_2 flow rate 40 ml min^{-1} and N_2 flow rate 56 ml min^{-1}.All data were collected within the first 10 min.

Table 4.5. Apparent activation energies for n-butane dehydrogenation and cracking over 1.2Cr2.8V/S (S=M-41, Z-5, M-22, mesoZ-5) catalysts. Reaction temperature, 525°C-600°C; catalyst weight, 0.15g, *n*-butane flow rate, 4 ml min^{-1}, CO_2 flow rate 40 ml min^{-1} and N_2 flow rate 56 ml min^{-1}.

Catalyst	Apparent activation energy (kJ/mol)		$E_{app,crack}/E_{app,dehyd}$
	Dehydrogenation ($E_{app,dehyd}$)	Cracking ($E_{app,crack}$)	
1.2Cr2.8V/M-41	72	157	2.18
1.2Cr2.8V/M-22	69	80	1.16
1.2Cr2.8V/Z-5	71	113	1.59
1.2Cr2.8V/mesoZ-5	67	131	1.96

Elsewhere, reactions over three distinct aluminiumphosphate based molecular sieves were tested and it was reported that the contribution of dehydrogenation was more pronounced at low temperature (500°C) than at high temperature (560°C) [88]. This is a direct consequence of the higher apparent activation energy for cracking (110-140kJ/mol) than for dehydrogenation (70-100kJ/mol).

4.2.2.6. Olefin/Paraffin Ratio

The olefin/paraffin ratio was measured at the temperature range of 525°C to 600°C for 10 min time on stream (Fig.4.21). This ratio gives a clue about the dehydrogenation/cracking ratio since only cracking reaction contributes to paraffin products. The selectivity to dehydrogenation and cracking over 1.2Cr2.8V/M-41, 1.2Cr2.8V/mesoZ-5 and 1.2Cr2.8V/Z-5 were found to be strongly influenced by temperature. The olefin/paraffin ratio is especially high at low temperatures and steadily reduces for the temperature range under study. Cracking products involves rupture of the C-C bond [89]; therefore, they are thermodynamically favored at high temperatures (endothermic reaction). However, for 1.2Cr2.8V/M-22 this ratio was maintained below 4.0. The stability of this ratio may be as a result of the low apparent activation energy of cracking (80kJ/mol). It is noteworthy to point out that for 1.2Cr2.8V/M-22 the ratio of dehydrogenation apparent activation energy (69kJ/mol) and cracking activation energy is the lowest among four catalysts indicating a pronounced competition between dehydrogenation and cracking reactions.

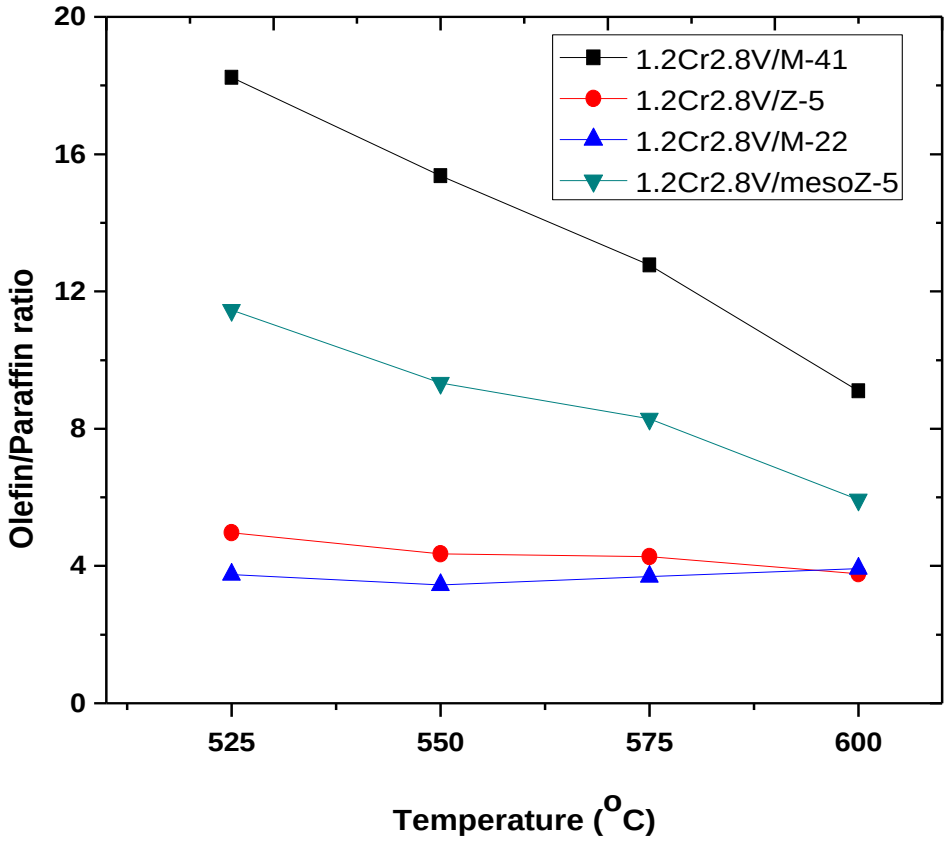

Fig.4.21. Olefin to paraffin ratio at the reaction time of 10 min as a function of temperature.

Table 4.6 Coke formation for n-butane dehydrogenation and cracking reactions at given reaction condition.

Catalyst	Temp(° C)	Time(min)	Conv.(%)	Coke(wt%)	Conv./Coke
1.2Cr2.8V/M-41	600	30	9.24	1.02	9.06
1.2Cr2.8V/M-22	600	30	6.89	3.74	1.84
1.2Cr2.8V/Z-5	600	30	12.39	1.55	7.99
1.2Cr2.8V/mesoZ-5	600	30	5.55	0.91	6.10

4.2.2.7 Coke studies

The amount of coke formation was measured after dehydrogenation at 600°C for 30 minutes of reaction time (Table 4.6). The results show that the amount of coke deposited over 1.2Cr2.8V /M-22 catalyst was found to be the highest among the four catalysts. From observation, both micro-structured derived catalysts (1.2Cr2.8V/M-22 & 1.2Cr2.8V/Z-5) gave a higher coke formation as compared with their meso-structured counterparts. Though the tested catalysts activity decreases with time on stream, the difference in coke formation on each catalyst may be due to pore size and/or surface acidity variations. Bazyari et al. [90] attributed coke formation to the cracked products with low molecular weights. According to them, these molecules usually have low diffusional limitations which are said to be responsible for coke formation. The molecule of these cracked products combine with the acid sites to form ionic radicals which then polymerize with other unsaturated hydrocarbons, and then dehydrogenate to form aggregates of coke [91]. As expected, the catalyst which promotes cracking (1.2Cr2.8V/M-22) gave the highest coke content. The ratio of conversion to coke weight per cent over the four catalysts at same reaction condition, ranges from 1.84 to 9.01 (Table 4), and remains in the following order: 1.2Cr2.8V/M-41>1.2Cr2.8V/Z-5>1.2Cr2.8V/mesoZ-5>1.2Cr2.8V/M-22.

4.3 Kinetic Modeling of *n*-Butane Dehydrogenation over 1.2Cr2.8V/MCM-41 Catalyst in a Fixed Bed Reactor

4.3.1 Model development

It is instructive to develop a model with a reasonably low number of reaction steps and kinetic parameters that will be just adequate to enable us to describe the essential features of *n*-butane dehydrogenation and cracking reactions. Rather than develop a detailed model incorporating all GC detected chemical species and possible reaction steps, we simplified the model by lumping all cracked products consisting of methane, ethane, ethene, propane, propene as one entity, and the butene isomers; namely 1-butene, cis-2-butene, trans-2-butene were regarded as a single specie called C_4 olefin. Also, some reaction steps with no significant contribution to the overall rate were ignored. Examples of such cases are Eq. 4.10 and Eq. 4.11 which is the single and double step bi-olefin route respectively. The selectivity to butadiene in the entire sample size was less than 5%, so the reaction steps leading to butadiene in the system were neglected. See Table 2 for product distribution.

Dehydrogenation steps

$$C_4H_{10} \rightleftharpoons C_4H_8 + H_2 \quad (4.10)$$

$$C_4H_8 \rightleftharpoons C_4H_6 + H_2 \quad (4.11)$$

$$C_4H_{10} \rightleftharpoons C_4H_6 + 2H_2 \quad (4.12)$$

Cracking steps

$$C_4H_{10} \longrightarrow C_2H_4 + C_2H_6 \quad (4.13)$$

$$C_4H_{10} \longrightarrow CH_4 + C_3H_6 \quad (4.14)$$

$$C_4H_8 \longrightarrow 2C_2H_4 \quad (4.15)$$

Therefore, scheme 1 was proposed after making the simplifications explained in the foregoing paragraph:

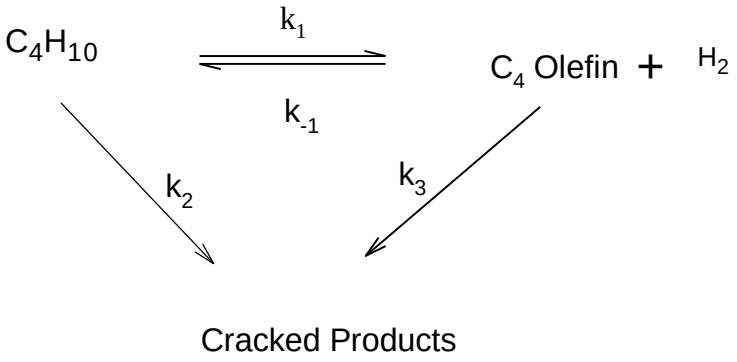

Scheme 1: Catalytic reaction scheme of *n*-butane dehydrogenation

Further modification was made to scheme 1 after the model failed to work. As can be seen by Eq. 4.12, the stoichiometric proportion of ethene to ethane is 1:1 which is

expected to increase if the secondary cracking reactions (Eq. 4.14) were to be factored in. However, the product distribution table suggested a decrease in the ratio (Table 4.7), hence secondary monomolecular cracking of olefin was neglected in the new scheme:

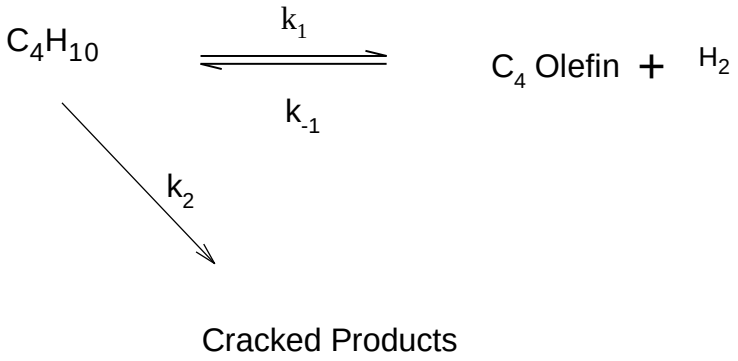

Scheme 2: Modified catalytic reaction scheme of *n*-butane dehydrogenation

The experimental results were modeled using catalyst deactivation function model based on reaction conversion catalyst decay function which was developed by Al-Khattaf and de Lasa [92]. In this model, deactivation is dependent on the conversion of *n*-butane which in turn is linked to the coke formed on the surface of the active sites of the catalysts. This approach appears to be more accurate than the time-on-stream approach widely used in literature to account for catalyst deactivation. Based on the fact that the temperature difference across the catalyst bed is negligible, the fixed bed was considered to be an isothermal plug flow reactor. The total reaction rate for each chemical specie *i* expressed by r_i was evaluated by summing up all the reaction rates at every step *j* which specie *i* was involved. For n_R number of reaction steps, the rate is given by:

Table 4.7: Product distribution of *n*-butane dehydrogenation over 1.2Cr2.8V/M-41

Contact Time $\left(\frac{g_{cat}min}{g_{butane}}\right)$	Yield (wt.%)										Conv. (%)
	CH_4	C_2H_6	C_2H_4	C_3H_8	C_3H_6	*trans-2* C_4H_8	nC_4H_8	iC_4H_8	*cis-2-* C_4H_8	C_4H_6	
525°C											
1.5	0.02	0.02	0.02	0.06	0.04	0.57	0.46	0.01	0.43	0.04	1.95
3	0.03	0.03	0.03	0.07	0.07	0.89	0.70	0.02	0.67	0.07	2.97
8	0.06	0.05	0.05	0.07	0.14	1.43	1.11	0.09	1.09	0.18	4.87
12	0.10	0.09	0.09	0.12	0.23	1.78	1.40	0.14	1.36	0.27	7.38
16	0.24	0.23	0.15	0.14	0.50	1.77	1.84	0.45	1.55	0.18	10.00
19	0.29	0.28	0.17	0.20	0.57	1.98	2.11	0.58	1.75	0.20	11.52
24	0.35	0.35	0.19	0.25	0.64	2.35	2.72	0.67	2.18	0.25	14.91
550°C											
1.5	0.03	0.02	0.05	0.06	0.09	1.24	1.03	0.05	0.94	0.39	2.55
3	0.06	0.05	0.06	0.07	0.15	1.16	0.96	0.05	0.89	0.14	3.97
8	0.13	0.10	0.13	0.08	0.33	1.40	1.14	0.12	1.07	0.27	6.70
12	0.19	0.17	0.18	0.11	0.48	2.10	1.72	0.21	1.62	0.41	10.03
16	0.58	0.55	0.41	0.26	1.27	2.01	2.23	0.58	1.79	0.33	13.74
19	0.64	0.60	0.43	0.32	1.33	2.25	2.62	0.81	2.06	0.37	15.22
24	0.83	0.82	0.47	0.46	1.56	2.84	3.61	1.02	2.72	0.46	19.56
575°C											
1.5	0.09	0.08	0.10	0.07	0.24	1.09	0.95	0.05	0.84	0.15	3.74
3	0.14	0.12	0.15	0.09	0.37	1.38	1.20	0.09	1.06	0.22	4.90
8	0.36	0.30	0.37	0.16	0.86	3.14	2.20	0.47	2.22	0.59	10.86
12	0.39	0.29	0.43	0.14	1.00	1.99	1.72	0.21	1.54	0.65	16.59
16	1.35	1.33	0.84	0.71	2.48	3.39	4.64	1.70	3.35	0.68	20.88
19	1.67	1.51	1.16	0.63	3.29	2.75	3.48	1.09	2.59	0.7	23.12
24	1.72	1.69	0.99	0.90	2.92	3.79	5.07	2.15	3.70	0.77	27.24

$$r_i = \frac{dC_i}{d\tau} = \sum_{j=1}^{n_R} (\mu_i)_j r_j \qquad (4.15)$$

where μ_i is the stoichiometric coefficient of specie *i*. From the reaction network shown in scheme 2 and on the assumption that butadiene formation is neglected, the following set of mole balance can be written:

Rate of disappearance of *n*-butane, r_B

$$-r_B = -\frac{dC_B}{d\tau} = \left[k_1(C_B - C_{B\square}\, C_H \frac{1}{K_c}) + k_2 C_B\right]\varphi \qquad (4.16)$$

Rate of appearance of C_4 olefin, r_{B^*}

$$r_{B\square} = \frac{dC_{B\square}}{d\tau} = \left[k_1\left(C_B - C_{B\square}\, C_H \frac{1}{K_c}\right)\right]\varphi \qquad (4.17)$$

Rate of appearance of cracked products, r_{CP}

$$r_{CP} = \frac{dC_{CP}}{d\tau} = k_2 C_B \varphi \qquad (4.18)$$

Rate of appearance of hydrogen, r_H

$$r_H = \frac{dC_H}{d\tau} = \left[k_1(C_B - C_{B\square}\, C_H \frac{1}{K_c})\right]\varphi \qquad (4.19)$$

where C_i is the molar concentration of each of the chemical species, *i* being *B* (*n*-Butane), B^*(C_4 Olefin), *CP* (Cracked Products) and *H* (Hydrogen), and the contact time, τ is given by:

$$\tau = \frac{W}{F} \qquad (4.20)$$

From which *W* is the catalyst weight (0.12g), F is total flow rate of the mixed gas into the reactor comprising of *n*-butane and nitrogen. *W* was fixed at 0.12g while *F* was varied keeping the partial pressure of *n*-butane constant in each case. φ is the catalyst decay function, which accounts for the loss of catalytic activity as a result of catalytic deactivation due to coking. For the reaction conversion model, the catalyst decay function is given by:

$$\varphi = exp(-\lambda . X_B) \qquad (4.21)$$

where λ is the catalyst decay constant and X_B is the conversion of *n*-butane given by:

$$X_B = \frac{C_B^0 - C_B}{C_B^0} \qquad (4.22)$$

$C_B^0 = C_B(t = 0)$.

The temperature dependent equilibrium constant (K_c) for the reversible reaction was found to be [93]:

$$K_c = 2.1 \times 10^7 exp\left(-\frac{122kJ/mol}{RT}\right) \qquad (4.23)$$

The activation energy of reaction step j, E_j, is related to the temperature dependent rate constant k_j by the Arrhenius equation:

$$k_j = k_{0j} exp\left(-\frac{E_j}{RT}\right) \qquad (4.24)$$

k_{oj} is the pre-exponential factor. Elswhere[94], it has been suggested that reparameterization of the Arrhenius equation will help reduce parameter interaction during modeling. As a result Eq. 4.24 was reparameterized by centering the values around k_{oj} which is the value of rate constant at reaction step j at the average temperature T_0 :

$$k_j = k_{0j} exp\left\{-\frac{E_j}{R}\left(\frac{1}{T}-\frac{1}{T_0}\right)\right\} \qquad (4.25)$$

The experimental runs were carried out at 525, 550, 575°C, therefore 550°C was selected as the average temperature, $T_{0.}$

4.3.2 Model Assumptions:

Below are the premise on which the model was developed.

1. Mass transfer limitation is negligible
2. Catalyst deactivation is a function of *n*-butane conversion.
3. A single deactivation constant is adopted for all reaction steps
4. Effectiness factor is unity
5. Reactor operates isothermally
6. Butadiene yield is negligible
7. Secondary cracking of olefin is neglected

8. Model assumes only catalytic conversion.

4.3.3 Determination of model parameters and model discrimination

The kinetic parameters in Eq 4.16-4.19 were estimated using a non-linear regression analysis. To estimate the parameters and evaluate the models, individual specific rate equations were combined with mole balance equations. The obtained ordinary differential equations were then solved numerically together with a least square fitting of the experimental *n*-butane dehydrogenation data. MATLAB ODE 45 subroutine (Runge-Kutta-Gill method) was applied in solving the ODE while LSQCURVEFIT subroutine (Modified Marquad method) was used for parameter estimation. To obtain more reliable model and model parameters, the experiments were conducted at three different reaction temperatures (525, 550, 575 °C) and seven different contact times (1.5, 3, 8, 12, 16, 19, 24 $g_{cat}.min.g_{butane}^{-1}$) . Because there is sufficient data for iteration, the degrees of freedom is more than is needed, hence we have a very accurate model results.

The model evaluation criteria are that all the rate parameters should be consistent with physical principles which are the specific reaction and adsorption rates, the activation energies for reactions and the heat of adsorption positive. The optimization criteria used was based on a minimum sum of squares criteria defined by:

$$SS = \sqrt{\sum_{i=1}^{n} \left(C_{i,exp} - C_{i,mod}\right)^2} \qquad (4.26)$$

Model discrimination was based on:

1. Correlation coefficient closer to one
2. Lower sum of square residuals
3. Lower confidence interval for model parameters

The values of the model parameters with their corresponding 95% confidence intervals are shown by Table 4.8 while the cross correlation matrix is as depicted by Table 4.9. As can be seen from Table 4.8, the estimated apparent activation energies of dehydrogenation and cracking are 90.2 and 130.4 kJ/mol respectively. The apparent activation energy of *n*-butane dehydrogenation was found to be lower than those found in literature [93, 95, 96 and 97]. Similar trend exists for the apparent activation energy of cracking (refer to Table 4.10). It was also observed that the apparent activation energy for the production of C_4 olefin is found to be much smaller (96.2 kJ/mol) than the cracking reactions producing methane, ethane, ethene and propene (130.4 kJ/ mol). These results were expected since the 1.2Cr2.8V/M-41 catalyst is more favorable for the dehydrogenation to give C_4 olefin than cracking reaction which requires high activation energy to produce the undesired products [76]. In Table 4, the correlation between E_1-k_1 and E_1-λ for all estimated parameters for dehydrogenation reaction and the correlation between E_2-k_2 and E_2-λ for all estimated parameters for cracking reaction have low to medium parameter interaction, however; there are exceptions. The parameter interactions between k_1-λ and k_2-λ for dehydrogenation and cracking reactions have been found to be significant. The yield of butene as seen from Figure 4.22 was found to increase with both contact time and temperature, which is also true for *n*-butane conversion. Maximum yield

Table 4.8: Estimated values of the kinetic parameters at 95% confidence intervals

Parameters	Reaction conversion model		
	E(kJ/mol)	Pre-exponential factor	R^2
k_1	96.2 ±12.2	$(5.9\pm 0.5) \times 10^{-3}$	0.9994
k_2	130.4±16.9	$(5.0\pm0.5) \times 10^{-3}$	
λ	0.97± 0.71		

Table 4.9: Correlation matrix for *n*-butane dehydrogenation over 1.2Cr2.8V/M-41 catalyst

	k_1	E_1	k_2	E_2	λ
k_1	1.00	0.29	0.60	0.41	0.88
E_1	0.29	1.00	0.50	0.01	0.53
k_2	0.60	0.50	1.00	-0.07	0.77
E_2	0.41	0.01	-0.07	1.00	0.38
Λ	0.88	0.53	0.77	0.38	1.00

Table 4.10: Apparent activation energy of *n*-butane dehydrogenation and cracking reactions reported in selected works.

Author	Catalyst	Apparent activation energy(kJ/mol)	
		Dehydrogenation	Cracking
J.A. Lecher et al[96]	H-ZSM-5	105	140
R. Gounder et al[97]	$H_{100}Na_0$MOR-T	177	191
"	$H_{100}Na_0$MOR-Z	194	208
"	$H_{45}Na_{55}$MOR-Z	186	205
J.Macgregor et al[95]	VO_x/Al_2O_3	132	-
Airaksinen et al[93]	CrO_x/Al_2O_3	137	-
This Study	1.2Cr2.8V/M-41	96	130

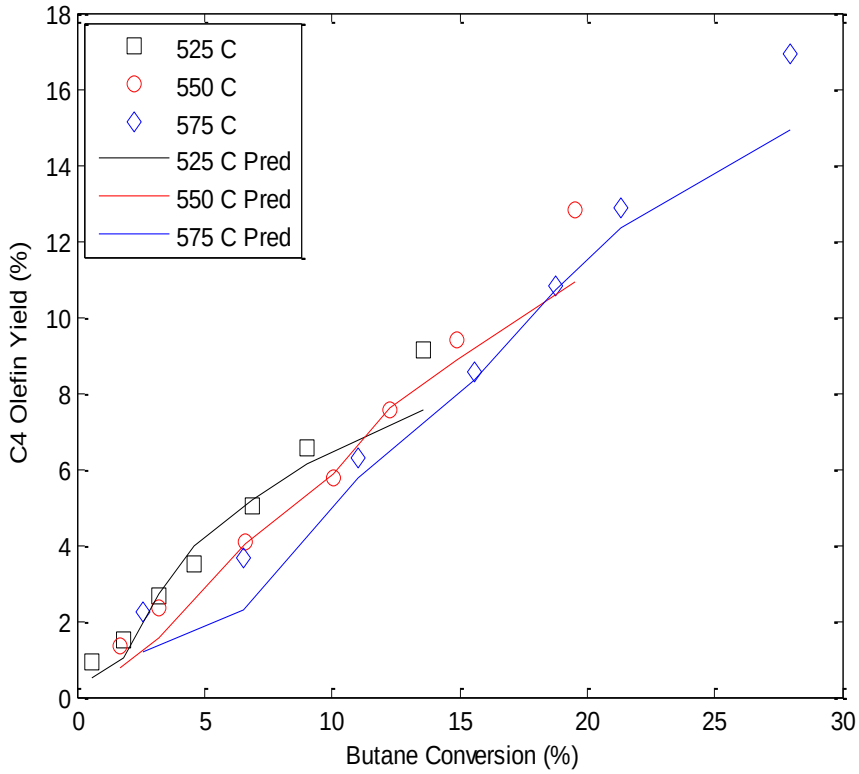

Figure 4.22: C_4 Olefin yields against *n*-butane conversion at various temperatures for 1.2Cr2.8V/M-41

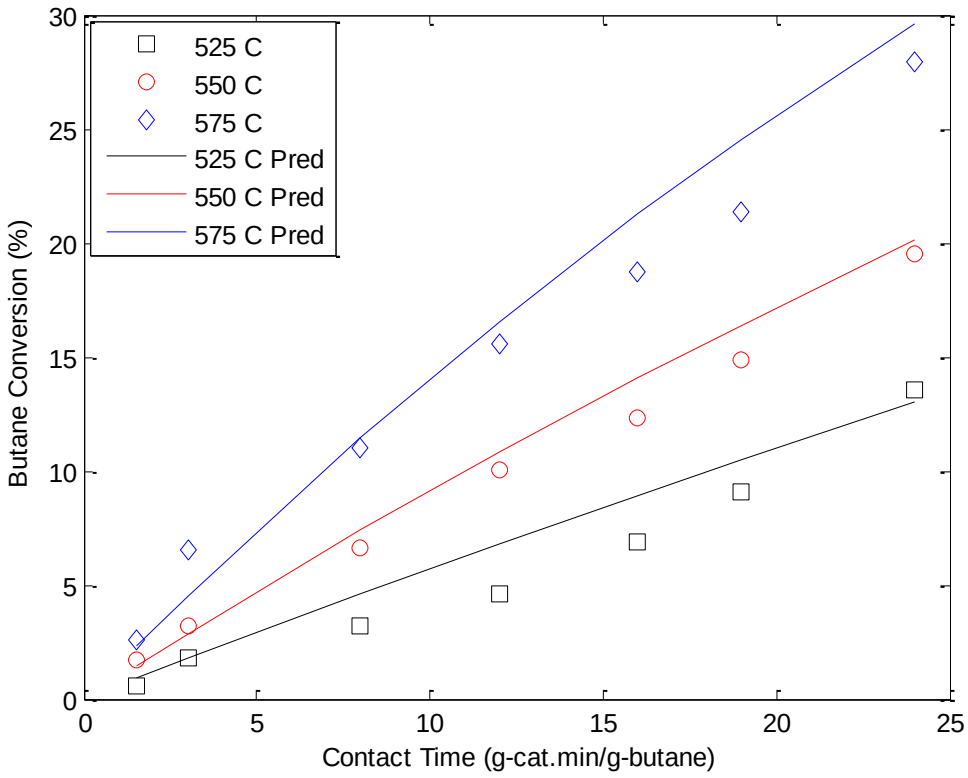

Figure 4.23: Comparison of experimental and model predicted conversion at different temperatures.

of 17, 13 and 9% were recorded at 575, 550 and 525°C respectively. The numerical results were compared with experimental data as depicted by Figure 4.23. As illustrated by the figure, the model prediction compares favorably with the experimental data. This is a proof that the proposed kinetic model is a good fit for the obtained experimental results. To further give credence to the determined model, a parity plot (Figure 4.24) showing the overall agreement of the experimental data and the model predictions was done. Also, the value of the regression coefficient was close to unity (R^2=0.99) suggesting a strong correlation between the experimental results and the model.

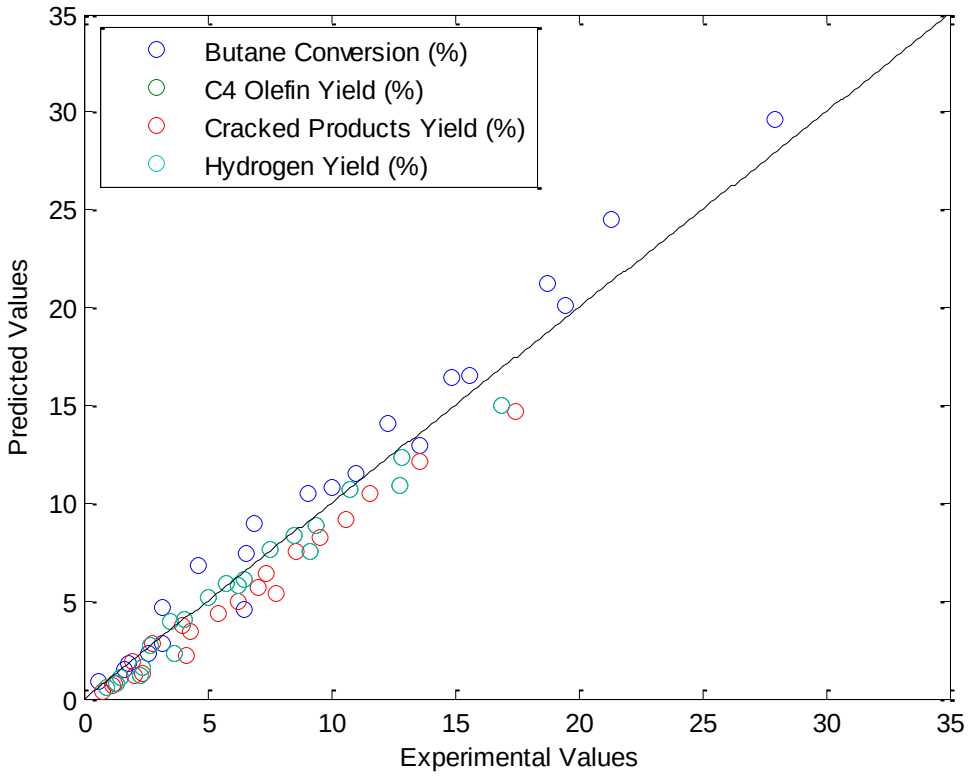

Figure 4.24: Parity plot between the experimental results and model predictions of 1.2Cr2.8V/M-41

CHAPTER 5

CONCLUSIONS & RECOMMENDATIONS

5.1 Conclusions

The study shows the preparation and characterization of mono (Cr or V) and bimetallic (Cr-V) based MCM-41 catalysts. The XRD results reveal that the CrOx and VOx species are well dispersed without any detectable crystalline peaks. The BET results indicate that in impregnated samples the mesoporous hexagonal is well retained with uniform pore size distributions. According to TPR results, the absence of considerable amount of polymeric vanadium species in bimetallic system clearly indicates a promoted dispersion of VOx species in the presence of CrOx species. The H_2 consumptions (mmol/g) were in the following order: 1.2Cr2.8V/M-41 > 3.8V/M-41 (0.655) > 2.0Cr2.0V/M-41 (0.605) > 2.7Cr1.2V/M-41 (0.495) > CrM-41 (0.385) > 3.5Cr/M-41 (0.285), respectively. The amount of ammonia consumed in the samples is as follows: 1.2Cr2.8V/M-41 ~ 2.7Cr1.2V/M-41 > 2Cr2V/M-41 > 3.5Cr/M-41 ~ 3.8V/M-41 > CrM-41 > SiMCM-41. The increased surface acidity shows the stronger interaction of mixed oxides over support than that of the mono metal oxide supported catalysts. Concomitantly, the catalytic selectivity can be related to the uniform dispersion of Cr, V and surface acidity of the catalysts. 1.2Cr2.8V/M-41 showed highest butane conversion of 20.1% and butenes selectivity 88.5% at 600 ^{o}C. In addition, it is shown that CO_2 atmosphere has a promoting effect on catalysts stability accompanied with slightly increased butane conversion.

The activity of bimetallic Cr-V impregnated mesoporous and microporous catalysts are tested in the oxidative dehydrogenation of *n*-butane using CO_2 as oxidant. The results show that the high activity of 1.2Cr2.8V/M-41 depends on the reducibility and acid to base functionality for the production of butenes. H_2 consumptions over the four samples were in the following order: 1.2Cr2.8V/M-41 > 1.2Cr2.8V/Z-5 > 1.2Cr2.8V/MesoZ-5 > 2.7Cr1.2V/M-22. The total acidity to basicity ratio of samples was observed as follows: 1.2Cr2.8V/M-41 > 1.2Cr2.8V/Z-5 > 1.2Cr2.8V/mesoZ-5 > 1.2Cr2.8V/M-22. For 1.2Cr2.8V/M-41 catalyst, the major product was found to be 1, 3-butadiene (6.6 wt %), while less amounts of trans 2-butene, 1-butene, cis 2-butene (< 2wt.%), isobutene (0.21wt.%) were observed. The enhanced selectivity of olefins over 1.2Cr2.8V/M-41 catalysts could be attributed to the mild adsorption on the catalyst acid surface with moderate strength. With respect to CO_2 activation, 1.2Cr2.8V/M-22 shows highest CO_2 conversion in the range 2.35-2.2% at 550 ^oC. While 1.2Cr2.8V/M-41 remains the best of the four samples as per dehydrogenation activity, further results show that it is not active towards CO_2 at low temperatures as compared with the other three samples. However, its CO_2 activation improves at higher temperatures. The apparent activation energies of dehydrogenation reaction over the four catalysts remain similar ranging from 67-72 kJ/mol. However, variation in the activation energies of cracking (80-157 kJ/mol) indicates different cracking mechanisms, invariably; this variation determines the performance of each catalyst for dehydrogenation reactions. The ratio of conversion to coke weight per cent over the four catalysts at same reaction condition are

in the following order: 1.2Cr2.8V/M-41>1.2Cr2.8V/Z-5>1.2Cr2.8V/mesoZ-5>1.2Cr2.8V/M-22.

Comprehensive experimental kinetic data were obtained for *n*-butane dehydrogenation over 1.2Cr2.8V/M-41 catalyst in a fixed bed reactor. Power law model was adopted for evaluating the kinetic parameters based on the reaction conversion catalyst decay function. The experimental data showed reasonable fit for the model at 95% confidence interval with a correlation coefficient of R^2=0.9994. The apparent activation energies of dehydrogenation and cracking are 96.2 and 130.4 kJ/mol respectively. From these results, the catalyst can be said to be a reliable catalyst for dehydrogenation when compared with some catalysts from literature because of its lower apparent activation energy. Also, the catalyst was observed to be selective towards dehydrogenation rather than cracking based on its lower apparent activation energy for dehydrogenation over cracking.

5.2 Recommendation

While 1.2Cr2.8V/M-41 enjoys a good activity for dehydrogenation, same cannot be said of its stability at steady state. This study results for the activity of 1.2Cr2.8V/M-41 could be fine-tuned for industrial applications if composite support comprising of MCM-41 and ZSM-5 hierarchical support type could be implemented in future work.

NOTATION

B = *n-butane specie*

B^* = C_4 *olefin specie*

CP = *cracked products lump*

C_B^0 = *initial concentration of n-butane (mmol/ml.*g_{cat}*)*

C_i^{exp} = *experimental concentration of specie i (mmol/ml.*g_{cat}*)*

C_i^{mod} = *predicted concentration of specie i (mmol/ml.*g_{cat}*)*

$d_{spacing}$ = *inter-atomic spacing (Å)*

E_j = *apparent activation energy for reaction step j (kJ/mol)*

H = *hydrogen*

F = *inlet mixed gas flow rate (ml/min)*

k_j = *specific reaction rate constants for step j at a particular temperature*

K_c = *equilibrium constant (bar)*

k_{0j} = *pre-exponential factor of step j*

r_i = *total reaction rate of specie i*

R = *universal gas constant (kJ/mol.K)*

R^2 = *correlation coefficient*

S_{BET} = *BET surface area (*m^2*/g)*

T = *reaction temperature (°C)*

T_0 = *average or reference temperature (°C)*

W = *weight of the catalyst (g)*

Z = *atomic number*

GREEK LETTERS

φ = *catalyst decay function*

λ = *decay constant*

μ_i = *stoichiometric coefficient of specie i*

τ = *contact time* (g_{cat} .min/g_{butane})

APPENDIX

(Flow diagram of the BELLCAT reactor with standard specification)

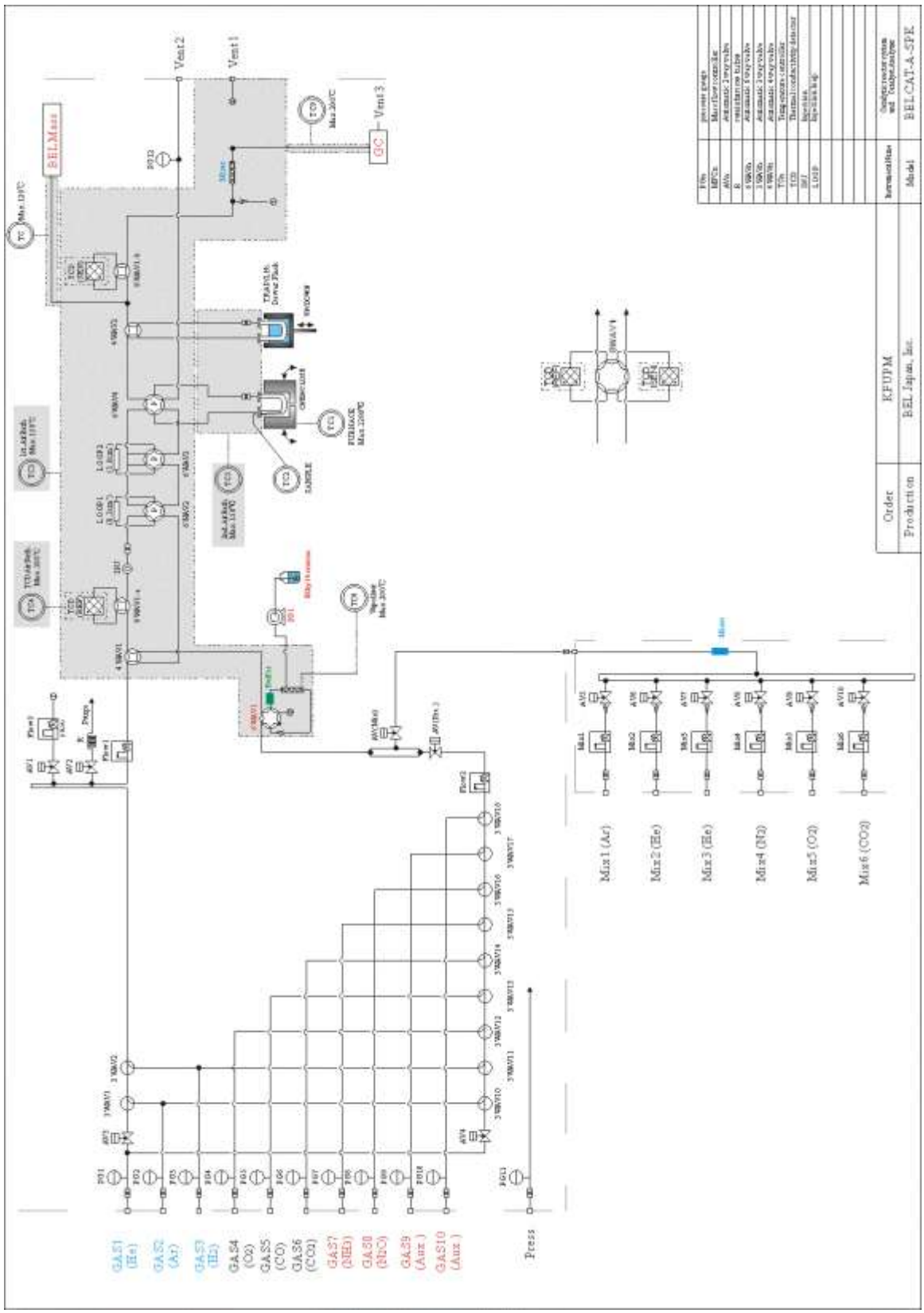
Vent2
Vent1
Vent3
BELMass
GAS1 (Ele)
GAS2 (Ar)
GAS3 (He)
GAS4 (O2)
GAS5 (CO)
GAS6 (CO2)
GAS7 (NH3)
GAS8 (NO)
GAS9 (Aux.)
GAS10 (Aux.)
Press
Mix1 (Ar)
Mix2 (He)
Mix3 (He)
Mix4 (N2)
Mix5 (O2)
Mix6 (CO2)
KFUPM
BEL Japan, Inc.
BELCAT-A-SPE

REFERENCES

1. Brazdil, J.F., Topics in Catalysis, 2009; 38: 289
2. Cavani F, Ballarini N, Cericola A. Oxidative dehydrogenation of ethane and propane: How far from commercial implementation? Catal. Today, 2007; 127: 113-131
3. Zhang F, Wu R, Yue Y, Yang W, Gu S, Miao C, Hua W, Gao Z. Chromium oxide supported on ZSM-5 as a novel efficient catalyst for dehydrogenation of propane with CO_2, Micropor. Mesopor. Mater., 2011; 145: 194–199
4. Qi G., Wang Y., Estevez L., Switzer A.K., Duan X, Yang X., Giannelis E.P., Chem. Mater., 2010; 122:2693.
5. Poole C.P, MacIver D.S. The physicalchemical properties of chromia-alumina catalysts, in: Advances in Catalysis, Academic Press, New York, 1967:17, 223–314
6. M. Larsson, M. Hulten, E.A. Blekkan, B. Anderson, J. Catal., 1996:164,44
7. Y.M. Liu, Y. Cao, S.R. Yan, W.L. Dai, K.N. Fan, Catal Lett, 88 (2003) 61.A.
8. De Rossi S, Casaletto M, Ferraris G, Cimino A., Minelli G., Chromia/zirconia catalysts with Cr content exceeding the monolayer. A comparison with chromia/alumina and chromia/silica for isobutane dehydrogenation Appl. Catal. A. 1998, 167: 257–270
9. Hakuli A, Harlin M.E, Backman L.B, Krause A.O.I, Dehydrogenation of i-butane on CrOx/SiO2 catalysts, J. Catal. 1999; 184: 349-356.

10. Botavina M.A., Martra G., Agafonov Yu.A., Gaidai N.A., Nekrasov N.V., Trushin D.V., Coluccia S., Lapidus A.L., Oxidative dehydrogenation of C3–C4 paraffins in the presence of CO2 over CrOx/SiO2 catalystsAppl. Catal. A. 2008 ; 347 : 126–132.
11. Volpe M, Tonetto G, de Lasa H. Butane dehydrogenation on vanadium supported catalysts under oxygen free atmosphere, Appl. Catal. A 2004 ; 272 : 69–78.
12. Malleswara Rao T.V, Mamoune Zahidi El, Sayari A. Ethane dehydrogenation over pore-expanded mesoporous silica-supported chromium oxide: 2. Catalytic properties and nature of active sites, J. Mol. Catal. A 2009; 301:159–165.
13. Setnicka M, Bulanek R, Capek L, Cicmanec P. n-Butane oxidative dehydrogenation over VOX-HMS catalysts, J. Mol. Catal. A 2011; 344: 1– 10
14. Bulanek R, Kaluzova A, Setnicka M, Zukal A, Cicmanec P, Mayerova J. Study of vanadium based mesoporous silicas for oxidative dehydrogenation of propane and n-butane, Catal. Today 2012 ; 179 : 149– 158
15. Wang S., Lu G.Q., Millar G.J., Energy & Fuels, Carbon Dioxide Reforming of Methane To Produce Synthesis Gas over Metal-Supported Catalysts: State of the Art. 1996, 10 : 896.
16. Nakagawa K., Kajita C., Okumura K., Ikenaga N., Nishitani-Gamo N., Ando T., Kobayashi T., Suzuki T., Application of the unique redox properties of magnesium ortho-vanadate incorporated with palladium in the unsteady-state operation of the oxidative dehydrogenation of propane, J. Catal. 2001, 203: 87-93.

17. Wang Y., Ohishi Y., Shishido T., Zhang Q., Takehira K., CO2 dehydrogenation of Propane over Cr-MCM-41 catalyst Stud. Surf. Sci. & Catal. 2003, 146:725-728
18. Shimada H., Akazawa T., Ikenaga N, Suzuki T., Dehydrogenation of isobutane to isobutene with iron-loaded activated carbon catalyst, Appl. Catal. A. 1998, 168 :243-250
19. Parvulescu V., Anastasescu C., Constantin C., Su B.L., Mono (V, Nb) or bimetallic (V–Ti, Nb–Ti) ions modified MCM-41 catalysts: synthesis, characterization and catalysis in oxidation of hydrocarbons (aromatics and alcohols) Catal. Today 2003, 78 :477–485.
20. Yuan Z.Y., Wang J.Z., Zhang Z.L., Chen T.H., Li H.X., Vanadium- and chromium-containing mesoporous MCM-41 molecular sieves with hierarchical structure Micropor. Mesopor. Mater. 2001, 43 :227.
21. Tuel A., Modification of mesoporous silicas by incorporation of heteroelements in the framework Micropor. Mesopor. Mater. 1999, 27: 151–167.
22. Wei D., Wang H., Feng X., Chueh W.-T., Ravikovich P., Lyubovsky M., Li C., Takeguchi T., Haller G.L., J. Phys. Chem.B Synthesis and Characterization of Vanadium-Substituted Mesoporous Molecular Sieves,1999, 103 : 2113–2121.
23. Parvelescu V., Su B.L., Synthesis and gas separation performance of zeolite membranes with orientation-controlled hexagonal crystals supported on γ-Al2O3 Stud. Surf. Sci. Catal. 2002, 143 : 575.
24. Ahmed S, Rahman F.,Al-Asiri H., Baduruthamal U., . Oxidative dehydrogenation of lower alkanes over metal incorporated MCM-41 catalysts,

Reaction Kinetics, Mechanisms and Catal. 20th Annual Saudi-Japan Symposium, KFUPM, Dhahran, December 5-6, 2010

25. Taguchi A, Schuth F, Ordered mesoporous materials in catalysis , Micropor. Mesopor. Mater. 2005, 77:1-45.
26. Rosa M. Martín-Aranda and Jiří Čejka, Recent Advances in Catalysis Over Mesoporous Molecular SievesTop Catal. 2010, 53:141-153
27. A. Olabode, L. Bentley, M. Radonjic, AIP Conf. Proc. 2012: **1453**, 347-352 doi:http://dx.doi.org/10.1063/1.4711198.
28. J.S. Chang, V.P. Vislovskiy, M.S. Park, D.Y. Hong, J.S. Yoo, S.E. Park, Green Chem.2003: **5**, 587–590
29. Y. Wang, Y. Ohishi, T. Shishido, Q. Zhang, W. Yang, Q. Guo, H. Wan, K. Takehira, J. Catal. 2003: **220**, 347–357.
30. F. Zhang, R. Wu, Y. Yue, W. Yang, S. Gu, C. Miao, W. Hua, Gao Z., Micropor. Mesopor. Mater. 2011: **145**, 194–199.
31. Operation manual Catalyst Analyzer BELCAT-A, ver.1.3.4, September 2011, BEL Japan, Inc.
32. Gardiner, D.J. Practical Raman spectroscopy. Springer-Verlag. (1989). ISBN 978-0-387-50254-0
33. Z. Pavlačkova, G. Košova´, N. Žilkova´, A. Zukal, J. Čejka, Stud. Surf. Sci. Catal. 2006: **162**, 905-912.
34. Beck J.S., Vartuli J.C., Roth W.J., Leonowicz M.E., Kresge C.T., Schmitt K.D., Chu C.T.-U., Olsen D.H., Sheppard E.W., McCullen S.B., Higgins J.B.,

Schlenker J.L., A new family of mesoporous molecular sieves prepared with liquid crystal templates J. Am. Chem. Soc. 1992, 114**:**10834

35. Zhu Z.**,** Chang Z., Kevan L., Synthesis and Characterization of Mesoporous Chromium-Containing Silica Tube Molecular Sieves CrMCM-41 J. Phys. Chem. B 1999, 103**:**2680
36. Chirayil T., Zavalij P.T. , . Whittingham M.S, Hydrothermal Synthesis of Vanadium OxidesChem. Mater. 1998, 10:2629
37. Cheng C-F., He H., Zhou W., Klinowski J., Goncüalves J. A. S., Gladden L. F., Synthesis and Characterization of the Gallosilicate Mesoporous Molecular Sieve MCM-41, J. Phys. Chem. 1996, 100, 390-396
38. Jha R.K., Shylesh S., Bhoware S.S., Singh A.P., Oxidation of ethyl benzene and diphenyl methane over ordered mesoporous M-MCM-41 (M = Ti, V, Cr): Synthesis, characterization and structure–activity correlations Micropor. Mesopor. Mater. 2006, 95: 154–156
39. Dai H.X., Bell A.T., Iglesia E., Effects of molybdena on the catalytic properties of vanadia domains supported on alumina for oxidative dehydrogenation of propane, J. Catal. 2004, 221:491–499
40. Kondratenko E.V., Cherian M., Baerns M., Su D., Schlogl R., Wang X., Wachs I.E., Activation of dihydrogen on supported and unsupported silver catalysts , J Catal. 2005, 234:141
41. Zhang F, Wu R, Yue Y, Yang W, Gu S, Miao C, Hua W, Gao Z. Chromium oxide supported on ZSM-5 as a novel efficient catalyst for dehydrogenation of propane with CO_2, Micropor. Mesopor. Mater., 2011; 145: 194–199

42. Ellison A., Overton T.L., Benzce L., J. Chem. Soc., Faraday Trans. Characterisation of Cr–silica polymerisation catalysts, 1993, 89: 843
43. Qiao Y., Miao C., Yue Y., Xie Z., Yang W., Hua W., Gao Z., Vanadium oxide supported on mesoporous MCM-41 as new catalysts for dehydrogenation of ethylbenzene with CO2 Micropor. Mesopor. Mater. 2009, 119 :150.
44. Sokolovskii V, Arena F., Giordano N., Parmaliana A., Role of Acid–Base Properties of SiO2-Based Catalysts in the Selective Oxidation of PropaneJ Catal. 1997, 167: 66.
45. Owens L., Kung H.H., The Effect of Loading of Vanadia on Silica in the Oxidation of Butane, J Catal. 1993, 144 :202–213
46. Xingtao Gao, Miguel A. Banares and Israel E. Wachs. Ethane and n-Butane Oxidation over Supported Vanadium Oxide Catalysts: An in Situ UV–Visible Diffuse Reflectance Spectroscopic Investigation, J. Catal. 199: 188, 325–331
47. Shylesh S, Singh A.P. Synthesis, characterization, and catalytic activity of vanadium-incorporated, -grafted, and -immobilized mesoporous MCM-41 in the oxidation of aromatics, J.Catal. 2004; 228: 333
48. Gaspar A., Brito J., Dieguez L., Characterization of chromium species in catalysts for dehydrogenation and polymerization, J. Mol. Catal. A. 2003, 203:251–266
49. Mitra B., Wachs I.E., Deo G., Promotion of the propane ODH reaction over supported V2O5/Al2O3 catalyst with secondary surface metal oxide additives J. Catal. 2006, 240:151–159,

50. Michorczyk P., Ogonowski J., Kustrowski P., Chmielarz L., Chromium oxide supported on MCM-41 as a highly active and selective catalyst for dehydrogenation of propane with CO2 Appl. Catal. A. 2008, 349:62
51. Airaksinen, S. M. K., Krause, A. O. I., Sainio, J., Lahtinen, J., Chao, K.-j.,Guerrero-Pérez, M. O., Bañares, M. A., Reduction of Chromia/Alumina Catalyst Monitored by DRIFTS-Mass Spectrometry and TPR-Raman Spectroscopy,Phys. Chem. Chem. Phys. 2003, 5: 4371–4377
52. Weckhuysen M., Wachs I. E., Zeolite-Encapsulated Copper(II) Amino Acid Complexes: Synthesis, Spectroscopy, and Catalysis J. Phys. Chem. 1996, 100:437-442.
53. Hoang D.L., Dittmar A., Schneider M., Trunschke A., Lieske H., Brzezinka K.-W., Witke K., Evidence of lanthanum–chromium mixed oxides formed in CrOx/La2O3 model catalysts, Thermochimica Acta, 2003, 400:153–163
54. Solsona B., Blasco T., López Nieto J.M.,. Peña M.L, Rey F., Vidal-Moya A., Vanadium Oxide Supported on Mesoporous MCM-41 as Selective Catalysts in the Oxidative Dehydrogenation of Alkanes , J. Catal. 2001, 203 :443
55. Santamaria-Gonzalez J, Luque-Zambrana J, Merida-Robles J, Maireles-Torres P, Rodriguez-Castellon E, Jimenez-Lopez A. Catalytic behavior of vanadium-containing mesoporous silicas in the oxidative dehydrogenation of propane, Catal. Lett. 2000; 68: 67–73
56. Raju G, Reddy B. M, Abhishek B, Mob Y-H, Park S-E. Synthesis of C4 olefins from *n*-butane over a novel VOx/SnO2–ZrO2 catalyst using CO2 as soft oxidant, Appl. Catal. A: Gen. 2012; 423– 424: 168– 175

57. Bulanek R, Kaluzova A, Setnicka M, Zukal A, Cicmanec P, Mayerova J. Study of vanadium based mesoporous silicas for oxidative dehydrogenation of propane and *n*-butane, Catal. Today 2012 ; 179 : 149– 158
58. Capek L., Adam J., Grygar T., Bulanek R., Vradman L., Kosova-Kucerova G., Cicmanec P., Knotek P., Nature of active sites in decane-SCR-NOx and NO decomposition over Cu-ZSM-5 zeolites Appl. Catal. A. 2008, 342:99
59. Karamullaoglu G., Dogu T., Oxidative Dehydrogenation of Ethane over Chromium−Vanadium Mixed Oxide and Chromium Oxide Catalysts Ind. Eng. Chem. Res. 2007, 46:7079-7086
60. Ruettinger W., Benderly A., Han S., Shen X., Ding Y., Suib S. L., Catal Lett. 2011, 141:15
61. Blasco T., Nieto J.M.L., Dejoz A., Vazquez M.I., Influence of the Acid-Base Character of Supported Vanadium Catalysts on Their Catalytic Properties for the Oxidative Dehydrogenation of n-Butane, J. Catal. 1995, 157: 271–282
62. Corma A., Nieto J.M.L., Parades N., Dejoz A., Vazquez I., in: Corbern V.C., Bellon S.V. (Eds.), Stud. in Surf. Sci. Catal., Elsevier, 1994, 113–123,
63. Du G., Lim S., Pinault M., Wang C., Fang F., Pfefferle L., Haller G. L., J. Catal. 2008, 253 :74–90
64. Le Bars J, Vedrine J.C., Auroux A., Appl. Catal. A 1992 88: 179.
65. Krannila H, Haag W.O, Gates B.C. Monomolecular and bimolecular mechanisms of paraffin cracking: n-*butane* cracking catalyzed by HZSM-5, J. Catal. 1992; 135: 115-124

66. Wakui K, Satoh K, Sawada G, Shiozawa K, Matano K, Suzuki K, Hayakawa T, Yoshimura Y, Murata K, Mizukami F. Dehydrogenative cracking of *n*-butane using double-stage reaction, Appl. Catal. A 2002; 230: 195-202.

67. Narbeshuber T.F, Thesis, University of Twente, ISBN 90-9007754-5, The Netherlands, 1994.

68. Narbeshuber T.F, Vinek H, Lercher J.A. Monomolecular Conversion of Light Alkanes over H-ZSM-5, J. Catal. 1995; 157: 388-395

69. Gil B, Zones S.I, Hwang S.J, Bejblova M, Cejka J. Acidic Properties of SSZ-33 and SSZ-35 Novel Zeolites: a Complex Infrared and MAS NMR Study, J Phys Chem C, 2008; 112: 2997.

70. Madeira L.M, Aranda R.M.M, Hodar F.J.M, Fierro J.L.G, Portela M.F. Oxidative Dehydrogenation of *n*-Butane over Alkali and Alkaline Earth-Promoted α-NiMoO4Catalysts, J. Catal. 1997; 169: 469–479.

71. Y-M. Liu, Y. Cao, N. Yi, W-L. Feng, W-L. Dai, S-R. Yan, H-Y. He, K-N. Fan, J. Catal., 2004:**224**, 417-428.

72. H. Berndt, A. Martin, A. Bruckner, E. Schreier, D. Muller, H. Kosslick, G.-U. Wolf, B. Lucke, J. Catal. 2000: **191**, 384-401.

73. Deng J, Zhang L, Liu C, Xia Y, Dai H. Single-crystalline mesoporous CaO supported Cr–V binary oxides: Highly active catalysts for the oxidative dehydrogenation of isobutene, Catal. Today 2011; 164: 347–352.

74. Cristiani C, Forzatti P, Busca G. On the surface structure of vanadia-titania catalysts: Combined laser-Raman and fourier transform-infrared investigation, J. Catal., 1989; 116: 586.

75. Chao K. J, Wu C. V, Chang H, Lee L. J, Hu S.-F. Incorporation of Vanadium in Mesoporous MCM-41 and Microporous AFI Zeolites, J. Phys Chem B. 1997; 101: 6341.

76. Ajayi B.P., Rabindran Jermy B., Ogunronbi K.E., Abussaud B.A., Al-Khattaf S, *n*-Butane Dehydrogenation Over Mono and Bimetallic Chromium and Vanadium Catalyst Under Oxygen Free Atmosphere, Catal. Today, 2013, 204:189-196A.

77. Takehira K, Ohishi Y, Shishido T, Kawabata T, Takaki K, Zhang Q, Wang Y. Behavior of active sites on Cr-MCM-41 catalysts during the dehydrogenation of propane with CO_2, J. Catal. 2004; 224: 404-416.

78. Cavani F, Ballarini N, Cericola A. Oxidative dehydrogenation of ethane and propane: How far from commercial implementation? Catal. Today, 2007; 127: 113-131

79. Ogonowski J, Skrzynska E. Carbon dioxide in the dehydrogenation of isobutane over VmgOx, Catal. Commun. 2009; 11: 132-136

80. Sun A, Qin Z, Chen S, Wang J. Role of carbon dioxide in the ethylbenzene dehydrogenation coupled with reverse water–gas shift J. Mol. Catal. A: Chem. 2004; 210: 189–195

81. Wakui K, Satoh K, Sawada G, Shiozawa K, Matano K, Suzuki K, Hayakawa T, Murata K, Yoshimura Y, Mizukami F. Catalytic cracking of *n*-butane over rare earth — loaded HZSM-5 catalysts, Stud. Surf. Sci. Catal. 1999; 125: 449..

82. Wang X, Carabineiro H, Lemos M.A.N.D.A, Ramoa Ribeiro F. Propane conversion over a H-ZSM5 acid catalyst: Part 1. Observed kinetics, J. of Mol. Catal. A: Chem. 2004; 216: 131-137

83. Ono Y, Osako K, Yamawaki M. Mechanism of the Activation of Butanes and Pentanes over ZSM-5 Zeolites, Stud. Surf. Sci. Catal. 1994; 83: 303.

84. Ahmed S, Rahman F, Al-Amer A.M. J, Al-Mutairi E.M, Baduruthamal U, Alam K. Oxidative dehydrogenation of lower alkanes over metal incorporated MCM-41 catalysts, Reaction Kinetics, Mechanisms and Catal. 2012; 105: 483-493.

85. Wang Y, Ohishi Y, Shishido T, Zhang Q, Yang W, Guo Q, Wan H, Takehira K. Characterizations and catalytic properties of Cr-MCM-41 prepared by direct hydrothermal synthesis and template-ion exchange, J.Catal. 2003; 220: 347–357.

86. Pirngruber G.D, Seshan K, Lercher J.A. Dehydroisomerization of *n*-Butane over Pt–ZSM5 (I): Effect of the Metal Loading and Acid Site Concentration, J. of Catal. 1999; 186: 188-200.

87. Solsona B., Lopez Nieto J. M., Concepcion P., Dejoz A.,. Ivars F., Vلzquez M.I., J. Catal. 2011; **280**: 28

88. Meusinger J, Vinek H, Lercher J.A. Cracking of n-hexane and n-butane over SAPO5, MgAPO5 and CoAPO5, J. Mol. Catal. 1994; 87: 263-274.

89. Toledo J.A, Armendariz H, Lopez-Salinas E. Oxidative dehydrogenation of *n*-butane: a comparative study of thermal and catalytic reaction using Fe-Zn mixed oxides, Catal. Lett., 2000; 66: 19-24.

90. Bazyari A, Khodadadi A.A, Hosseinpour N, Mortazavi Y. Effects of steaming-made changes in physicochemical properties of Y-zeolite on cracking of bulky 1,3,5-triisopropylbenzene and coke formation, Fuel Process Technol. 2009; 90: 1226-1233
91. Hosseinpour N, Khodadadi A.A, Mortazavi Y, Bazyari A. Nano-ceria–zirconia promoter effects on enhanced coke combustion and oxidation of CO formed in regeneration of silica–alumina coked during cracking of triisopropylbenzene, Appl. Catal. A 2009; 353: 271-281.
92. Al-Khattaf S., de Lasa H., Catalytic Cracking Of Cumene In A Riser Simulator: A Catalyst Activity Decay Model., Ind. Eng. Chem. Res. 2001, 40:5398-5404
93. Airaksinen S.M.K., Harlin M. E., Krause A.O. I., Kinetic Modeling of Dehydrogenation of Isobutane on Chromia/Alumina Catalyst, Ind. Eng. Chem. Res. 2002, 40:5619-5626
94. Agarwal A.K., Brisk M.L., Sequential Experimental Design For Precise Paramter Estimation: Use Of Reparameterization. Ind. Eng. Chem. Proc. Des. Dev. 1985, 24:203-207
95. Jiménez-López A., Rodriguez-Castellón E., Maireles-Torres P., Diaz L, Mérida-Robles J., Chromium oxide supported on zirconium- and lanthanum-doped mesoporous silica for oxidative dehydrogenation of propane, Appl. Catal. A. 2001,218: 295–306.,
96. Lercher J.A.,. van Santen R.A, Vinek H., Carbonium Ion Formation In Zeolite Catalysis, Catal. Lett. 1994, 269:91-96

97. Gounder R., Iglesia E., Effects of Partial Confinement on the Specificity of Monomolecular Alkane Reactions for Acid Sites in Side Pockets of Mordenite, Angew. Chem. Int. Ed. 2010, 49:808-811

Vitae

Name	:Babajide Patrick Ajayi
Nationality	Nigerian
Email	:jide.ajayi@ymail.com
Academic Background	:BSc(Chemical Engineering) Obafemi Awolowo University
	:MSc(Chemical Engineering) King Fahd Univ. of Petrol.
Contact Address	Lagos, Nigeria

Research Outcomes

a. PUBLICATIONS

- **B.P. Ajayi**, R. Rabindran Jermy, K.E. Ogunronbi, B.A. Abussaud, S. Al-Khattaf, n-Butane dehydrogenation over mono- and bi-metallic MCM-41 catalysts under oxygen free atmosphere, *Catal. Today* , 204(2013)189-196
- **B.P. Ajayi**, R. Rabindran Jermy, B.A. Abussaud, S. Al-Khattaf, Oxidative dehydrogenation of *n*-butane over bimetallic mesoporous and micro-porous zeolites with CO_2 as mild oxidant, *J. of Porous Mater., accepted.*

b. CONFERENCE PROCEEDINGS

- **B.P. Ajayi**, R. Rabindran Jermy, B.A. Abussaud, K.E. Ogunronbi, S. Al-Khattaf, n-Butane dehydrogenation over mono- and bi-metallic MCM-41 catalysts under oxygen free atmosphere, *Proceedings of the International Zeolite Workshop, Jejune* Island, South-Korea, *3rd-5th August, 2012.*
- **B.P. Ajayi**, R. Rabindran Jermy, B.A. Abussaud, S. Al-Khattaf, Oxidative dehydrogenation of *n*-butane over bimetallic mesoporous and micro-porous zeolites with CO_2 as mild oxidant, *4th Scientific Student Conf., Makkah, 28th April- May 2nd, 2013*
- **B.P. Ajayi**, Kinetic modeling of *n*-butane dehydrogenation over CrO_xVO_x/MCM-41 catalyst in a fixed bed reactor, *4th Scientific Student Conf., Makkah, 28th April-May 2nd, 2013*